A 22 GHz WATER MASER RADIOMETER

A thesis submitted for the degree of Master of Science

at Rhodes University

Grahamstown

By

BRIAN J. NUNN

September, 1974.

Supervisor ~~Promotor~~: Professor E. E. BAART

" From harmony, from heavenly harmony,
This universal frame began;
When nature underneath a heap
Of jarring atoms lay,
And could not heave her head,
The tuneful voice was heard from high,
"Arise, ye more than dead!" "

from John Dryden (1687),

"A song for St. Cecilia's day".

Acknowledgements

I wish to express my sincere thanks to the following people, without whose assistance this project would have been impossible:

Professor E. E. Baart for his constant guidance and constructive criticism, and his comments on the first draft of this manuscript,

Dr. G. de Jager for his help and unfailing optimism,

Mr. C. Way-Jones for his expert advice rendered during the many fruitful discussions on the various aspects of the project,

Mr. Arnott for his help in the design of the antenna structure, and his and Mr. A. Barnard's precise machining of this structure,

Mr. J. Walters who produced photographs and xerox copies of figures for the text, and

Mrs Estment for her patience with my handwriting, and her expertise with the typewriter.

I also appreciate the help and encouragement of all my friends, including especially the people mentioned above, Laurie Mutch, Dr. G. Gruber, Professor J. Gledhill, and Kathy, and of my parents and family.

Finally, the financial assistance provided by Mr. F. J. J. Furter ~~Furtur~~ during 1973 and the Muirhead and C. S. I. R. Grants during 1973 and 1974 was invaluable, and deeply appreciated.

CONTENTS

CHAPTER THREE

CHAPTER FOUR

CHAPTER FIVE

CHAPTER SIX

CHAPTER SEVEN

Appendix A

A1 General Radio Astronomy Theory:

Brightness-, Spin-, and Kinetic-temperatures

A2 Derivation of equation 4.10

Appendix B

B2, B.3, B.4, B.5 & B.6: Supplementary figures

Bibliography

Supplementary Bibliography

ABSTRACT

This thesis describes the properties of interstellar water maser sources, and other sources near 22 GHz. Calculations based on manufacturer's specifications of the 22 GHz mixer, which was to be used in a water radiometer, and on the size of the proposed antenna ~~apeture~~ aperture, show the viability of constructing such a radiometer for spectral line and continuum work. Various sections of the radiometer were constructed, including the Cassegrain feed system and its support, an intermediate frequency amplifier and buffer, a timing control unit, and a data processor. These units are part of the radiometer, which is almost ready for observations of sources.

CHAPTER I

WATER MASER AND OTHER ASTRONOMICAL SOURCES AT 22 GHz

1.1 Historical background

1.2 The discovery of water sources and the need for further study

1.3 Water masers : occurrence and properties

- 1.3a Late sequence stars
- 1.3b Early main sequence stars
- 1.3c Other objects possibly associated with H_2O masers

1.4 Summary of the possible uses of a 22 GHz telescope

- 1.4a Spectral lines near 22 GHz
- 1.4b Continuum sources at 22 GHz

CHAPTER I

WATER MASERS AND OTHER ASTRONOMICAL SOURCES AT 22 GHz

1.1 Historical Background

The theory that the solar system is heliocentric - first proposed by Aristarchus in the second century B.C., and subsequently rediscovered by Copernicus seventeen centuries later - was the first major breakthrough in man's understanding of the universe. A breakthrough as important as the first was heralded by the reception and identification of radio noise from extraterrestrial sources by Jansky in 1931.

This breakthrough is the opportunity to study the universe with radiation in parts of the electromagnetic spectrum other than the 'optical window'. The subsequent study of the universe with optical- and radio- wavelength techniques together has yielded a vast amount of information on stars, interstellar matter, and galaxies.

The discovery of interstellar line emission from the hydroxyl radical at 1665 MHz and 1667 MHz by Weinreb startled many people (Dieter 1963, 1966, Kerr 1968). This discovery wasn't altogether unexpected, for Merril had discovered two diffuse interstellar lines optically in 1934, which Swings in 1937 attributed to CO_2 bands (McNally 1968). Townes later (1957) listed about thirty simple molecules which might be detected in the interstellar medium by their microwave rotational-level transitions.

OH was one of these 'molecules' which, after its initial discovery in absorption, was discovered in emission in several H II (ionised hydrogen) regions by Weaver in 1965.

This discovery sparked off a series of microwave frequency line studies of interstellar clouds. In 1968 and 1969, the discovery and analysis of interstellar microwave transitions of ammonia, water, and formaldehyde (Litvak 1972) - of which the former two were also predicted by Townes (1957) - indicated that a wealth of new interstellar molecules awaited discovery and that thermal equilibrium of the molecules concerned was hardly likely in many cases. Maser action was proposed to account for the non-thermal behaviour.

Up to the present 36 interstellar molecules have been discovered; about 30 of these since 1969 (Snyder 1970a, 1970b).

In this thesis the design of a telescope suitable for studying the water microwave sources at 22 GHz is described. The rest of this chapter is devoted to a description of these sources, with emphasis on those features which affected the telescope design.

1.2 The discovery of water sources and the need for further study

The discovery of water vapour emission at 22,235 GHz was made by Cheung et al (1969) in Sgr. B2, Orion A, and W 49 with the Hat Creek 20 ft. parabolic antenna. They excluded the 22,234 GHz ammonia inversion transition as a possible explanation of the line.

Since this discovery, water has been found in more than 50 sources, most of which occur in the galactic plane, especially towards the galactic center. Figure 1.1 (Johnston 1972b) shows the water sources known in 1972, and indicates that they are associated with two types of object, as shown in extensive surveys by American and Australian astronomers.

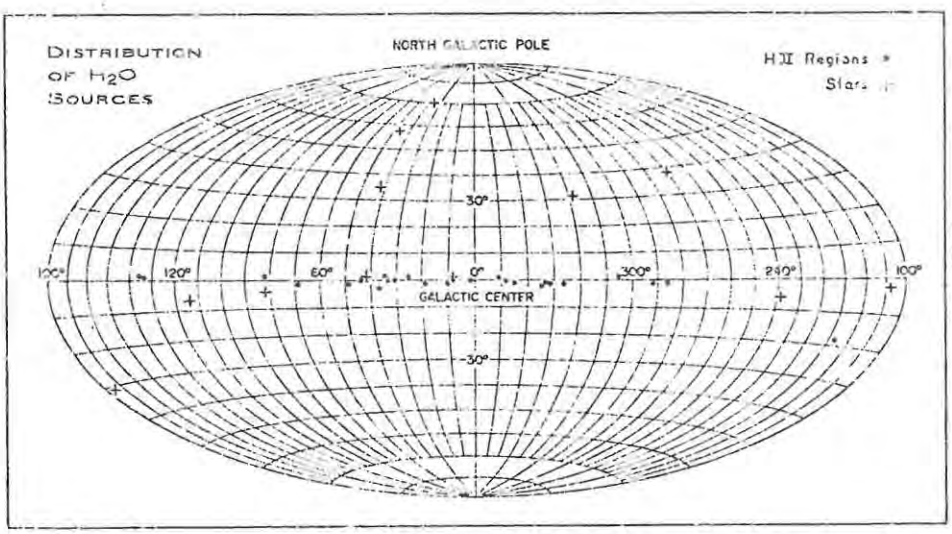

Figure 1.1. Map of the entire sky showing celestial sources of water radiation known before 1972. Sources associated with interstellar clouds are concentrated towards the galactic equator (horizontal diameter) (Johnston 1972b).

The first type, consisting of OH emission sources linked to H II regions, are interstellar clouds which lie very close to the galactic plane, and are presumably young Population 1 objects. The other sources of H_2O radiation are cool, late M-type stars, which have greater dispersion in galactic latitude, indicating that they are older Population 1. Figure 1.2 shows a plan view of the distribution of water sources in the galaxy (Johnston 1973).

The observed microwave transition of water corresponds to the $6_{16} - 5_{23}$ transition, the numbers 5 and 6 defining the angular momentum. The first subscript refers to the average projection of the angular momentum along the axis of the least moment of inertia, the second is that along the axis of the greatest moment of inertia (Burke 1969). The reference frequency, the mean of the frequencies of the hyperfine components weighted by their L.T.E. (local thermodynamic equilibrium) intensities, is 22 235,07986 MHz (Moran 1973).

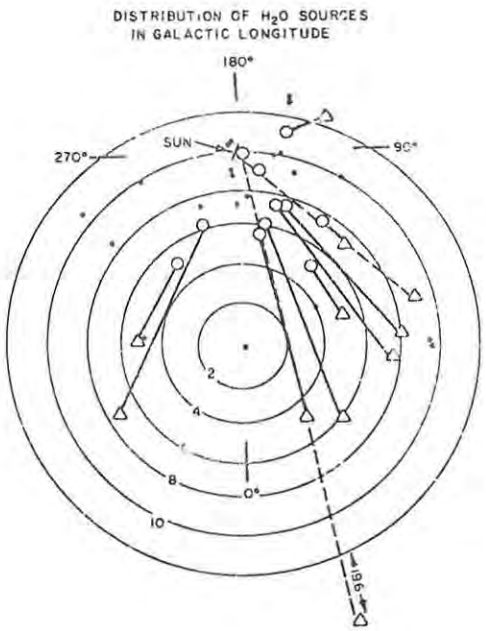

Figure 1.2 Distribution of H_2O sources in galactic longitude. Filled circles denote sources having known distances. Open circles and triangles denote the possible distance limits of sources with uncertain distances (Johnston 1973).

Apart from surveys of hydrogen, systematic surveys of large areas around the galactic plane have been made only for the "molecules" OH (at wavelengths of 18 cm) and H_2CO (at wavelengths of 6 cm) (Wickrama-singhe 1972). Because both lines are seen predominantly in absorption against galactic continuum sources, the results may be biased. In the case of H_2O surveys, the results are biased, for water has been sought only in localised sources such as dark clouds, I.R. (infra-red) objects, late M-type stars, and OH sources, and many of these observations have been done in the Northern Hemisphere only. An unbiased, full-sky survey of H_2O sources is thus needed to supplement existing data, and the equipment described in this thesis was constructed to that end. So far, all the information on H_2O masers indicates that they are associated with star formation (in H II regions) and decay (if the late M-type stars are in fact late main sequence stars). Hence it would seem that further knowledge of H_2O sources is essential to our understanding of stars.

1.3 Water Masers : Occurrence and Properties

As already mentioned, water maser observations are associated with two types of object, late - sequence - type stars, and early main - sequence stars. Since the radiometer was to be built to study mainly these water sources, a thorough knowledge of the characteristics and occurrence of these two types of object was highly desirable. ~~Having calculated the~~ Once the sensitivity of the proposed radiometer had been calculated, the feasibility of studying the water masers could be estimated. This feasibility study is discussed in chapter II. This information would, further, influence the design of the 100-channel receiver, and provide a starting-point for water maser searches. Sections 1.3a and 1.3b deal with these two types of object, and the properties of the masers associated with them. In section 1.3c the association of water masers with supernova remnants and globular clusters, which has been proposed by some workers in the field, is discussed.

1.3a Late Sequence Stars

The ~~late-~~sequence ~~type~~ stars, late-type main, with which water masers are associated, all show 18 cm wavelength hydroxyl-radical maser emission. More than 50 late-sequence type stars exhibit OH maser emission. These oxygen-rich, late M-type stars have photospheric temperatures of about 2 000 K. Some of them have large excess radiations at 5 μm and 10 μm (Neugebauer 1971) due to circumstellar gas clouds. Of these 50 stars, ~~more than~~ at least 19 have H_2O masers. These 19 stars have been divided into two groups (Wilson 1973, Winnberg 1973) depending on their OH emission characteristics (Raimond 1969, Kerr 1968). The first group consists of Mira Ceti type variables for which the OH emission is strongest in the two main lines at 1665 MHz and 1667 MHz (Dieter 1966). These variables do not show a large 10 micron I.R. excess above the radiation predicted ~~by~~ from the photospheric temperature (Goss 1973, Wilson 1972), as opposed to the second class. The second class of OH/I.R. star, the Supergiant group, consists of three stars, VY C.Ma., VX Sgr., and NML Cyg. (Herbig 1970, Hyland 1970, Wilson 1970, 1973).

The 1612 MHz OH emission of these irregular variables isn't highly polarised, as opposed to the significantly polarised 'main line' emission at 1665 MHz and 1667 MHz, which is also weaker than the 1612 MHz emission in this case.

Both these types of water sources exhibit brightness temperatures of up to 10^{10} K. (The concepts of brightness temperature and flux density are discussed in appendix A.) Litvak (1969) derived cloud lengths of 2×10^{15} cm and hydrogen densities of about 10^{9} cm^{-3} with kinetic temperatures of 100-1 000 K at a radius of 3×10^{15} cm (in the outer stellar atmosphere) for these sources. Excitation of both OH and H_2O is probably caused by I.R. pumping (Johnson 1966, Wallerstein 1971).

The OH/I.R. stars are typically less than the 18th magnitude visually, and the maximum in the H_2O emission corresponds with the maximum light (Dickinson 1973, Johnston 1972b). Cohen (1973) notes that there is an anticorrelation between the visible and the I.R. maxima. The correlations, shown in figure 1.3 for the H_2O and I.R. emission, could more easily be studied by a small telescope than by a large instrument, which is too expensive to allow it to be used to observe variable sources for long periods. Long integration times will, however, be necessary to make up for the lack of collecting area.

1.3b Early Main Sequence Stars

This type of H_2O maser source is located in or near H II regions where protostars and young T Tauri type stars are forming. These young massive stars are surrounded by dust "cocoons" having temperatures typically lower than 100 K (Solomon 1973), with radii of the order of 10^{17} cm. They are often associated with radio continuum (spatial) peaks due to enhanced electron densities. (These electrons produce continuum radiation by free-free emission). Several reviews on these objects have appeared recently (Knowles 1969a, b, Litvak 1969, Heiles 1971, Bok 1972, Henderson 1972,

Wickramasinghe 1972, Buhl 1973, Larson 1973, Turner 1973, Sullivan 1973).

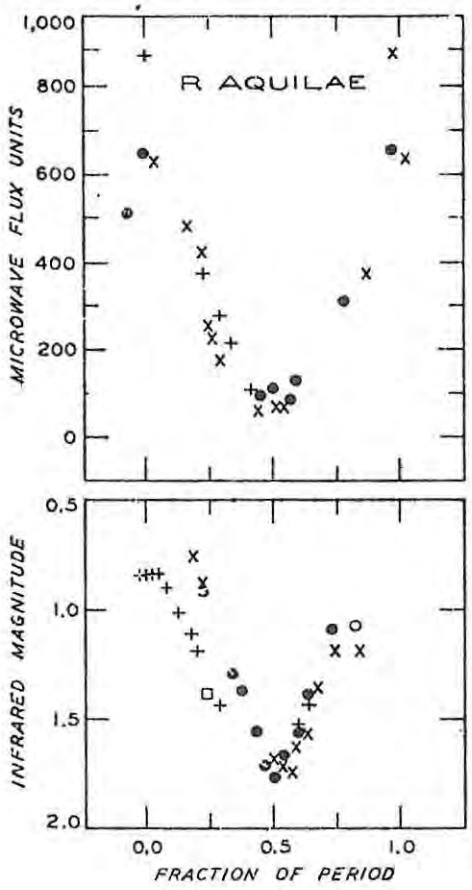

Figure 1.3 : The H_2O emission of the Mira-type variable star R Aquilae (top frame) changes in much the same manner as the infrared magnitude measured at a wavelength of 1,04 microns. Similar large variations have been observed for the Supergiant NML Cyg. (Moran 1973). Davies (1972) and Wallerstein (1973) give kinematical models for NML Cyg.

The dust cocoons surrounding the protostars or protostar clusters are surrounded by or close to H II regions, and radio condensations where "interstellar" organic molecular emission originates. The H_2O sources, located frequently <u>in</u> collapsing protostars, are generally a hundred times brighter than the late-sequence type star sources often with brightness temperatures of over 10^{15} K. This value corresponds to a flux density of 30 000 f.u. for a feature in W49 which has a diameter of 4,5 astronomical units. (The actual masering region is up to 200 times the observed dimension, as one observes "hot spots" of the maser (Litvak 1971,1973)).

Figure 1.4 shows the relative flux densities of the thirty seven known H_2O sources in H II regions. All of these are associated with type I OH emission sources - for which the

two main-lines at 18 cm are the most intense.

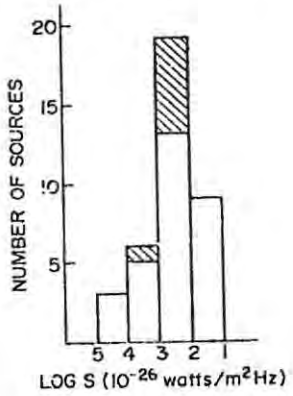

Figure 1.4 (Johnston 1973) : Histograms of the flux S of all known H_2O sources associated with H II regions. The crosshatched areas are for sources found in Johnston's southern hemisphere survey (Johnston 1972a).

The protostars are probably formed from dense gas clouds of 1 000 $M_\odot$ to 30 $M_\odot$ (Robinson 1973) in the shock fronts accompanying the galactic spiral waves of Shu et al (1970a, b, 1972). This process is discussed by Parker (1966), and Field (1970b). Once the O-stars reach the M.S. (main sequence) they ionise the remnant of the protocluster and star formation in this subgroup comes to a halt. This remnant appears to be tightly packed around the O-stars in the form of a shell or cocoon, and the ionised gas is therefore first observed as a very compact H II region of high density, which subsequently rapidly expands.

It has been confirmed that in W3, W49, and W51 the H_2O and OH sources are close to, but not always coincident with, the other molecular and continuum sources and I.R. objects. In some cases, however, the H_2O sources are clearly separated from the compact H II regions (Hills 1972, Emerson 1973, Moran 1973), and OH sources (Mezger 1971, Johnston 1973).

Figure 1.5 (Johnston 1972) shows a typical low spatial-resolution H_2O spectrum - in this case of the Orion Nebula.

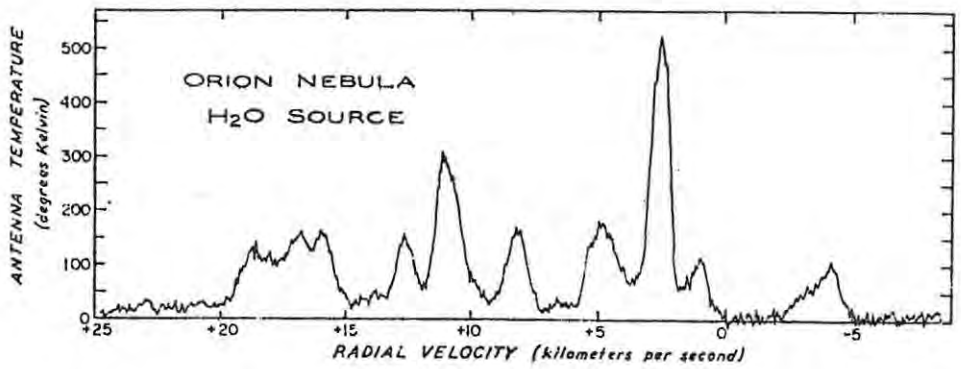

Figure 1.5 : The H_2O radiation source in the Orion nebula is highly complex in structure. As this spectrum shows, its microwave line of 1,35 centimeters wavelength consists of at least eight discrete peaks, each indicating a separate source with its own radial velocity.

Very long baseline interferometry has to be used to resolve individual sources which are small and packed close to each other. (Angular diameters of 0,000 3" have been measured, and 12 separate sources appear in an angular area of two square seconds in W49)

It would be useful to conduct variability studies of the known H_2O sources, which all exhibit ~~complitude~~ complicated variations over different periods of time (Buhl 1969, Becklin 1973). For example, a feature of 3 160 f.u. was discovered in M17 in 1973 where in 1971 no H_2O had been detected above 200 f.u. On the other hand a feature in Orion B dropped to half ~~it's~~ its intensity in three days in 1972. (Johnson 1972). Other possible candidates for H_2O searches have been mentioned. These are discussed below.

1.3c Other objects possibly associated with H_2O masers.

H_2O and OH sources have been associated by some authors with supernova remnants (Litvak 1973, Gardner 1972). However, some OH and H_2O regions have recently been reclassified from "supernova" classification to "H II regions" (Caswell, 1972). Litvak classes the three supergiant late-type stars discussed earlier as supernova remnants, but these are regarded by many

other workers as late-M type stars, which are red supergiants. However, supernova remnants are usually white dwarfs surrounded by expanding nebulae. There is thus some doubt attached to the association of H_2O with these objects.

Globular clusters and extreme population II objects have previously been searched for OH and H_2O masers. Each cluster contains about ten variable metal-deficient red giants. Poor H_2O and OH abundances are, however, expected for these objects because of the poor heavy element abundances. Knapp (1973b) gives a few exceptions which are too southerly for observations from Maryland and which could be searched from Grahamstown. White (1970) lists colour-magnitude diagrams for these objects, which would aid searchers for them.

Many theories have been proposed to account for the existance of the many molecules, including H_2O, in the hostile conditions in interstellar "space". It is probable that one or more of the mechanisms of Aanestad (1973b), Watson (1973), Brown (1973), Dalgarno (1973), or Williams (1971) operate to produce the molecules, but the position is still confused. Pumping mechanisms to explain the H_2O maser line in the regions of occurrence of these molecules have been investigated by Dickinson (1970), Johnston (1973), Gwinn (1973), Knapp (1973), Litvak (1969a, 1972, 1973a, 1973b), and others.

1.4 Summary of the possible uses for a 22 GHz telescope.

From the foregoing discussion of the occurrence and properties of water masers, it can be seen that a telescope operating at 22 GHz could usefully be used to study the variability of the H_2O masers, and to survey selected objects for H_2O masers. Suitable objects to survey include known Southern Hemisphere H II regions (Gardner 1968), radio condensations, globular clusters (Knapp 1973b), infrared objects (Schwartz 1970), OH emitters (Turner 1970), and Mira variables showing H_2O absorption

(Spinrad 1965). In addition, an unselective (full sky) survey could probably be undertaken with reasonable sensitivity in a period of about 12 months, because of the large beamwidth of the proposed telescope.

However, other uses for a small telescope will further increase its viability, and greatly strengthened the motivation for its construction. These other uses include the study of other spectral lines near 22 GHz, and of continuum sources, mostly free-free electron transition sources and thermally radiating sources. The properties of the other sources near 22 GHz, besides H_2O masers, are surveyed briefly in this section. The feasibility of studying such sources with a small telescope will be demonstrated in chapter II.

1.4a Spectral lines near 22 GHz.

Four molecules have been detected by their emission in lines close to 22 GHz. Ammonia, the most abundant of these, was discovered by Cheung et al. (1968) in a few sources in the interstellar medium at 23,7 GHz. It has since been found in numerous sources in absorption (Mayer 1973, Mezger 1972, 1973, Foley 1973) and in emission in ten sources, at seven frequencies - from 23,7 GHz to 25,1 GHz (Barret 1969).

Methyl alcohol has been discovered in four sources at 25,3 GHz (Litvak 1973); a weak Q-branch has been discovered at 26,3 GHz (Lees 1972). Isocyanic acid whose microwave spectrum is given by Hocking (1972), was discovered in SgrB2 by Buhl (1972), at 21,9 GHz. He worked out an excitation temperature of 12,8 K for this observed cloud. The last of these molecules, found in emission in two sources, is cyanoacetylene (Dickinson 1972). It was discovered by Snyder (1972) at 18,2 GHz with a flux density of 7 f.u. in SgrB2.

There are other simple molecules which would be expected in reasonable quantities in molecular clouds, but which have not yet

been found. Meeks (1969) failed to detect one of these, HDO, at 22,3 GHz corresponding to the $S_{32} - S_{33}$ transition. He put an upper limit on the intensity of 1/1000 that of H_2O sources. Two other important molecular lines are those of glycaldehyde at 23,4 GHz (Brown 1973), and of N_2O at 25,1 GHz (Townes 1957). These too have not been found.

It will be shown in chapter II that the proposed telescope would probably be too insensitive to detect the above lines - but a few searches for them might still yield fruitful results. It will also be shown, however, that many continuum sources could be meaningfully studied.

1.4b Continuum Sources at 22 GHz

There are a large number of interesting radio objects which could be studied at 22 GHz. The need for studying objects such as the Crab Nebula (Matveenko 1972, 1973), ~~Saggitarius~~ Sagittarius A (Jones 1973), and other sources at 'high' frequencies (above 10 GHz) has been pointed out by many authors. Continuum studies would be started on sources listed in the many available cataloques (Baars 1965, Kraus 1966, Blake 1970, Wynn-Williams 1970, Kurichik 1972, Jones 1973, and Strull 1973). Suitable sources for study are those which have reasonably flat spectra and high fluxes at the lower frequencies. As will be seen in chapter II, the solar system contains seven microwave sources powerful enough to be detected by the proposed equipment. These are discussed briefly in order of their decreasing ease of detection. The first of these is the sun.

The sun's emission at 22 GHz consists of a slowly varying component (Steinberg 1963) superimposed on a background with an equivalent temperature of $1,3 \times 10^4$ K (Harvey 1963). In addition solar flares of 10^6 f.u. to 10^7 f.u. have been observed (Bhatia 1970, Fürst 1971). The next most easily detectable body in our solar system at 22 GHz is the moon, which has a large phase-variation between 200 K ~~to~~ and 270 K (Steinberg 1963, Hey 1971) in its equivalent temperature.

The centimeter wavelength radiation from the planets has been extensively studied and is the subject of reviews by Barber (1963), Steinberg (1963), Harvey (1963), Gulkis (1973), and Newburn and Gulkis (1973). Venus is the most easily detectable planet (excluding the earth!) at 22 GHz. Its microwave spectrum is interesting in that it is enhanced at 22, 23 GHz by its atmospheric water (Barret 1970, Jones 1972), and exhibits intensity phase-variations at 10 Ghz but not at 15 GHz (Morrison 1969). The other planets which could be detected are mentioned in chapter II.

CHAPTER 2

THE 22 GHz RADIOMETER

CHAPTER II

THE 22 GHz RADIOMETER

The radiometer described in this thesis incorporates an equatorially mounted parabolic dish antenna as the main reflector of a Cassegrain feed system, the design of which is detailed in chapter III. The received signal is fed directly to a low-noise Schottky-barrier diode mixer (Irvin 1969, Elder 1969), as no cheap low noise amplifiers exist for 22 GHz. An electrically tunable Gunn-effect diode oscillator serves as the local oscillator. An i.f. (intermediate frequency) preamplifier, which has a bandwidth of 110 MHz and a gain of 35 dB, is matched directly to the mixer to reduce noise. The receiver section following the high-frequency 'front-end' and this preamplifier consists of two separate receivers. These are the continuum receiver with a bandwidth of 110 MHz, and the spectral line receiver, consisting initially of 50 narrowband amplifier channels. The spectral line receiver will eventually contain 100 such contiguous bandpass channels with bandwidths of 50 KHz each, typical of many spectral line water radiometers (Balister 1968, Sarma 1972, Henderson 1972). In this chapter the major factors influencing the radiometer design are discussed, including the receiver stability and sensitivity.

2.1 The theory of noise and radiometer sensitivity

The signal being investigated by radiometers is invariably buried in noise signals from background sources and from the receiver. A short summary of the concepts involved follows. (A more detailed treatment is given in Kraus 1966).

A resistor at a temperature To will deliver to a matched load a noise power W_G, given by the Nyquist formula for Johnson noise.

$$W_G = k\ To\ B \qquad 2.1$$

where k is Boltzmann's constant, and B is the bandwidth of the instrument measuring W_G. The 'noise temperature' T of an amplifier with gain G and bandwidth B is defined analogously by

$$W_N = G\ k\ T\ B \qquad 2.2$$

where W_N in this case is the exchangeable output noise power of the amplifier due to its noise sources, usually contributed mainly by the first high gain stage and the noise source at its input. The amplifier noise figure F is defined by

$$F = 1 + T/To \qquad 2.3$$

where To is the ambient temperature. The corresponding noise temperature T of an attenuator, with a loss L and at a temperature To, is

$$T = (t\ L - 1)To. \qquad 2.4$$

The factor t is 1 for passive attenuators. Its value lies between one and two for modern mixers (or active attenuators), and in this case L is the conversion loss of the mixer.

The total 'antenna temperature' T_A is composed of two parts; T_{sky} is the contribution to the antenna noise temperature due to background sky noise entering the antenna sidelobes, while Tu is the contribution due to the source being investigated in the antenna main beam. The background 'sky' noise comprises the extended galactic background radiation, the atmospheric contribution due to the radiation by the atmosphere at a temperature of about 0^oC (figure 2.2), and the small contribution from the ground radiation which leaks into the sidelobes. The atmospheric radiation introduces an equivalent noise temperature of about 50 K for well designed Cassegrain systems, and is the main contributor to T_{sky}. The antenna noise temperature T_A is also defined in terms of the

Nyquist formula,

$$T_A = T_{sky} + T_u = W/kB \qquad 2.5$$

where k is Boltzmann's constant, and W is the total power received in bandwidth B. The antenna temperature due to the source, T_u, can be expressed in terms of the source temperature T_s, if the Rayleigh-Jeans law holds (see appendix A),

$$T_u = \frac{1}{\Omega_A} \int_{\Omega \text{ source}} T_s (\theta, \psi) P_{n\nu} (\theta, \psi) d\Omega, \qquad 2.6$$

where Ω_A is the antenna main-lobe solid angle, and $P_{n\nu}$ is the normalised power pattern of the antenna. The value of T_u is usually much less than that of T_{sky}, and is neglected in calculations involving T_A. The radiometer system temperature is given by

$$T_{system} = T_A + (L-1)T_o + L\, T_R \qquad 2.7$$

where L is the loss factor of the transmission line between the horn and the mixer, and T_o is its temperature. T_R is the noise temperature of the receiver, and is determined almost entirely by the mixer-preamplifier combination.

The minimum detectable signal ΔT_{min} of the radiometer is defined to be the signal noise temperature ΔT_u which produces a receiver d.c. output power equal to the total d.c. noise output power, which is due to the noise temperature contribution given by T_{system} in equation 2.7, and

$$\Delta T_{min} = K_s\, T_{system}/(\Delta \nu \tau)^{\frac{1}{2}} \qquad 2.8$$

K_s is the sensitivity constant of the receiver (Kraus p 258) $\Delta \nu$ is the predetection equivalent bandwidth (Kraus p 245), and τ is the postdetection integration time. The integration time is limited by the receiver stability, and may be increased by adding records of successive integration periods. The minimum detectable flux density (appendix A), Δ Smin,

derived from equation 2.8.

$$\Delta S \text{ min} = 2k \Delta T\text{min}/Ae. \qquad 2.9$$

Ae is the effective aperture area of the antenna, and is usually about 50% to 70% of the physical ~~apeture~~ aperture area.

2.2 The receiver stability and stabilisation by modulation methods

Low frequency gain instabilities inherent in all radiometers (Colvin 1961) stop them from attaining the sensitivity given by equation 2.8, unless the receivers are modulated. In modulation receivers the input is switched at a low audio-frequency alternately to a reference source and to the antenna signal being measured. The difference in power between the unknown and reference sources appears as a modulation on the detected output of the receiver, and may be converted to a d.c. signal by synchronous rectification. The output d.c. level will be proportional to the difference in power between the unknown and reference signals, if the receiver detector is a square-law device.

The square wave modulation technique is depicted in figure 2.1. The power levels of the input signals may be

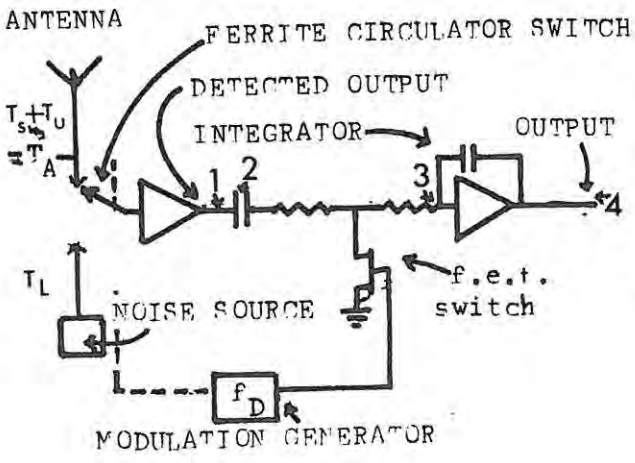

Figure 2.1a Modulated Receiver

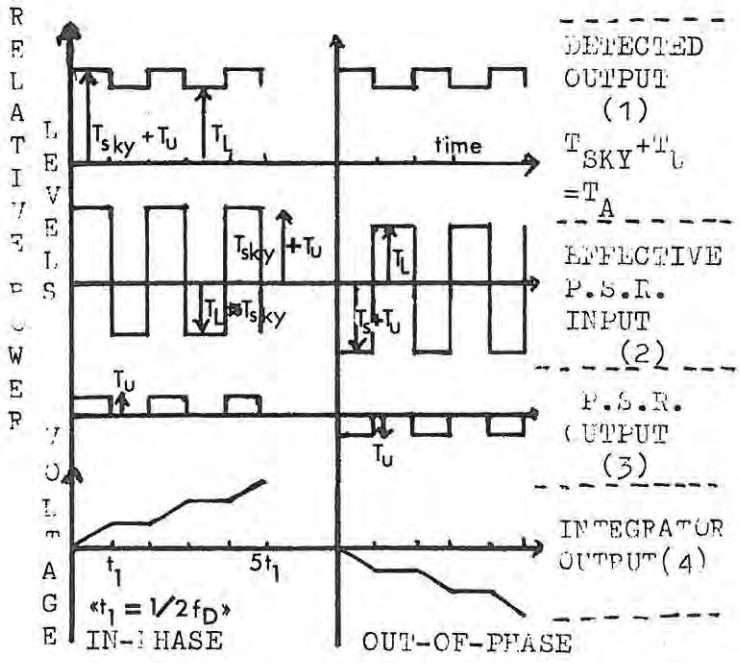

Figure 2.1b Phase-sensitive Rectification

defined in terms of noise temperatures, as was seen in the last section. The source signal being investigated, with noise temperature T_u, is always buried in the antenna noise temperature T_A. The receiver input is switched between the antenna with noise temperature T_A, and the reference source with noise temperature T_L, which is made as close to T_A as possible. After amplification and square-law detection the signals from the front-end are fed to the phase sensitive rectifier (p.s.r.). This rectifier is controlled by a field effect transistor (fet) which is switched at a frequency f_D by the modulator. When the front-end and the p.s.r. are switched in phase, the effect of the phase sensitive rectification is to subtract the signal due to T_L from that due to T_A resulting in the integrator output being proportional to the unknown source noise temperature T_u. The receiver noise T_R is added to both signals, and so is also subtracted out in the phase sensitive rectifier. Out of phase switching results in a negative output voltage of the same magnitude, as shown in figure 2.1b. If the modulation frequency f_D is greater than the ~~low~~ frequency of the gain instabilities, then their effect, which is random, is minimised (Kraus 1966, Kuz'min 1966). The sensitivity constant K_s in equation 2.8 is '2' for square wave modulation.

For stabilisation purposes the reference noise source may be a gas discharge tube, in which case the radiometer is a standard 'Dicke' type. Beam switching, on the other hand, involves switching the input between two horns in the Cassegrain focal plane; the one directs the antenna beam at the source, the other directs it at a slightly offset sky region which acts as the reference (Baars 1966, 1970, Conway 1963). This method can only be used for small sources, and will only be introduced into the radiometer when the rest of the system is fully operational. The third method of switching, 'frequency switching', is used only for spectral line work. The local oscillator frequency is switched so that the receiver is tuned alternately to the water spectral line frequency, and to a nearby frequency where no spectral lines are likely to occur. Precautions are taken to ensure that the receiver image channel never

receives spectral line emission. The comparison noise source in this case is the continuum background radiation, and since the signal and reference noise paths are exactly the same, excellent stability results. The radiation from the earths atmosphere is

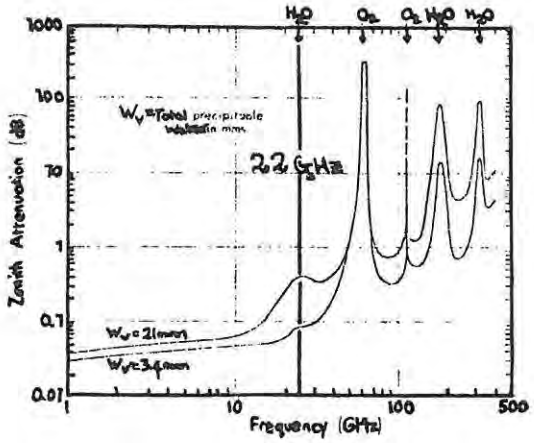

Figure 2.2. Total Atmospheric Absorption (Findlay 1971)

related to the attenuation it produces by equation 2.4. The 22 GHz atmospheric water emission line is pressure-broadened, and it can be seen from figure 2.2. that if frequency switching of 100 MHz is employed, the attenuation-change will be less than one percent. Combinations of the switching methods have recently been used by Albaugh (1968) and Dolan (1970).

2.3 Sensitivity of the proposed telescope

Before the minimum detectable flux density can be evaluated from equation 2.9, the system temperature T_{system} must be evaluated from equation 2.7.

It has already been noted that the antenna noise temperature due to the sky background, T_{sky}, is around 50 K for Cassegrain telescopes at 22 GHz. This will be the value assumed for the telescope as it is independent of ~~apeture~~ aperture size. The second and third terms on the right hand side of equation 2.7 depend on the transmission line loss. The loss factor is 0,14 dB for the estimated length of 22 cm for the waveguide to the mixer (Benson 1969), plus an estimated loss of 0,1 dB for the three joins in

this waveguide (Harvey 1963). The total loss factor L is thus 0.24 dB, or (if not expressed in dB) 1,057. The double channel noise figure for the mixer - i.f. preamplifier combination which has been acquired is 4.4 dB, or 2,75 when expressed linearly. The receiver noise temperature T_R is determined by this noise figure, and is given from equation 2.3 as

$$T_R = (F-1)\, T_o = 509 \text{ K}, \qquad 2.10$$

if an ambient temperature T_o of 290 K is assumed. The effective noise temperature of the receiver when it is used for spectral line work is double this value, as only one channel is used (Harvey 1963, Kraus 1966). The system temperature given by equation 2.7 can now be evaluated for double channel (continuum) and single channel (spectral line) work, and

$$T_{system} = T_{sky} + (L-1)\, T_o + L\, T_R$$

$$= 604 \text{ K and } 1084 \text{ K respectively.} \qquad 2.11$$

The modulation technique of receiver stabilisation could conceivably allow total integration times of an hour or more, but these times are limited by integrator drift. However, the addition of successive records could result in effective integration times of many hours. The minimum detectable flux is evaluated from equation 2.8 and ~~2.29~~ 2.9 assuming an integration time of 10 hours, using equation 2.11 for the system temperature, and assuming a sensitivity constant K_s of 2. The values of the minimum detectable flux for the continuum work and for the spectral line work are given by

$$\Delta S_{min} \; (\Delta\nu = 110 \text{ MHz}, \tau = 10 \text{ hours}) = 1{,}05 \text{ f.u.} \qquad 2.12$$

$$\Delta S_{min} \; (\Delta\nu = 50 \text{ KHz}, \tau = 10 \text{ hours}) = 99 \text{ f.u.} \qquad 2.13$$

respectively. The efficiency of the 1,83 m diameter ~~apeture~~ aperture was assumed to be 60%. However, this calculation assumes that the

contribution to the noise figure of the receiver section following the intermediate-frequency preamplifier is negligible.

2.4 Spectral line studies and sky surveys

The minimum detectable flux density for spectral line work is 99 f.u. for an integration time of 10 hours. From figure 1.4 it can easily be shown that about 75 percent of the known water masers would be above the detection limit of the telescope, making it very useful for variability studies of these sources.

However, the other molecules mentioned, whose emission lines occur close to 22 GHz, would probably all be undetectable. Not only are the known sources below the detectable threshold of 99 f.u., but also this threshold is considerably higher at frequencies different from 22 GHz, as the mixer double channel noise figure rises from 4,4 dB at 22 GHz to 6,5 dB at 24 GHz and 18 GHz.

Before the detection limit attainable in a rapid sky survey can be evaluated, the antenna half-power beamwidth (H.P.B.W.) must be known. The H.P.B.W. can be minimised by illuminating the parabolic dish uniformly - this maximises the antenna gain, as will be shown later. (The sidelobes are increased at the same time, but as they are directed at the sky they don't contribute much to the antenna noise temperature). In this case (Harvey 1963)

$$1{,}02\ \lambda/D \lesssim \text{HPBW} < 1{,}20\ \lambda/D, \qquad 2.14$$

where λ is the wavelength (1,35 cm) and D the ~~apeture~~ aperture diameter (1,83 m for the paraboloids which had been bought). Thus

$$26' < \text{HPBW} < 30' \qquad 2.15$$

The beam area is given by

$$\Omega_A = (\text{HPBW})^2 / \varepsilon \qquad 2.16$$

where ε, the beam efficiency, is usually 0,75 (Kraus 1966). The expected beam area corresponding to the pessimistic value of the HPBW (30') is thus

$$\Omega_A = 10{,}3 \times 10^5 \text{ rad}^2 = 0{,}33 \text{ deg}^2 \qquad 2.17$$

As mentioned previously, the radiometer will eventually have 100 50 KHz channels. The Doppler velocity range covered with this resolution is 68 km s^{-1} (from equation 1.5). Provided that the central frequency of the receiver is placed at the frequencies corresponding to the most probable Doppler shifts for the region being searched, this coverage of $\pm$ 34 km s^{-1} should suffice for the survey.

If a year say is spent on a full sky survey, the integration time available per search grid point is

$$\tau = (t_{survey} \times \Omega_A)/\Omega_{sky}. \qquad 2.18$$

Antennas are seldom directed below about 25^o above the horizon, and are usually unable to point below 15^o above the horizon. If the latter figure is taken as an extreme limit, then figure 2.3 shows the radio sky visible from Grahamstown (at a lattitude of 33^o 19' South). (It will be noticed that the galactic centre region $\ell_{II} = b_{II} = 0$ which is thought to comprise a vast molecular cloud, and which contains many H_2O sources, passes almost directly overhead.) The sky area visible from Grahamstown is thus

$$\Omega_{sky} = \int_{90^o\ S}^{41^o\ 41'\ N} 2\pi \cos\theta \, d\theta = 10{,}46 \text{ ster.} \qquad 2.19$$

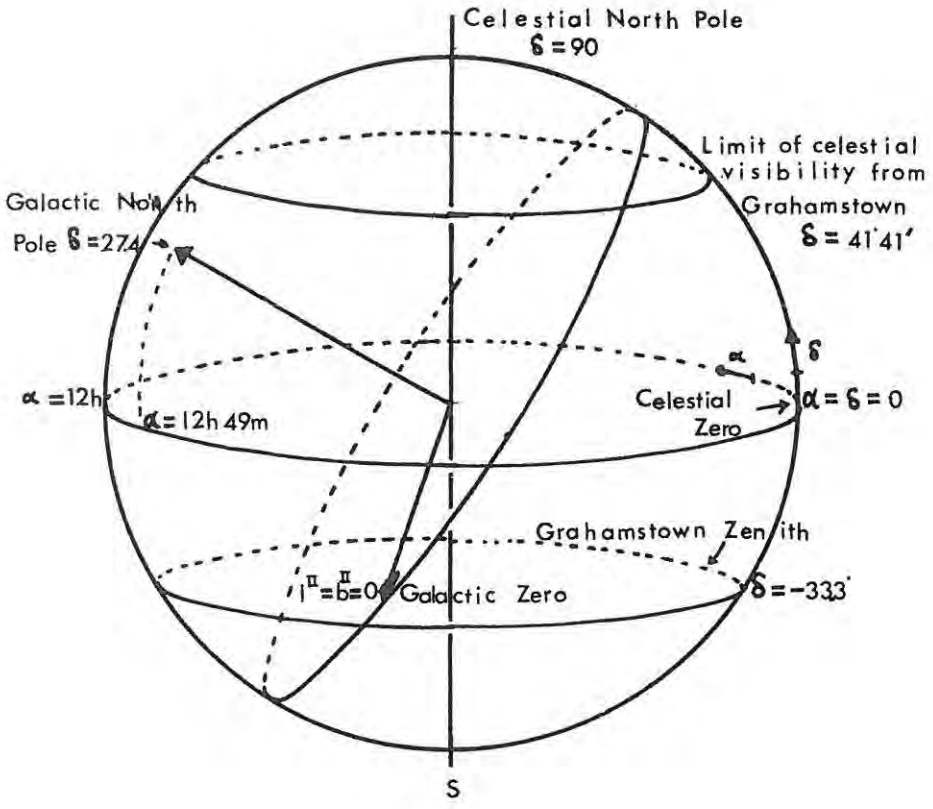

Figure 2.3 Celestial and Galactic Coordinates

Equation 2.21 to 2.23 can be used to find the integration time per search point:

$$\tau = 310 \text{ seconds} \qquad 2.20$$

The corresponding sensitivity is

$$\Delta S \text{ min, survey} = 1050 \text{ f.u.} \qquad 2.21$$

Figure 1.4 shows that a survey with this detection limit would 'pick up' about 16 percent of all known water sources associated with H_{II} regions.

Previous surveys from the northern hemisphere have been conducted with a sensitivity of 20 f.u. The only survey from the southern hemisphere was conducted at Parkes, Australia, to a limit of 125 f.u., in which 5 new sources were found (Johnston 1971, 1972). However, as has been mentioned, these surveys were conducted by searching late M-type stars, H_{II} regions etc. The proposed search would be unselective and still have a good chance of locating new sources in a short time (see also Rudnitskii 1973). This probability is further increased by the knowledge that many H_{II} regions which haven't been discovered in optical surveys are being discovered all the time (Grasdalen 1973). A higher sensitivity could be achieved by spending more time surveying the galactic plane only where the probability of detecting sources is greatest.

There are only two radiometers in the southern hemisphere capable of working at 22 GHz, the Parkes dish in Australia, and the McKenzie University dish in Brazil. The Parkes dish centre section (diameter 32m), which has an ~~apeture~~ aperture efficiency of 14% and a beamwidth of 1,6 arc minutes at 22 GHz, was used to search for water masers in 1972 (Johnston 1972a). The mixer used had a single sideband noise temperature of 3200 K, and 64 channels with bandwidths of 33 KHz were used, corresponding to a radial velocity search range of only 28 kms^{-1}. If the Parkes dish were to be used for an unselective full sky survey with a detection limit of 1156 f.u. (equation 2.21), and for a range of about 60 kms^{-1}, it would need 19 years of full-time observation to do so! This is obviously completely impracticable for a large telescope, which in any case is in demand for other studies.

2.5 Continuum studies and a sky survey

If a power splitter is used to simultaneously feed the spectral-line and continuum receivers, the latter receiver could be used during the full sky survey. ~~It's~~ Its corresponding sensitivity would be (from sections 2.3 and 2.4)

$$T_u = \Omega_{source}\, T_{b\nu\ source} / \Omega_A \qquad 2.23$$

where $T_{b\nu\ source}$ is the source brightness temperature discussed in appendix A. The received flux S_u, is given by

$$S_u = 2k\, T_u / A_e \qquad 2.24$$

where A_e is the effective antenna ~~apeture~~ aperture. The results of the calculation in equation 2.23 and 2.24 are shown in figure 2.4 for the bodies in the solar system, which are listed in the order of their ease of detection. Seven of these bodies will be detectable; the weakest of these, Saturn, would appear above the detection limit in just 285 seconds (from equation 2.9).

This section has shown the usefulness of a small telescope operating at 22 GHz in the southern hemisphere. In the next section a description of the full system design is given.

2.6 The 22 GHz Radiometer System design

The operation of the 22 GHz radiometer system is described in this section in sufficient detail to put the rest of this thesis in context.

2.6a The receiver section

The design of the Cassegrain feed system, and the antenna- and front-end-mounts was part of the work performed for this thesis, and is detailed in chapter III. Provision was made in the front-end for the three methods of modulation described in section 2.2, as shown in figure 2.5a. The 22 GHz Gunn-diode oscillator was to be frequency-stabilised by phase-locking it to a harmonic of a stable 5 MHz oscillator. Frequency switching of the Gunn-diode would be achieved by frequency switching the 5 MHz oscillator.

Object	Measured Brightness Temperature (k)	at wavelength (cm)	Average solid angle at earth $(deg)^2$	Expected received flux (f.u.)	Reference for Column two
Sun	10^4	1,35	0,22	1,42 $\times 10^6$	Harvey 1963
Moon	230	1,35	0,21	3,06 $\times 10^5$	Hey 1971
Venus	525 $\pm$ 25	2,00	2,4 $\times 10^{-4}$	7,97 $\times 10^2$	Law 1968 Janssen 1972, 1973b.
Jupiter	136 $\pm$ 5	1,35	1,2 $\times 10^{-4}$	1,03 $\times 10^2$	Janssen 1973 Wrixon 1971
	107 $\pm$ 12	1,35		81,6	Law 1968
	139 $\pm$ 6	1,33		106	Newburn 1973
Mars	181 $\pm$ 11	1,35	3,28 $\times 10^{-5}$	37,8	Ingersoll 1971
Mercury	280 $\pm$ 20	1,35	9,6 $\times 10^{-6}$	17,1	Morrison 1970
Saturn	127,2 $\pm$ 5,5	1,35	1,6 $\times 10^{-5}$	13,0	Newburn 1973
Instrument detection limit in sky survey (equation 2.22)				11,3	
10 hour integration (equation 2.12)				1,05	
Uranus	169 $\pm$ 20	1,35	2,78 $\times 10^{-7}$	0.30	Pauliny-Toth 1970
Neptune	255 I 20	2,7	6,74 $\times 10^{-8}$	0.90 f.u.	
Pluto + asteroids many orders of magnitude less detectable.					

Figure 2.4 Table of thermal sources in the solar system The average measured brightness temperatures were obtained from the references in column 6. The average solid angles subtended at the earth were evaluated from the mean distance to the earth and the diameter of the body concerned (Kraus 1966, Harvey 1963).

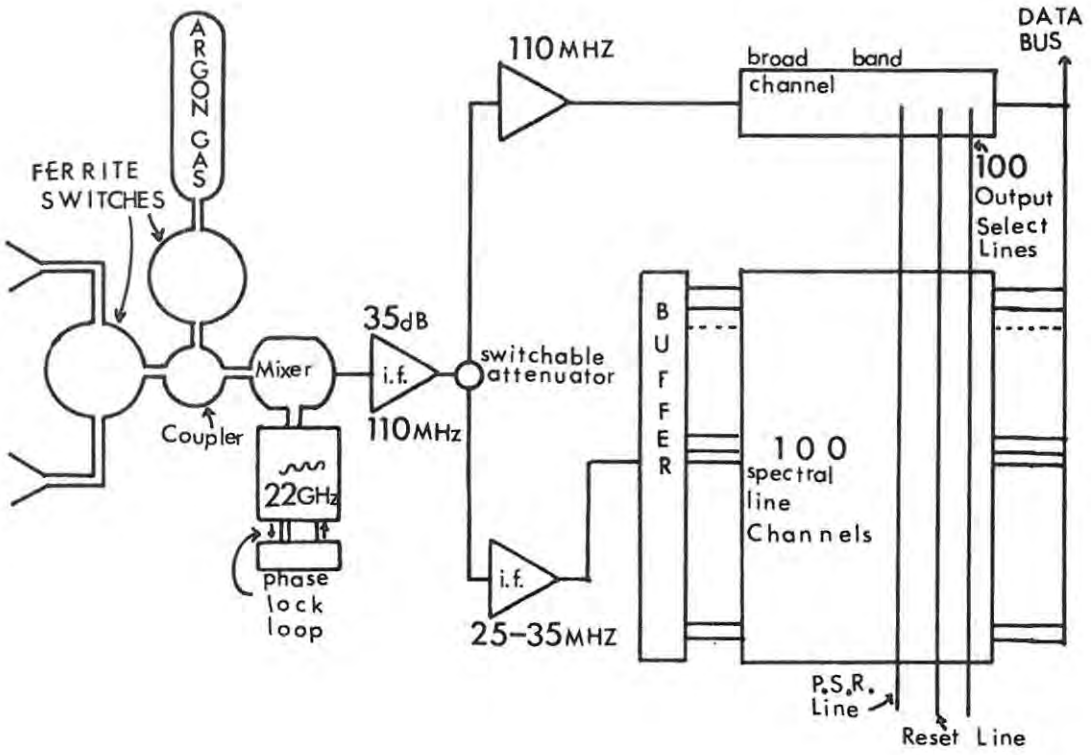

Figure 2.5a The Full Receiver

A 'f.e.t.' (field effect transistor) - controlled attenuator was to be attached to the output of the i.f. pre-amplifier for calibration purposes. A power splitter following the attenuator would feed the broad-band and spectral-line channels. The broad-band (continuum) channel provides a further 60 dB gain before detection. For spectral line work, however, the output of a 30 MHz i.f. amplifier- which has a bandwidth of 10 MHz and a gain of up to 80 dB - is fed via a buffer stage to the 100 channels. This buffer stage was designed for the work in this thesis (chapter V), and provides input- and output- impedance matching to the 50 ohm-impedance coaxial cable used, and also reduces interchannel 'crosstalk'. Each of the 100 channels selects the required bandwidth by mixing the signal with a second local oscillator, at an appropriate frequency near 30 MHz, and then passing the signal through a 25 KHz lowpass filter (figure 2.5b). The channel is then sensitive to frequencies within 25 KHz

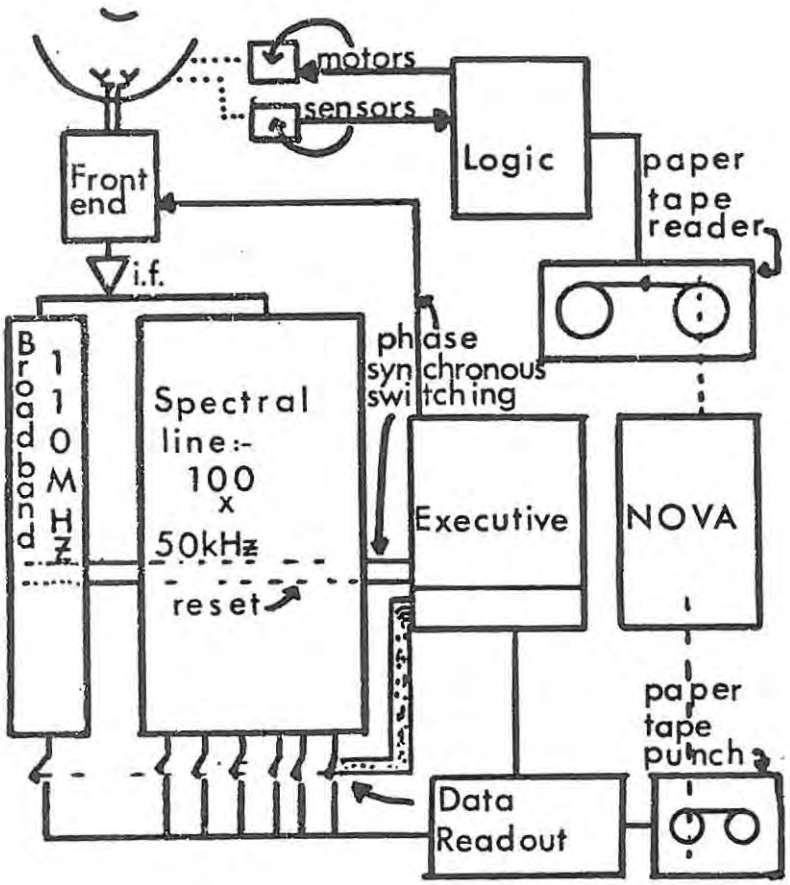

Figure 2.6 **RADIOMETER**

above and below the local oscillator frequency. The phase sensitive rectification is performed by the capacitor 'c' and the f.e.t. switch at the frequency f_D. The channel outputs may be switched selectively onto a common data bus line by f.e.t. switches, and the outputs may all be 'zeroed' by the reset line, again via f.e.t. switches, which short the integrating capacitors.

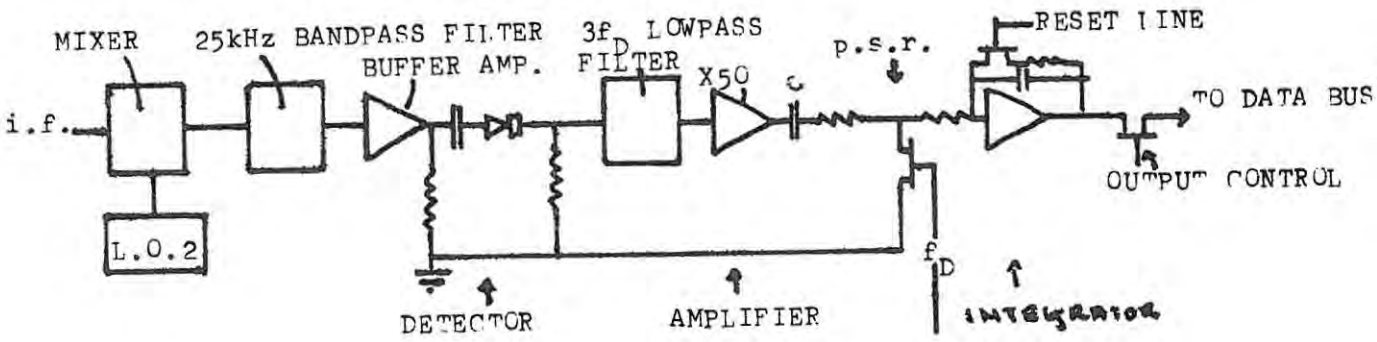

Figure 2.5b Layout of 100 Channels

2.6b The control section

The so-called 'receiver executive timing control', described in chapter VI, controls the switching of the front-ends and p.s.r.-modulators. The 'executive' also controls the switchable attenuator and the 'reset' line, and supervises the control of the 'output select lines' and the 'data processor'. The data processor, also described in chapter VI, digitises the output voltage values, and stores them at a rate of 200 characters per second in a 500 - character buffer memory. A paper tape punch then punches the contents of this memory at 20 characters per second, while the receiver proceeds with the next run. The complete block diagram of the radiometer appears opposite (figure 2.6), and in more detail in appendix B (figures B2.1, B2.2). Standard time signals and frequencies are obtained, from broadcasts such as "Z.U.O." and "W.W.V", for calibrating the system. The telescope drive system is being designed to allow tracking of several sources sequentially, with correction for instrument-pointing and atmospheric refraction effects. The telescope drive will be controlled by a program fed to a paper tape reader, which will also control the executive, and hence the entire radiometer. Output data will eventually be fed directly to an ~~outline~~ on-line NOVA computer instead of onto paper tape.

CHAPTER III

THE CASSEGRAIN FEED DESIGN

CHAPTER III

The Cassegrain Feed Design

Cassegrain antennas are frequently used in radio astronomy because of their inherent low noise, which results from the sidelobes being directed at the sky only, and not at the ground. The Physics Department at Rhodes University had bought several 1,83m diameter parabolic 'dish' reflectors before the work described in this thesis had been started; a Cassegrain antenna system incorporating one of these 'dishes' had to be designed for maximum gain.

3.1 Geometrical optics design equations

Figure 3.1 shows the elements of a Cassegrain feed system,

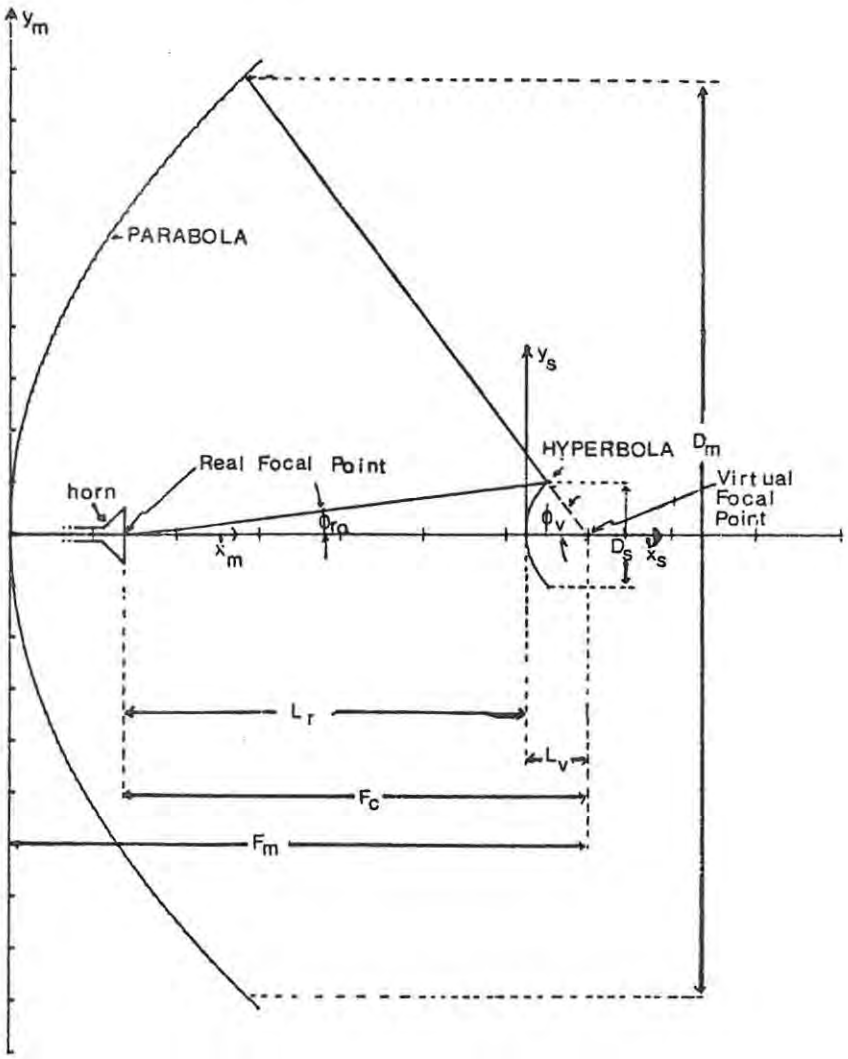

Figure 3.1 Cassegrain feed antenna

where the virtual focal point of the hyperbolic subreflector coincides with the focus of the parabolic dish, and the real focus of the hyperboloid coincides with the focal - or ~~apeture~~ aperture - plane of the horn. The analysis of the operation of the Cassegrain system may be performed semi-optically to a good approximation, when the wavelength is small with respect to the ~~apeture~~ aperture diameter (Rusch 1970). In the present case the approximation holds, as the ratio of the wavelength to the dish-diameter is 10^{-3}.

The optical description of the system requires four fixed parameters, two for each reflector (Hannan 1961). The equation describing the parabolic surface, with respect to the axis defined by x_m and y_m (figure 3.1), is

$$x_m = y^2_m/4\ Fm \qquad 3.1$$

where Fm is the focal length of the reflector. This focal length Fm and the diameter Dm completely describe the main reflector. These parameters may be obtained from measurements of the parabolic reflector surface, and used to evaluate the angle subtended by the reflector at it's focus, Φ_V :

$$\Phi_V = 2 \text{ arc tan } (Dm/4\ Fm) \qquad 3.2$$

The antenna gain is determined by the 'feed taper', which is the illumination by the feed system at the edge of the parabolic reflector, with respect to that at the centre of the reflector. The 'feed taper' is in turn determined by the cutoff angle of the feedhorn power pattern, Φ_{ro}, which is one of the two parameters needed to describe the hyperbolic surface of the subreflector. The other parameter needed to describe the subreflector, the interfocal distance F_c, is related to Φ_{ro} and Φ_V by the equation describing the hyperbolic surface, which is

$$x_s = a\ [(1 + (y_s/b)^2)^{\frac{1}{2}} - 1] \qquad 3.3$$

where x_s and y_s define a coordinate system as shown in figure 3.1, and where

$$a = F_c/2e \ , \quad b = (e^2 - 1)^{\frac{1}{2}} \ ,$$

and the eccentricity $e = \dfrac{\sin\left[\frac{1}{2}\left(\Phi_v + \Phi_{ro}\right)\right]}{\sin\left[\frac{1}{2}\left(\Phi_v - \Phi_{ro}\right)\right]}$

The two parameters F_c and Φ_{ro} completely determine the hyperbolic reflector for a given feedhorn and main reflector. Once these are determined the subreflector diameter D_s, and the distances to its focal points from its centre, L_v and L_r, can be evaluated from, respectively (Saad 1971):

$$D_s = \frac{D_m(F_c/F_m)(\tan \Phi_v \tan \Phi_{ro})}{(2 \tan \Phi_v/2)(\tan \Phi_r + \tan \Phi_{ro})} \qquad 3.4$$

$$L_v = F_c/(1 + D_m/4 F_m \tan \Phi_{ro}/2) \qquad 3.5$$

$$L_r = F_c - L_v \qquad 3.6$$

The design procedure for the Cassegrain system is shown in figure 3.2. It involves, initially, the determination of the paraboloid-defining parameters F_m, D_m and Φ_v. An edge illumination for the paraboloid is then chosen, and uniquely determines the feed angle Φ_{ro} for a chosen horn. The hyperboloid interfocal distance F_c is then chosen to satisfy certain physical conditions (to be discussed in section 3.5). A final choice of horn is then made on the basis of the size of the resulting subreflector (figure 3.2). When the choice of feedhorn has been made, the parameters L_v and L_r can be evaluated, as well as the subreflector shape (equation 3.5, 3.6, and 3.3 respectively). From the flowchart in figure 3.2 it can be seen that the feed angle Φ_{ro} depends on the horn chosen (once the feed taper has been fixed), and the parameter F_c is adjusted to suit design criteria for various horns. The best design resulting from the variation of F_c and the horn pattern (obtained by using various horns) is then chosen. The operations depicted in figure 3.2. will be detailed below.

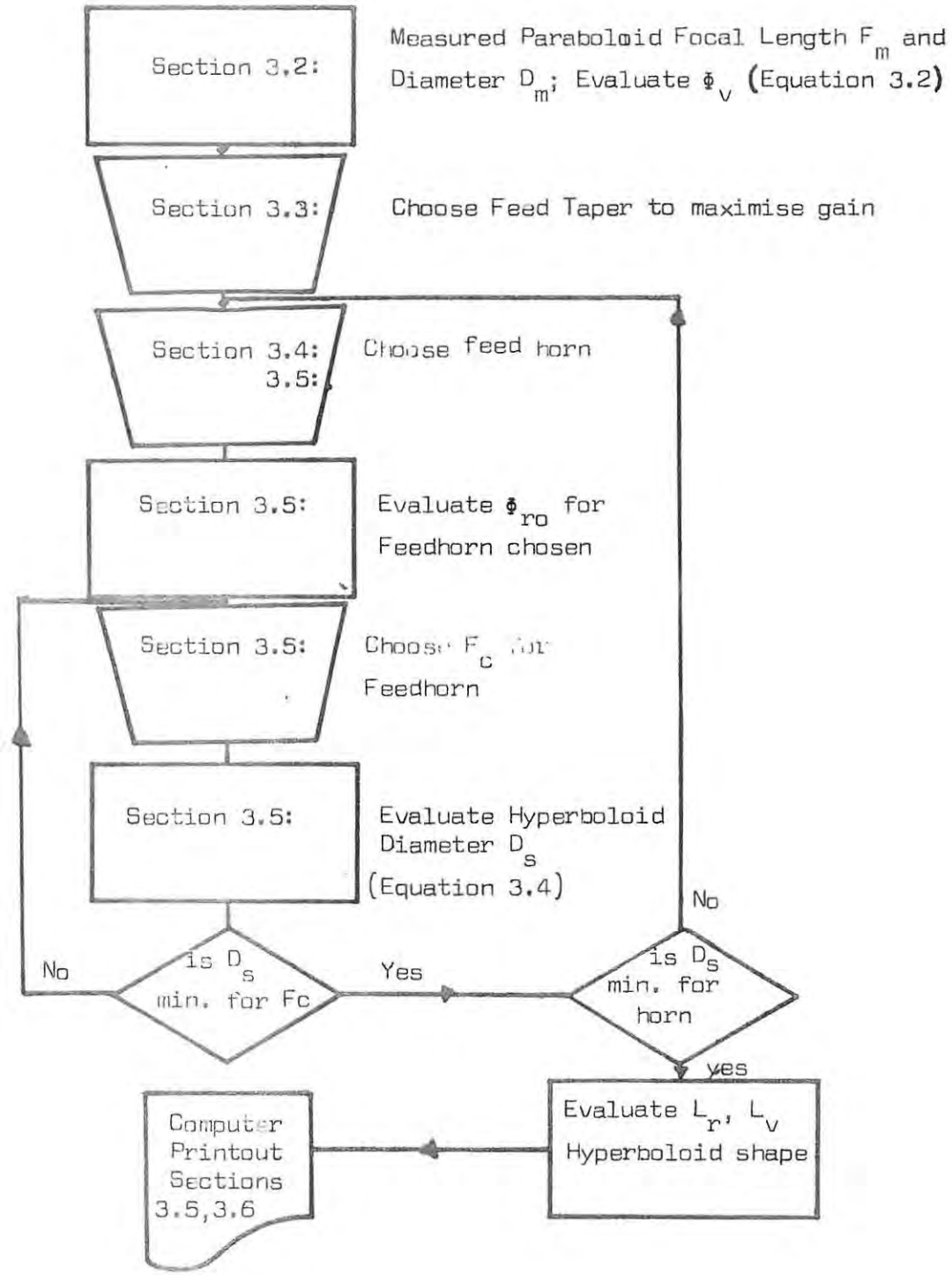

Figure 3.2. Flowchart of Cassegrain design

3.2. The determination of the paraboloid diameter and focal length

The diameter D_m of the paraboloid was measured between points near the rim of the paraboloid, where it was estimated that the parabolic shape is not yet deformed by the strengthening cylindrical rim. The value obtained was

$$D_m = 1,83 \pm 0,01 \text{ m} \qquad 3.7$$

The focal length F_m of the paraboloid was obtained by first measuring the depth of the parabola (x_m) at regular distances (y_m in figure 3.1) along several diameters of the paraboloid. The measurements were made on the inverted dish with two straight-edged steel rulers held at right angles by a slotted metal block. Plots of (x_m/y_m) versus y_m (figure B3.1, appendix B) yielded an average slope of $F_m/4$, i.e. $0,359\ m^{-1}$, from which $F_m = 0,70 \pm 0,01$ m. The large error in the value of F_m results from the fact that the measurements were made on a slightly damaged paraboloid. However, it will be shown that a knowledge of the exact values of F_m and D_m is not critical to the succeeding calculations. The angle Φ_V is obtained from equation 3.2, and is given by

$$\Phi_V = 66,6^0 \qquad 3.8$$

3.3 Choice of the paraboloid edge illumination

The edge illumination of the paraboloid by the feed (the horn plus the subreflector), with respect to that at the centre, determines the sidelobe levels and also the antenna gain. The gain increases, as the edge illumination increases, to a maximum when the edge illumination is about 8dB to 9dB less than that at the centre of the paraboloid (in which case the illumination across the paraboloid aperture plane is most nearly uniform). As the gain increases, so does the sidelobe level (Collin 1969). However, the sidelobes, which are directed at the sky (at a temperature of about 270 K), will not introduce much noise into the system in comparison with the receiver noise temperature (about 600 K, equation 2.11). It was thus decided to maximise the gain, even though the sidelobe levels would increase.

The directivity D of an antenna is the ratio of the maximum radiated power density (along the forward symmetry axis in this case) to the average power density over 4π steradians. The gain G takes the losses of a real antenna into account, and is defined by (Jasik 1961)

$$G = \eta D \qquad 3.9$$

where η is the antenna efficiency, and usually lies between 0,5 and 0,75. It has already been mentioned that the gain (and hence the directivity) depends on the paraboloid edge illumination. This edge illumination results from the feedhorn power pattern taper, and also from the unavoidable "space attenuation". This space attenuation results from the $1/r^2$ dependance of illumination from a point source, and from the parabolic shape of the main dish (Hosking 1973) and is given by (Silver 1965)

$$= 20 \log \sec^2 (\Phi_V/2) \quad (dB) \qquad 3.10$$
$$= 3,1 \text{ dB}$$

where Φ_V was obtained from equation 3.8. The space attenuation reduces the paraboloid edge illumination by 3.1 dB below the uniform illumination level, and adds to the edge attenuation produced by the feedhorn power pattern taper.

The overall directivity D of the antenna can be characterised by the E- and H-plane directivity factors of the feedhorn, which are D_E and D_H respectively. The appropriate expression is

$$D = D_E + D_H + 10 \log (A/\lambda^2), \quad (dB) \qquad 3.11$$

where A is the area of the reflector ~~aperture~~ aperture $(=\pi D_m^2/4)$ (Hosking 1973). The directivity factors takes into account the illumination taper and the type of feedhorn, and are plotted in figure 3.3 for pyramidal feedhorns.

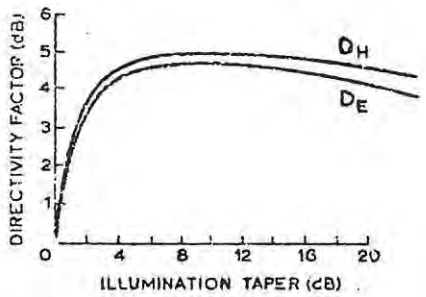

Figure 3.3 The E- and H- directivity factor D_E and D_H for a pyramidal feedhorn.

It can be seen from figure ~~3.4~~ 3.3 that D_E and D_H both have maxima, corresponding to a maximum in D, when the ~~aperture~~ aperture edge illumination is between 7 dB and 9 dB (below the central illumination of the paraboloid). The value chosen for the paraboloid edge illumination was 8,6 dB, to minimise the sidelobe level while retaining the maximum gain (as the sidelobe level decreases with decreasing edge illumination). Since the space attenuation is 3,1 dB (equation 3.10), the attenuation at the edge of the paraboloid due to the feed must be 5,5 dB, for an overall edge illumination of 8,6 dB for the paraboloid below the central value. A feedhorn at the focus of the paraboloid would need a taper of 5,5 dB at an angle of Φ_v degrees to provide an edge illumination of 5,5 dB (at the paraboloid edge due to the feed alone). Since the feed is at the second focus of the hyperboloid, it must have a taper of 5,5 dB at Φ_{ro} degrees (figure 3.1) to provide the same edge illumination for the paraboloid.

3.4 Measurement of feedhorn power patterns

The angle Φ_{ro} from the central axis of a horn, at which the power level (emitted by the horn) is 5,5 dB below the maximum power level, is dependent on the horn power pattern. The power patterns of the three horns available, with gains of 10 dB, 15 dB, and 20 dB, were measured to allow an evaluation of the cutoff angles (Φ_{ro}) for these horns.

The horn whose power pattern was to be measured was attached via an attenuator to a Hewlett-Packard power meter, and mounted securely in a horizontal position on top of a spectrometer table by means of an adjustable support. This arrangement allowed the horn to be rotated about a vertical axis in its ~~apeture~~ aperture plane, while the vernier scales on the spectrometer table allowed the angles of rotation to be measured accurately. Spurious reflections were avoided by mounting the spectrometer table and horn assembly on a 1 m high stand in the middle of a hockey field. The horn was covered with black paper to prevent sunlight from influencing the thermistor. A small transmitting horn, attached to a Gunn diode oscillator, was placed 6 m from the receiving horn 1 m above the ground to simulate an isotropic point source. The separation of 6 m satisfies the far field condition proposed by Steinberg (1963). This is

$$R > 10\ D^2/\lambda \qquad 3.12$$

where R is the (far field) distance between the horns, D is the receiving horn ~~apeture~~ aperture diameter, and λ is the wavelength (1,35 cm). This far field distance for the largest horn (D = 6 cm) is 3 m.

The power meter was first calibrated. The 'E-plane' power pattern was then obtained at half-degree intervals for each receiving horn (to an accuracy of $\pm$ 1 percent in power level, and to $\pm$ 2' arc in angle), while the E-planes of both the transmitting and receiving horns were horizontal. The H-plane patterns were obtained similarly. The two patterns obtained for the 20- dB horn are shown in figures B3.2 and B3.3 (Appendix B). The cutoff angles (Φ_{ro}) were now obtained for each horn as discussed at the beginning of this section. Since the cutoff angles for the E- and H-planes of each horn differed slightly, an average of the two values was taken to be $\bar{\Phi}_{ro}$. For example, the E- and H-plane cutoff angles for the 20 dB horn are $12^o\ 30'$ and $11^o\ 45'$ respectively. The value chosen for $\bar{\Phi}_{ro}$ was taken to be $12^o\ 0'$. The illumination taper around the

paraboloid rim will vary slightly because of this averaging process. However, this will not noticeably affect the directivity of the antenna which changes only slightly for even large variations of illumination taper between 6 dB and 9 dB (see figure 3.3 and equation 3.11).

3.5 Choice of subreflector-determining parameters

The choice of feedhorn and the hyperboloid interfocal distance F_c are linked as shown in figure 3.2. The choice of F_c depends on constraints relating to the feedhorn position, and also on the subreflector blockage. The choice of the feedhorn position was limited by two factors. First, the feedhorn had to be located on the concave side of the parabolic reflector, due to the small size of the hole in the middle of the reflector, and as close to the parabolic surface as possible, to avoid mechanical flexing of the supporting waveguide and to reduce attenuation of the signal in this waveguide. Second, room had to be allowed between the parabolic surface and the end of the feedhorn for a ferrite switch to be used with two focal-plane horns for beam-switching. The focal length of the paraboloid is 70 cm (section 3.2), and as the available horns are between 5 cm and 11 cm long and the switch is 5 cm long, the distance F_c had to be between 50 cm and 60 cm to satisfy the above two conditions.

Within the above ~~limitations~~ limits, the value of F_c had to be chosen to minimise the subreflector blockage. For a chosen horn the value of the subreflector diameter can be evaluated from equation 3.4. There exists a minimum value of the subreflector diameter, D_{smin}, for the paraboloid at the operating wavelength of 1,35 cm, as is shown in figure 3.4, where (Hannan 1961)

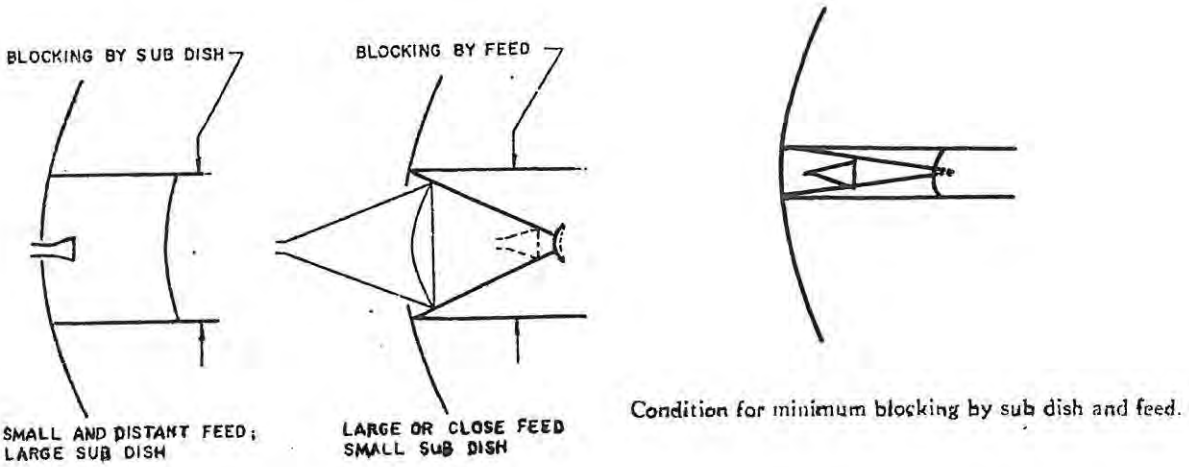

Figure 3.4 Type of apeture blocking - illustrating the minimum blocking condition

$$D_{s\ min} = 2\ Fm\ \lambda/k \qquad 3.13$$

$$= 15{,}3\ cm$$

where k is the ratio of the effective - to the blocking - feed aperture ~~apeture~~ diameter (about 0,8), and where F_m is the paraboloid focal length (70 cm) (Hannan 1961).

The choice of F_c was simplified by writing a FORTRAN program (figure B3.4, appendix B) to evaluate D_s, L_r, L_v, and the constants e, a, and c (= $F_e/2$) relating to the hyperboloid surface (from equations in sections 3.1), for values of F_c between 50 cm and 60 cm. The program printout revealed that the use of the 10 dB, 15 dB, and 20 dB horns would necessitate subreflector diameters of about 50 cm, 30 cm, and 20 cm respectively. The 20 dB horn results in the least aperture ~~apeture~~ blocking by the subreflector and was chosen for the feedhorn. The printout of the program in figure B3.4 for the 20 dB horn appears in figure 3.5

GEOMETRICAL RELATIONS OF CASSEGRAIN ANTENNAS.

DM = 1,830 METERS (DIAM OF MAIN DISH)
FM = 0,696 METERS (FOCAL LENGTH OF MAIN DISH)
PHIV = 66,636 DEGREES (ANGLE SUBTENDED AT FOCUS)
= 1,163 RADIANS
PHIR = 12,000 DEGREES (ANGLE SUBTENDED BY HYPERBOLA)
= 0,209 RADIANS
FE = 4,353 METERS (FOCAL LENGTH OF EQUIVALENT PARABOLA)

FC METERS.	DS METERS.	LR METERS.	LV METERS.	C METERS.	A METERS.	E
0,500	0,195	0,431	0,069	0,250	0,181	1,381
0,510	0,199	0,440	0,070	0,255	0,185	1,381
0,520	0,202	0,448	0,072	0,260	0,188	1,381
0,530	0,206	0,457	0,073	0,265	0,192	1,381
0,540	0,210	0,466	0,074	0,270	0,196	1,381
0,550	0,214	0,474	0,076	0,275	0,199	1,381
0,514	0,200	0,443	0,071	0,257	0,186	1,381

Figure 3.5 Cassegrain parameters for the 20 dB gain horn

The closest that the ~~apeture~~ aperture plane of this horn can be to the paraboloid is limited by the horn length (11 cm) and the ferrite switch length (5 cm) to 16 cm. This value results in a value of F_c (F_m - 16 cm, figure 3.1) of 54 cm. The value chosen for F_c was 53 cm, to allow a focussing movement towards the paraboloid of 1 cm. From figure 3.5 it can be seen that the resulting subreflector diameter is 20,6 cm, which is ~~sufficiently~~ close to the minimum blocking diameter of 15,3 cm (equation 3.12).

A program, designed by F. Jacot-Guillarmod (private communications) for use on a HP Model 10 calculator, was employed to check the above FORTRAN program for an interfocal distance F_c of 53 cm. This program was also used to plot the hyperboloid shape to scale. The plot was used as a rough check on the template described in the next section.

3.6 Hyperboloid-template and hyperboloid construction

A second FORTRAN program was written to first evaluate the hyperbolic surface points from equation 3.3, and then tabulate the

values of these coordinate points (x_s versus y_s in figure 3.1), at 0,1 mm intervals. The hyperboloid template was constructed with the aid of this table, a portion of which is shown with the program listing in figure B3.5 (appendix B). A strict criterion for a reflecting surface is that the surface be accurate to within a sixteenth of a wavelength to avoid phase errors (Silver 1965). This requirement necessitated a surface accuracy of $\pm$ 0.8 mm for the hyperboloid, and hence for the template.

After an unsuccessful attempt to use a precision densitometer as a two dimensional travelling microscope to map out the hyperbolic shape on a sheet of brass, it was decided to draw the shape, at double the scale, on plastic tracing paper. The portion of this tracing paper on the concave side of the hyperbolic so drawn was blackened, and the resulting pattern was photographically reduced to the correct size as a negative. Two such negatives were cut accurately along the hyperbolas, and checked with the densitometer They were found to be accurate to within $\pm$ 0,3 mm.

The sub-reflector was fabricated as follows in the Physics workshop. A steel template was made from one of the plastic ones by spraying marking paint onto the plastic template, which was held firmly in contact with a metal sheet. This sheet was filed to shape, and used to shape a block of wood on a lathe. A 1/8 inch aluminium sheet was heated and dipped in water to soften it, and then spun onto the shaped wooden face. The steel template was now used to ~~roughly~~ shape the aluminium face, which was then polished with abrasive papers with decreasing grain size, until it matched the plastic templates.

A depth ~~guage~~ gauge mounted on the lathe was used to measure the accuracy of the hyperbolic surface. It was found to be accurate to within 0,5 mm, corresponding to one-twenty-fifth of a wavelength, along several diameters. A 2 cm cylindrical edge for mounting was turned behind the surface, and a 2 mm hole was drilled through it's centre to facilitate lining-up of the surface with a laser beam.

3.7 Evaluation of Cassegrain design performance

The directivity D of the antenna is obtained from equation 3.11 (page 35), where D_E and D_H may be found from figure 3.3 for an aperture edge illumination of -8,6 dB:

$$D = 51,1 \text{ dB} \qquad 3.13$$

The gain is given from equation 3.9 as

$$G = 51,1 - 10 \log \eta \quad \text{dB}, \qquad 3.14$$

where η is the antenna efficiency. The theoretical upper limit of the value of η is a function of the frequency and ~~aperture~~ aperture angle and is 0,96 for the antenna being considered (Potter 1963, 1967), but η is decreased by spillover and other effects. Theoretical evaluations of these effects can be performed numerically, and yield reasonable results (Potter 1963, Weinreb 1970, Leonard 1973).

The only way of obtaining the actual value of η is by experiment, by measuring the astronomical "standard sources" mentioned earlier. It was also mentioned that η is commonly between 0,5 and 0,75. The pessimistic value (0,5) would yield a gain of 48,1 dB for the Cassegrain system designed above.

The next step in the design of the antenna is the design of the Cassegrain support framework: this is discussed in chapter four.

CHAPTER 4

CONSTRUCTION OF THE CASSEGRAIN AND FRONT-END SUPPORT FRAMEWORK

CHAPTER IV

CONSTRUCTION OF THE CASSEGRAIN AND FRONT-END SUPPORT FRAMEWORK

The Cassegrain system discussed in chapter 3 had to be mounted on the telescope support. The supporting framework was designed with the aid of a scale model. Since the framework would deform with antenna elevation angle changes, the next step in the design was an evaluation of the amount of defocussing, due to this effect, which could be allowed. The various framework structural beams or rods were then chosen to keep the deformations within the calculated tolerances. The above design steps are discussed in this chapter, which is concluded by a short description of the constructional details.

4.1 Front-end layout and the model telescope

The antenna and its support had to be light, and balanced about the horizontal rotation axis, to reduce the strain on the tracking motors, and had to allow the antenna beam to point to within 15^{o} of the horizontal. The paraboloid and its support had thus to be positioned as close to the horizontal rotation axis as possible to reduce the counterbalancing torque needed, while allowing the paraboloid symmetry axis to point to within 15^{o} of the horizontal without any projections interfering with the framework. It was decided to mount the front-end (waveguide) section behind the paraboloid in the yoke of the telescope mount, together with the counterweight. The design of the support structure was assisted by the building of a scale (1:3) balsa-wood model of the telescope mount and the parabolic dish. This model is shown in figure 4.1, together with the model of the framework which was chosen to suit the above criteria.

Because construction of the two supporting octagons would be relatively simple, and because these would allow easy mounting onto the telescope bearings, it was decided to mount the front-end

flat on a thick aluminium sheet, and to allow a length of waveguide, attached to the mixer, to project through the hole at the centre of the paraboloid to support the feedhorn. Positioning and focussing of the horn could then be achieved by moving the front-end plate.

Figure 4.1 Model of the telescope and Cassegrain support framework

Several layouts of the front-end (figure 2.6a) were set up in attempts to find one which could be mounted on a sheet of metal, and which still fitted inside the telescope mount. When a layout had been chosen a framework was built around the front-end plate for enclosing it against the weather. This framework was designed to house the counterweight at the bottom, as far from the horizontal axis as possible. Because of excessive flexing by the counterweight of the box framework, it was designed to be mounted on the telescope bearings almost independently of the front-end and paraboloid supports. The

subreflector was to be supported by four pairs of aluminium rods if possible, so as to reduce the weight, attached symmetrically to the paraboloid support framework.

The next step in the framework design was the evaluation of allowable deformations so that sufficiently rigid materials could be chosen for the construction of the telescope.

4.2 Evaluation of allowed tolerances

The hyperboloid subreflector and the feedhorn have to be aligned to within certain tolerances with respect to the parabolic reflector surface, and must stay aligned as the telescope tracks a source. The parabolic reflector itself must be rigidly supported to prevent sagging, and distortion of the parabolic shape. The usual requirement on reflecting surfaces is that on average they be kept to within an eighth of a wavelength of the required shape at the operating frequency. The paraboloid should thus be true to within 1,7 mm for operation at a wavelength of 1,35 cm. Deviations from this criterion will noticeably decrease the antenna efficiency (equation 3.4), given by

$$\eta = 1 - \overline{\delta^2}, \qquad 4.1$$

where $\overline{\delta^2}$ is the mean square phase-error (Findlay 1964). (The efficiency is commonly measured by measuring the system response to a standard source (Cogdell 1973).)

The allowable tolerance on the axial displacement of the subreflector is evaluated as follows: if it is displaced axially by a distance δ_o from the focussed position, the phase-error δ is (Silver 1965)

$$\delta = \delta_o \cos \Phi_{ro} \qquad 4.2$$

The focussing tolerance of the hyperboloid needed to satisfy the one-eighth wavelength criterion ($\delta = \lambda/8$) is thus

$$\delta_o = \pm \frac{\lambda}{8} \sec \Phi_{ro} = \pm 1{,}7 \text{ mm} \qquad 4.3$$

Baars (1973) discusses the case of radial displacements of the horn and subreflector (normal to the symmetry axis). The decrease in gain in this case is not much affected by even moderate feed displacements (used when two horns are positioned in the focal plane for beam-switching). However, the feed tilt from the symmetry axis should be restricted to a minimum, as the gain decreases by 0,1 percent when this tilt is one beamwidth ($0{,}5^o$), and decreases rapidly for larger tilt angles (Saad 1971). The maximum allowable tilt was chosen to be half a degree to keep the resulting loss in gain to below 0,1 percent. The tolerances on the reflector surface deformations and on the positioning of the subreflector and feedhorn were fixed, allowing of a choice of structural materials.

4.3 Choice of suitable structural beams with regard to loading and tolerances

The deflection of beams with uniform cross-section can easily be evaluated. However, complicated frameworks,such as the paraboloid support, are tedious to evaluate analytically, and simplifying assumptions were made to yield order-of-magnitude results for the deflections.

4.3a The parabolic dish support

There were two possible steel beams which could be used for the paraboloid supporting framework. Their cross-sections and dimensions are shown in figure 4.2, together with formulae for I, the second moment of elasticity about the neutral fibre axis (Boltz 1973). The values of I are 1,49 cm^3 for the square tube

and 1,08 cm^3 for the L-beam, which is thus more flexible. This, together with the fact that the square tube would yield a lighter structure (it has a mass of 1,18 kg m^{-1}, as opposed to 1,35 kg m^{-1} for the L-beam), make the square steel tube the obvious choice.

It can be seen from figure 4.1 that the parabolic dish would be supported around it's lip only, by the large octagon, which is in turn supported by eight struts attached to a smaller octagon and hence to the bearing mounts. Assuming that the hyperboloid supports remain completely rigid, it is highly probable that the axial defocussing of the Cassegrain system will be minimal as the telescope elevation angle changes, as such defocussing would have to be caused mainly by buckling of the struts between the two octagons. The main effect of the change in elevation angle will be to change the shape of the rim of the paraboloid from circular, due to elastic deformation of the large octagon.

When the antenna is pointing at the horizon, the top and bottom arms of the large octagon will have the maximum deformation. The loading of the two side arms of this octagon (vertical to the ground when the antenna is pointing at the horizon) will not contribute to the deformation of the paraboloid. If, as an approximation, the four arms of the octagon discussed above are each considered as carrying a quarter of the total weight of the antenna, distributed along their length, the deformation at the centre of the top and bottom arms can be evaluated from (Boltz 1973)

$$y\,(s/2) = W_o\, s^4/384\, E\, I \qquad 4.4$$

In equation 4.4. s is the beam length (74 cm), E is Young's modulus of elasticity for steel (2,11 x 10^6 kg cm^{-2}), and I has been evaluated above. W_o is the weight distributed along the bar, which, in the approximation mentioned, is a quarter of the total weight (40 kg) of the paraboloid (19 kg), subreflector (about 10 kg), and the large hexagon and its support struts (10 kg). W_o is thus

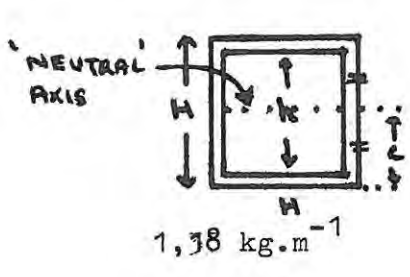

1,38 kg.m^{-1}

H = 2,53cm

h = 2,19cm

$I=(H^4-h^4)/H$

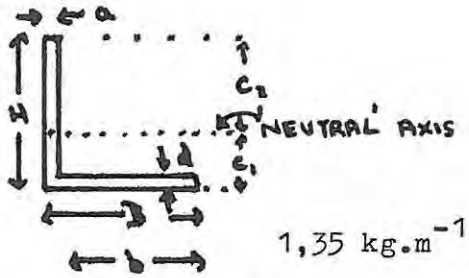

1,35 kg.m^{-1}

H=B= 2,64cm , b= 2,30cm

a=d= 0,34cm , ~~h= c-d~~

$c_1=(aH^2+bd^2)/(aH+bd).2$

$c_2=H-c_1$

$I=(Bc_1^3-bh^3+ac_2^3)/3$

FIGURE 4.2 Steel beams for antenna framework

10 kg. The value obtained for y (s/2) is

$$y\ (s/2) = 2{,}72\ \text{mm}, \qquad 4.5$$

which is about a fifth of a wavelength. However, the paraboloid and its strengthened cylindrical rim is firmly held onto the large octagon by 16 evenly spaced clamps, which probably stiffens the whole structure, so that the mean square phase-error over the whole dish (in equation 4.1) probably nearly satisfies the $\lambda/8$ criterion.

4.3b The Front-end, and counterweight supports

The L-beam in figure 4.2 was chosen both for the framework supporting the front-end plate, and for the counterweight support beams, even though the square cross-section tubing is stiffer. The reasons for this choice are detailed below.

The chosen front-end layout allows a supporting framework to be mounted behind the aluminium plate. The face of this framework had to be machined flat so as not to distort the aluminium plate when bolted to it. The sides of the L-beam are twice the thickness of the sides of the square-beam (figure 4.2), which are thus far less suited to flat machining. A further reason for using the L-beam for the front-end support is that the square-beam would tend to distort when bolted through two opposite sides onto the aluminium plate.

An L-beam was chosen for the counterweight support struts because flexing of the supports will not affect the focussing or pointing accuracy of the antenna, since the supports are mounted on the telescope bearings independently of the antenna and front-end. The L-beam allows more room inside the front-end box, and minimises the stresses in the supports. The stresses are less than for the square beam as demonstrated below.

When a moment M is applied to a beam, the maximum stress in the upper or lower boundary fibre, σ_{max}, is given by

$$\sigma_{max} = cM/I, \qquad 4.6$$

where c is the distance between the neutral fibre plane, and the appropriate boundary plane (Sommerfeld 1964). The beam with the lowest c/I ratio will subject the metal boundary fibres to the least stress. These may be evaluated from figure 4.2. For the square tube c/I is 0,84 cm^{-2}, while the two values for the L-beam are c_1/I, and c_2/I, which are 0,725 cm^{-2} and 1,72 cm^{-2} respectively. The smallest value is obtained for the L-beam, when the moment to which it is subjected tends to stretch the 'B side' (figure 4.2). The orientations of the various struts supporting the counterweight were all arranged so that the least stress was applied to the metal boundaries for all elevations of the telescope.

4.3c The Feedhorn support

The ensuing argument demonstrates that the waveguide alone can support the feedhorn without excessive tilting of the feed.

The H-plane of the waveguide (parallel to the two widest sides) supporting the feedhorn is parallel to the plane containing the front-end plate and the bearing mounts. The second moment of elasticity, I, for the flexing in the E-plane perpendicular to this can be evaluated (from Boltz, 1973) for the dimensions of the brass waveguide (figure 4.2).

$$I = 0,0213 \text{ cm}^3 \qquad 4.7$$

The horn is 11 cm long, and the waveguide section 5 cm long (Chapter 3). The additional length of unsupported waveguide behind the paraboloid is 2 cm. Assuming the horn to be as flexible as the waveguide (giving a pessimistic value for the flexing), the deflection of the horn at the ~~aperture~~ aperture plane, from its

undeflected position, when the horn is horizontal, is (Pipes 1946)

$$y(\ell) = \frac{P_o a^2}{EI} \left(\frac{\ell}{2} - \frac{a}{6}\right) . \qquad 4.8$$

P_o is the weight of the horn (0,24 kg), "a" the distance of the centre of gravity from the supported end of the waveguide (13 cm), and "ℓ" the length from this supported end to the horn ~~aperture~~ aperture (18 cm). The resultant (maximum) deflection will be

$$y(\ell) = 0,12 \text{ mm}, \qquad 4.9$$

which corresponds to a feedhorn tilt angle of 2,4 minutes of arc This is far less than the telescope beamwidth (30'), and is acceptable in terms of the tolerance allowance mentioned in section 4.2.

4.3d The subreflector supports

The subreflector supports consist of four pairs of rods, of which one pair is shown in figure 4.3.

A rough calculation showed that axial defocussing of the hyperboloid, with elevation-angle changes, would be negligible for even the thinnest-walled one-inch diameter aluminium tubing. The major effect contributing to the movement of the subreflector is the torque exerted by the subreflector and its support (the combined center of gravity of which is shown in figure 4.3), about the midpoint of the support connected to the aluminium rods. This torque is a maximum when the antenna symmetry axis is horizontal. A mathematical model representing a pair of support rods is shown in figure 4.4. This model is representative of the situation where the rotating joints (figure 4.3) are bolted down, and where all forces except the torque mentioned are supposed to act along the aluminium rods

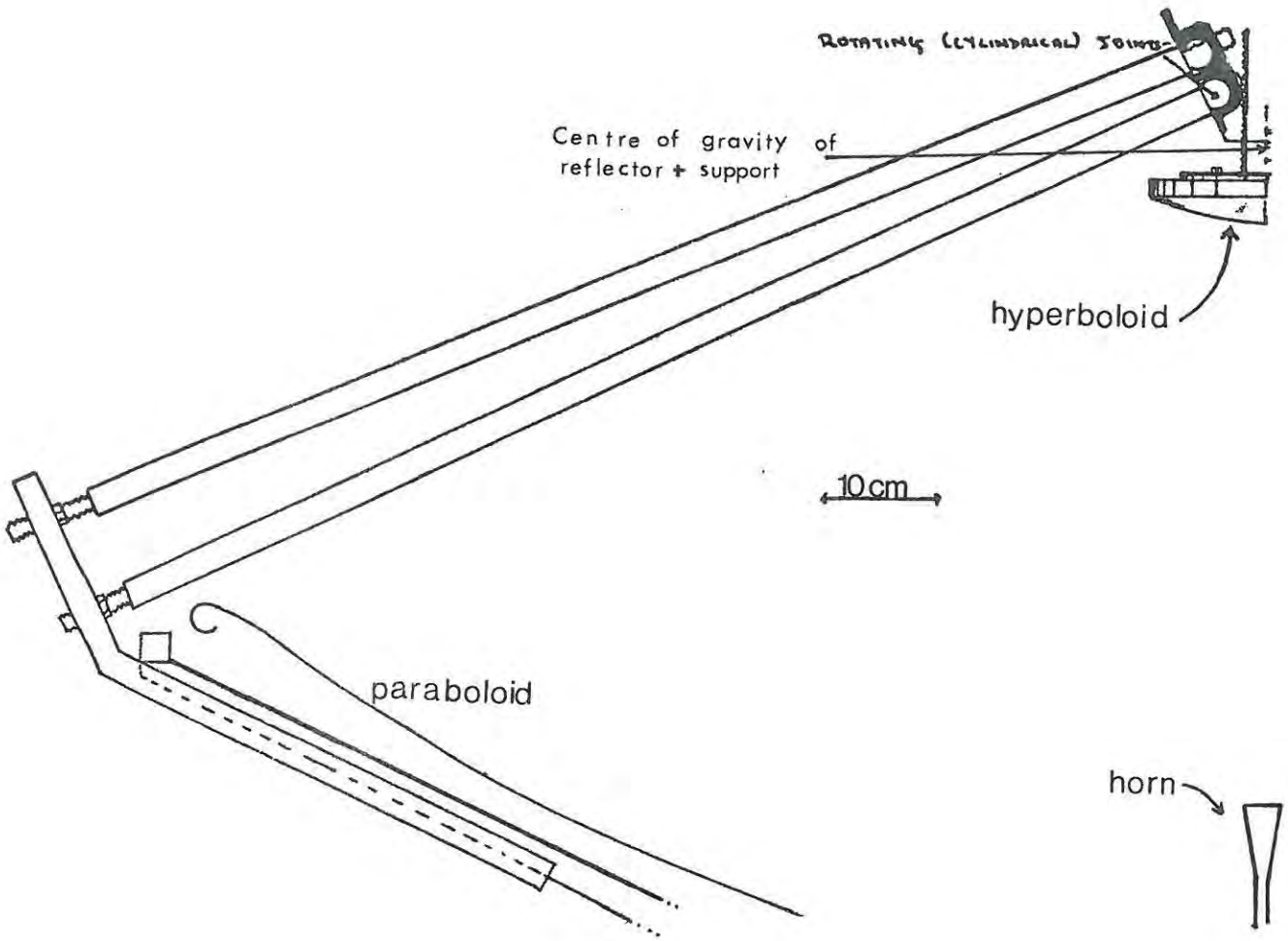

Figure 4.3 Hyperboloid Subreflector support

The amount of tilting of the subreflector is given by (Appendix A.2)

$$(dy/dx)_{x = \ell} = -T\ell/ EI. \qquad 4.10$$

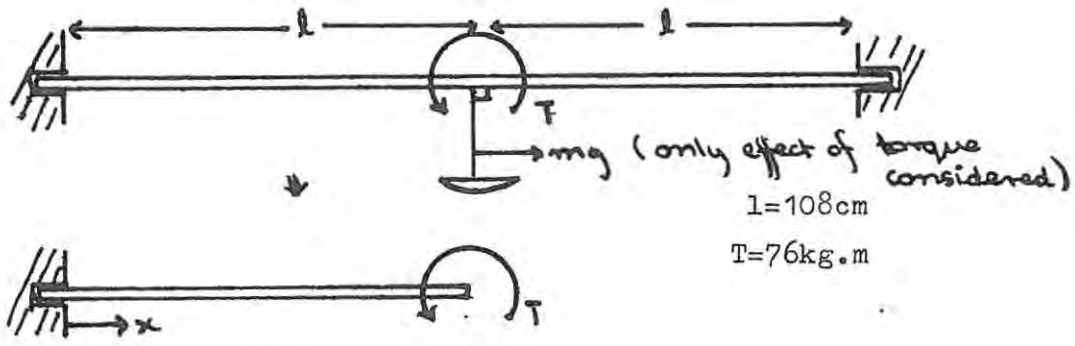

$y(x=0) = 0 = y(x=l)$

$dy/dx(x=0) = 0$

Figure 4.4. Mathematical model of subreflector support flexing

The value of E, Young's modulus was obtained from tables ($7{,}38 \times 10^5$ kg cm^{-2} for aluminium alloy), and I was evaluated from the relevant formula (Kotz 1973) to be 1,43 cm^3. The expected value for $(dy/dx)_{x = \ell}$ is $7{,}76 \times 10^{-3}$, which results in a lateral movement of the subreflector surface of 1,2 mm, which is negligible. This movement is halved by the pair of rods opposite to the two considered above.

4.4 The construction of the support framework

The model telescope in figure 4.1 was used, together with accurate measurements of the telescope bearing mounts, to produce the design diagrams for the antenna framework. The detailed diagrams used by the workshop in the construction of the framework appear as figures B4.1 to B4.4 (appendix B). Several design features which were included during the construction are discussed briefly.

The front-end-supporting plate was mounted, as discussed, on

a framework with a machined face. The aluminium plate and the framework were attached by means of bolts, through slotted holes, so as to allow the plate three mutually perpendicular degrees of freedom. This allows both coaxial alignment of the feedhorn with the paraboloid symmetry axis, and its focussing. The hyperboloid also had these three degrees of freedom. Two of these degrees of freedom were allowed by mounting the flat back-plate of the hyperboloid ~~to~~ onto a second plate, with the bolts passing through large holes in the second plate. These large holes allow lateral movements of the hyperboloid. Focussing of the hyperboloid is achieved by means of the threaded pipe connecting the second plate to the hyperboloid support (figure 4.3). Tilting of the hyperboloid is achieved by altering the supporting length of the aluminium rods (figure 4.3) by means of the locknuts.

A removable steel block was mounted with locating pins on the aluminium plate for lining-up. This block had a cylindrical hole in it the size of the hole in the paraboloid, and concentric with the central axis of the ~~hord~~ horn feed position. A cylindrical brass plug inserted in the hole in the steel block, and protruding above the level of the bottom of the paraboloid, was used to locate the position of the paraboloid hole. A narrow hole was also drilled through, and concentric with, the brass plug. A laser beam directed through this hole would locate the subreflector centre position.

Figures 4.5 and 4.6 shows the completed support structure on the telescope stand. A lead counterweight was later hung underneath the front-end box to allow more room inside this box, and to provide greater leverage.

The remainder of the work completed involved the design and construction of electronic circuits; this is described in the two following chapters.

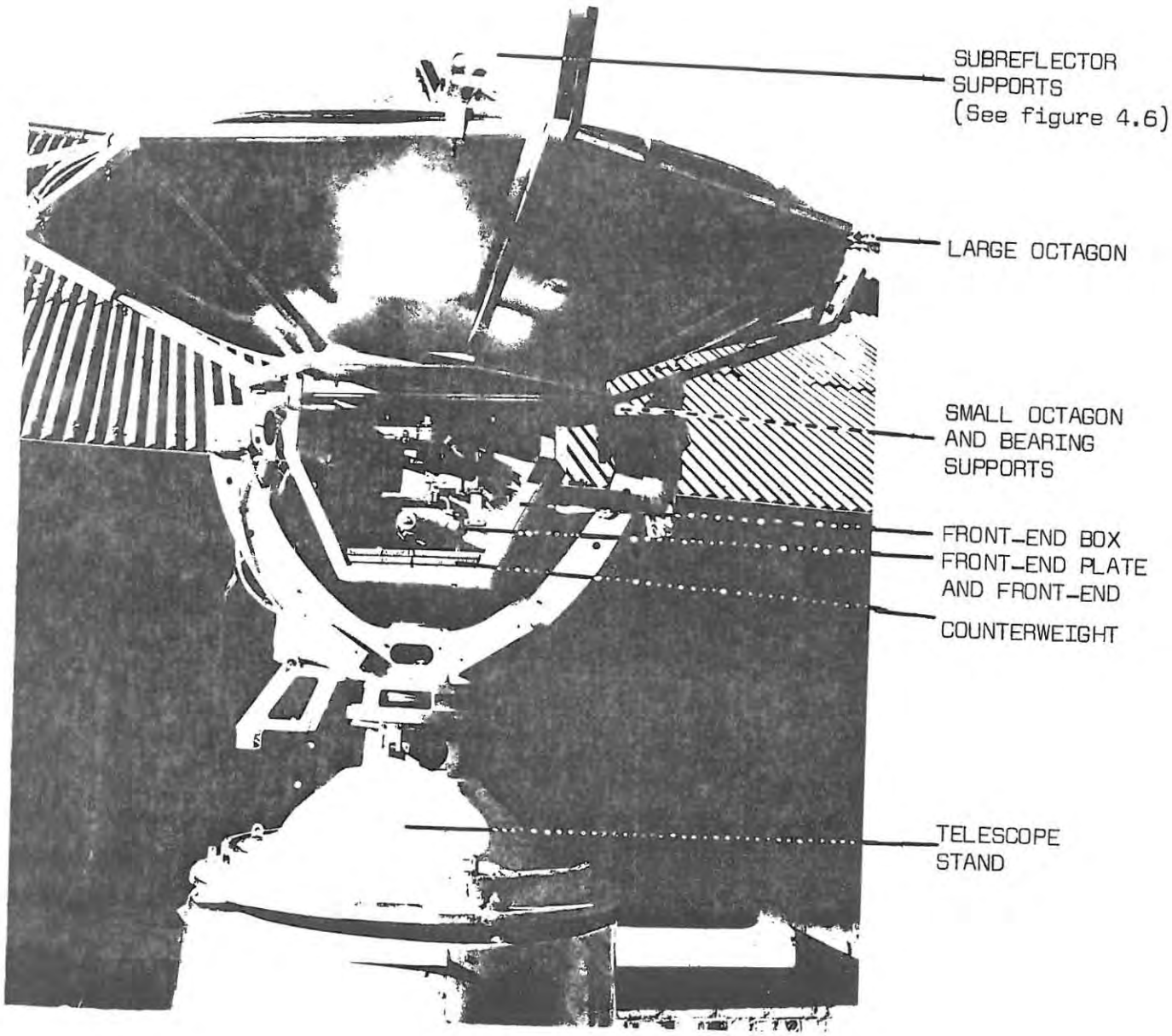

Figure 4.5 The completed support framework

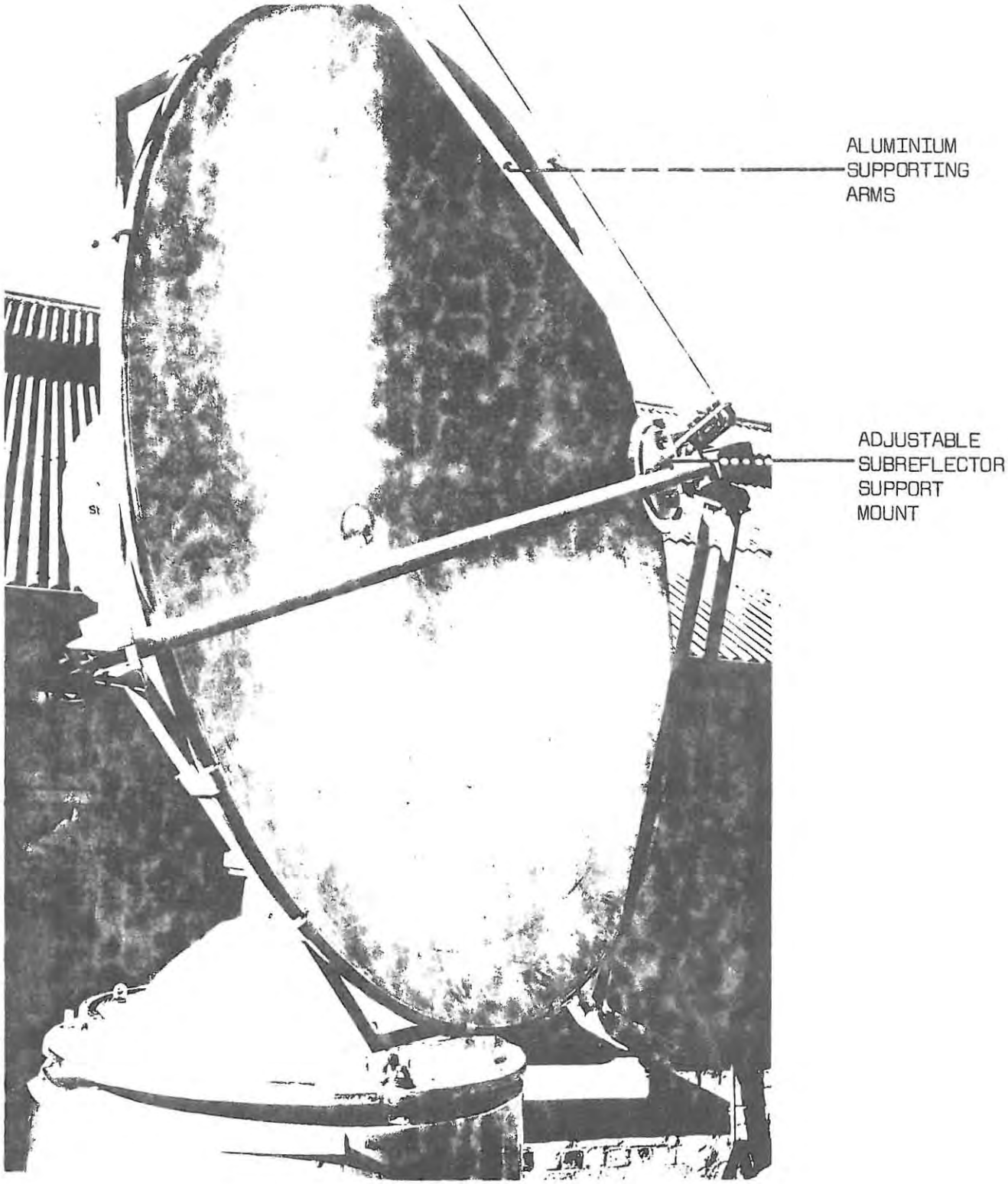

Figure 4.6 Close-up of the two reflectors, and the sub-reflector support.

CHAPTER V

THE INTERMEDIATE FREQUENCY AND DISTRIBUTION AMPLIFIERS

5.1 The 30MHz intermediate frequency amplifier

5.2 The 100-output buffer

5.2a The "attenuating and matching" distribution amplifiers

5.2b The eleven wideband amplifiers

5.2c Construction of the buffers

CHAPTER V

THE INTERMEDIATE FREQUENCY AND DISTRIBUTION AMPLIFIERS

The 25 MHz - 35 MHz amplifier, and the 100 channel buffer, shown in figure 2.5a (page 28) were both designed during the period of this thesis. The amplifier was not used, as it was replaced by a commercial model with better specifications. Its construction is, however, described briefly in the first section of this chapter. The second section (5.2) deals with the construction of the buffer.

5.1 The 30 MHz intermediate frequency amplifier

The gain required of the i.f. amplifier is determined by the mixer output power and the power needed to drive the detectors. This gain had to be evaluated before the amplifier could be built; this evaluation is described first.

If the factor t (in equation 2.4, page 16) is assumed to be unity for the mixer, then its output noise power is given by equation 2.1 as - 157 dB, in the bandwidth of 50 KHz of the individual spectral-line channels. The output noise power from the preamplifier attached to the mixer is - 122 dB, as it has a gain of 35 dB. The detectors require 1 mW or - 30 dB of noise power to function properly. Of the remaining amplification needed between the preamplifier and the detectors, 92 dB, a gain of 65 dB was to be supplied by the i.f. amplifier, and the remaining 27 dB by amplifiers in each of the 100 channels. It was decided to build a bandpass i.f. amplifier with a centre frequency of 30 MHz, and with a bandwidth of 10 MHz, to allow for a constant gain over the 5 MHz bandwidth of the spectral line receiver. It was also decided to incorporate an automatic gain control into the amplifier; this would necessitate a maximum gain in excess of 65 dB to allow the gain control to operate efficiently.

The i.f. amplifier block diagram appears in figure 5.1. The design of the six-stage tuned amplifier (shown in detail in figure

B5.1, appendix B) was based on a 45 MHz amplifier built at Cambridge University. This amplifier stage has a gain of 57½ dB from 26 MHz to 34 MHz. Further gain is provided by the 23 dB gain broad band

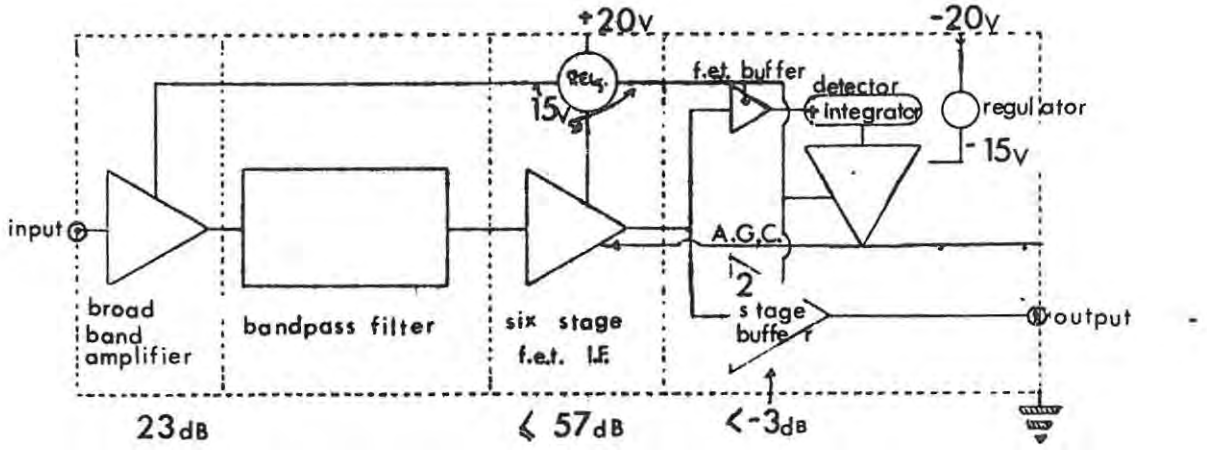

Figure 5.1 The 25 - 35 MHz i.f. amplifier with >65 dB gain

amplifier at the input (figure 5.1). The output of the tuned amplifier is fed to two buffers, one of which provides the 50 ohm impedance output to the distribution amplifier. The other buffer feeds a detector and integrator to provide the automatic gain control signal for the six stage amplifier.

Because of difficulties encountered during the construction of the i.f. amplifier, a commercial model was ordered. The difficulty found was that for large changes in the input voltage, the automatic gain control altered the individual gains of the six field effect transistor stages differently. These stages were stagger tuned as proposed by Fisher(1966), and so the amplification change over the band wasn't uniform. The commercial model arrived while this problem was being investigated, and was used because of its high gain (88 dB over 10 MHz), low noise, and excellent stability when controlled by its automatic gain control input. The model shown in figure 5.1 was abandoned in favour of the commercial i.f. amplifier.

5.2 The 100-output buffer

The buffer was mentioned in section 2.6. As can be seen from figure 2.5a (page 28), it is fed by the 30 MHz i.f. amplifier discussed in the last section, and feeds the 100 channels of the spectral line receiver. The various stages in the design of the buffer are discussed in this section.

The task of the buffer is to provide 100 isolated outputs to feed the 100 channels, with 50 ohm impedances to match that of the coaxial feeder cable. It is necessary to provide isolation between these outputs, so that the local oscillators in individual channels cannot affect the input signals of the other channels. The buffer consists of 100 identical stages, which contain attenuators to provide the isolation, and feedback amplifiers to provide further isolation and output impedances of 50 ohms. Since the 100 individual stages are preceded by attenuators, several amplifying stages are used to compensate for the resulting attenuation.

The 100 spectral line channels are arranged, ten in a row, in ten heated and thermally stabilised trays. It was decided to locate a ten-output buffer in each tray to feed the ten channels in that tray, and a further "master" buffer in an eleventh tray to feed the ten buffers. The block diagram of the buffer, consisting of the master buffer and ten buffers identical to it, is shown in figure 5.2a. It can be seen that each of the eleven buffers in turn consists of a wideband amplifier feeding ten identical "attenuating and matching" distribution amplifiers.

5.2a The "attenuating and matching" distribution amplifiers

The design of the 100 distribution amplifiers was determined by the expected input and output voltage levels, and the required frequency response. They must supply an output voltage of 100 mV to the channels, and have a flat frequency response up to 35 MHz or higher.

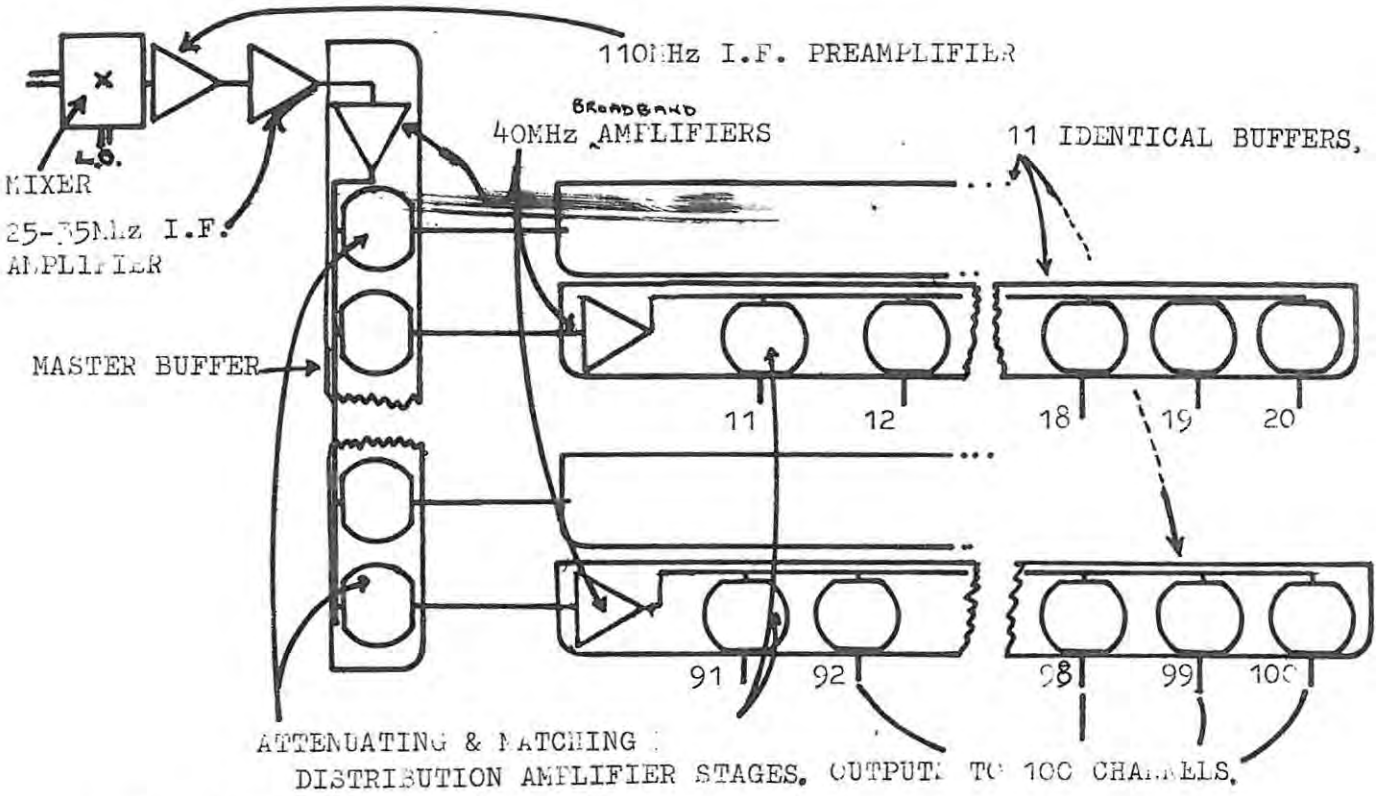

Figure 5.2a Spectral line receiver i.f. buffer

The proportion of noise introduced by the ten feeder cables, between the master buffer and the ten buffers in trays, is likely to be less if large signals are fed along these cables. The value chosen for the signal voltage level in these cables is 1 V peak-to-peak, which sets a lower limit on the required dynamic range of the buffer stages. The 40 MHz broadband amplifiers in each buffer feeds 10 distribution amplifier stages in parallel. For this to be an efficient process, the output impedance of the amplifier must be at most a half of the combined input impedances of the ten stages. A value of 50 ohms or lower was selected for the amplifier output impedance. This sets a lower limit on the input impedances of the ten distribution amplifier stages of ~~4k ohm~~ 1 kilo ohm, so that their combined input impedance is 100 ohms or more. The last criterion for the distribution amplifier stages was one of cost (as 110 of these were necessary).

Several distribution amplifiers were tested; the one chosen is shown in figure 5.2b. This buffer stage has an almost flat frequency

response from 25 MHz to 35 MHz, and a dynamic range of 1,4V. Its forward attenuation is 3x, and is controlled by the variable resistor R_2, while its reverse attenuation is 12x. The attenuator, consisting of the resistors R_1 and R_2 and the input impedance of transistor T_1 feeds the feedback amplifier, consisting of transistors T_1 and T_2 and

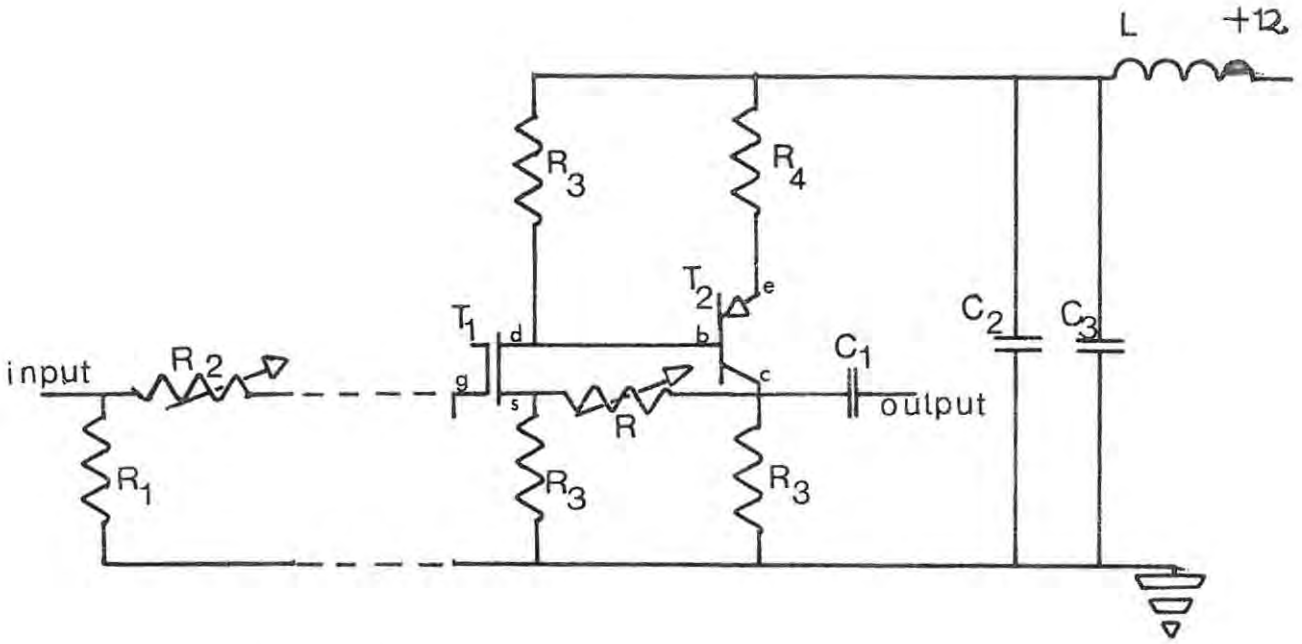

Figure 5.2b Design of a single distribution amplifier stage. (The component values are given in figure B5.2, appendix B.).

their biasing resistors. The resistor R controls the feedback fraction, and allows the output impedance to be controlled between 40 ohms and 65 ohms. (The input impedance is 1,5k ohms.) The power supply filter consisting of the coil L_f and the capacitors C_2 and C_3, isolates the supply lines between the stages. (There are two such filters between any two stages). The coil L consists of a few turns of wire on a ferrite bead capable of operating efficiently at 30 MHz, while two different types of capacitor were used to give a wide frequency response. The passive attenuator at the input of each channel attenuates signals by a factor of two in the forward direction, and ten in the reverse direction. The total attenuation or isolation factor, in the reverse direction between the channel

and the input to the distribution amplifier stage feeding it, is thus 120. The isolation factor in the forward direction (of the signal) is 6, due to the attenuations of 3x in the distribution amplifier, and 2x in the channel.

5.2b The eleven wideband amplifiers

It was mentioned in section 5.2a that the output impedance of the wideband amplifiers, each of which feeds 10 distribution amplifier stages, must be 50 ohms or lower. The input impedance of these amplifiers must be 50 ohms to match the cable impedance.

The circuit selected for the amplifier stage uses a linear integrated circuit, and is shown in figure 5.3. The input attenuator (consisting of the resistors R_7, R_8 and R_9) has an input impedance of

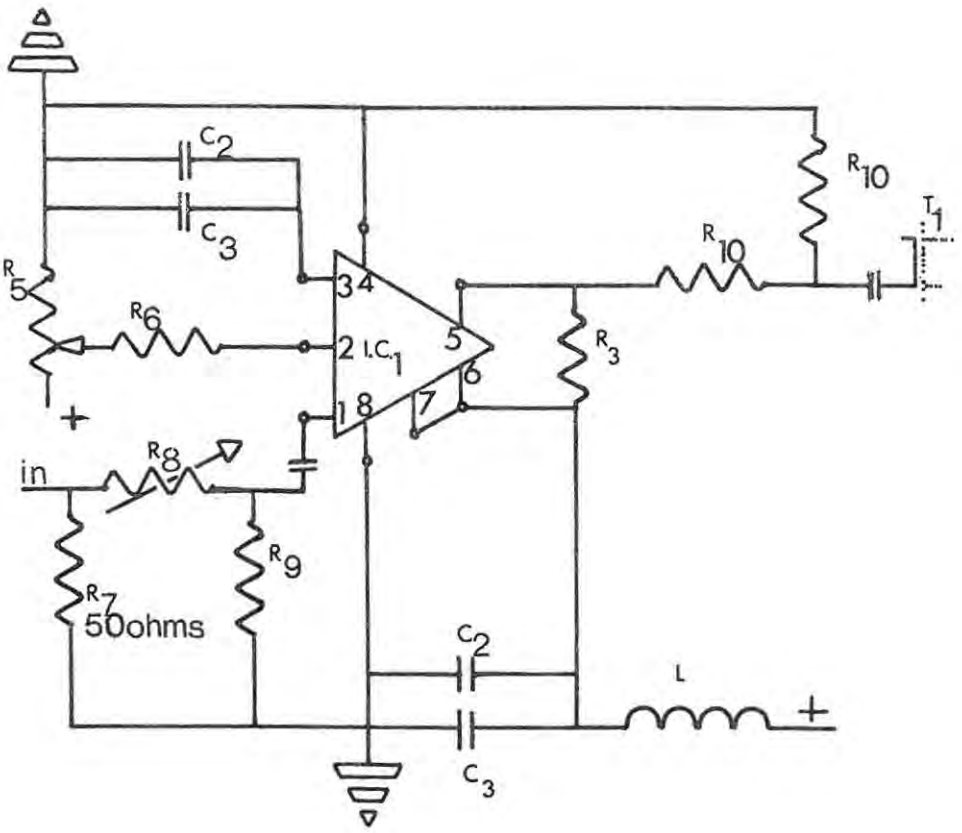

Figure 5.3 40 MHz high gain amplifier. (Component values are given in figure ~~B5.4~~ B5.a, appendix B.)

nearly 50 ohms, a forward attenuation of between 10x and 100x, and a reverse attenuation of five times the forward attenuation. The variable network R_5, and R_6, controls the voltage on pin 2 of the integrated circuit, and so controls its gain. The maximum value of the gain is 30. An LC circuit is again used to isolate the power supply. The output impedance at the output on pin 5 of the integrated circuit is 350 ohms, which is far too high for this output to feed the ten buffer stages (with a combined input impedance of 150 ohms). This impedance of 350 ohms is effectively reduced by adding a low output-impedance stage to the output. The stage chosen was the feedback stage of figure 5.2 (excluding the input resistors R_1 and R_2 at the input, on the left of figure 5.2b). The manner in which the broadband amplifier is attached to the gate of the transistor T_1 is shown in figure 5.3. The wideband amplifier, together with the added feedback stage, now has a minimum output impedance of 40 ohms, which is sufficiently low for driving ten distribution amplifier stages in parallel.

It was noted in the previous section that the forward and reverse isolation factors between the input to a channel, and the input to the buffer stage feeding it, are 6 and 120 respectively. The isolation factors between two channels in the same tray is thus 720. The isolation between individual trays is at least ten times this figure, due to the isolation by the first ten-stage buffer (of 720x again), and due to the attenuation factor of the attenuator at the input of the amplifying stages (10 or more).

5.2c Construction of the buffers

The buffer circuits were built up on double sided copper-clad printed circuit boards. The copper sheet on the side facing the components was used as an almost continuous ground-plane. The connections between the components were etched on the reverse side of the boards; these connecting strips were made narrow to avoid capacitive coupling between them. The ten distribution amplifier

stages were mounted on a single board, and the wideband amplifier and its impedance-matching stage on another. These boards were both placed in an aluminium box, with an aluminium partition between them. This box has a well fitting lid to completely shield the inside. The signals are fed to, and from, the buffer with 50 ohm impedance coaxial connectors. The regulated voltages are fed through inductances and feed-through capacitors to both boards. A completed buffer can be seen in figure 5.4.

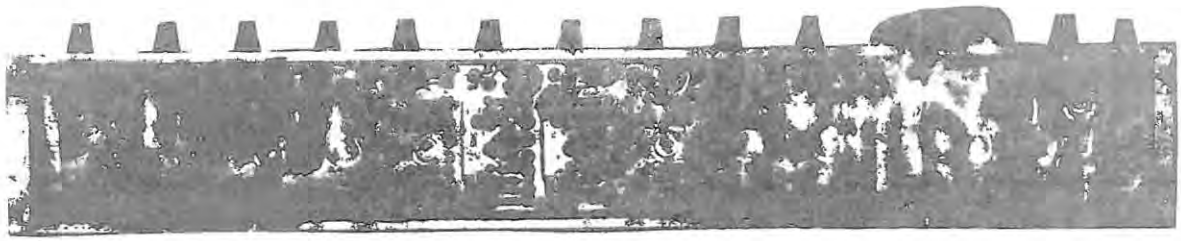

Figure ~~6.3~~ 5.4 A completed buffer

The isolation factors, the frequency responses, and the dynamic ranges quoted above are the result of measurements on the buffer in figure 5.4. Care had to be exercised to take into account the capacitive impedance of the oscilloscope probe used for measurements. This buffer has also been successfully used to feed ten channels in one tray. Tests for interaction between channels in this configuration yielded negative results. The design of the buffer is thus acceptable, and others are being constructed to feed the rest of the channels.

CHAPTER SIX

THE DIGITAL CONTROL SECTION

6.1 The executive timing control

- a The integration-run start, ~~stop~~, halt, restart, and stop controls
- b The receiver controls

6.2 The data processor

- a The data processor "memory signal input" logic
- b The buffer memory and punch control

6.3 Construction and testing of the data processor

Chapter VI

The Digital Control Section

The general operation of the digital control section, consisting of the "executive" and the "data readout" shown in figure 2.6, was discussed briefly in section 2.6 (page 29). The details of their operation are given below.

6.1 The executive timing control

The block diagram is shown in figure 6.1 (overleaf). The unit was built on six printed circuit (P.C.) boards, and can be controlled by the paper tape reader logic (figure 2.6), or by the controls on the front panel shown in figure 6.2. The light emitting diode (l.e.d.) displays on the front panel indicate the mode of operation of the executive. The executive controls the starting of integration runs, the phase synchronous modulation of the front-end and the channel detectors, and the length of integration runs. At the end of each integration run the executive stops the modulation switching, and allows the data readout system to digitise and store the channel output voltage value. When this process is completed, the executive resets the channel outputs to the ground potential, and restarts the next integration run. The executive also controls the i.f. attenuator (figure 2.5ø, page 28). The operation of the executive is detailed below.

6.1a The integration-run start, halt, restart, and stop controls

There are two methods of starting the executive. The first method, the "full start" controlled by the circuit board 5 (figure 6.1), first allows the digital values of the two frequencies, of the crystal oscillator used in frequency switching, to be entered into the data readout buffer memory. (It will be recalled that the frequency of the 22 GHz Gunn oscillator is stabilised by a harmonic of the crystal oscillator, in a phase-locked loop, and that the Gunn oscillator is frequency-switched by switching the crystal oscillator.) The first frequency value is stored in a counter, and entered into the memory

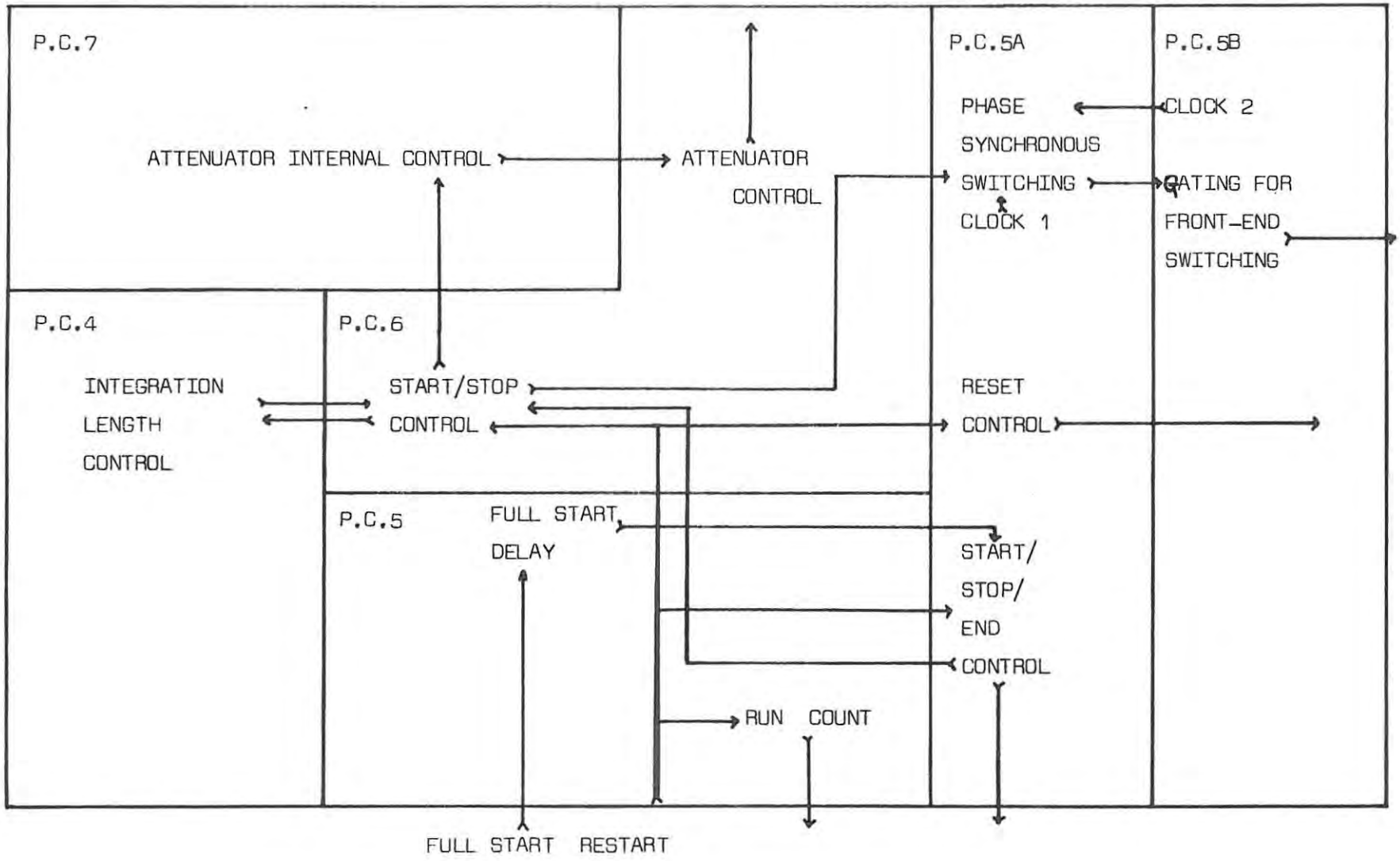

Figure 6.1 "Executive" control block diagram

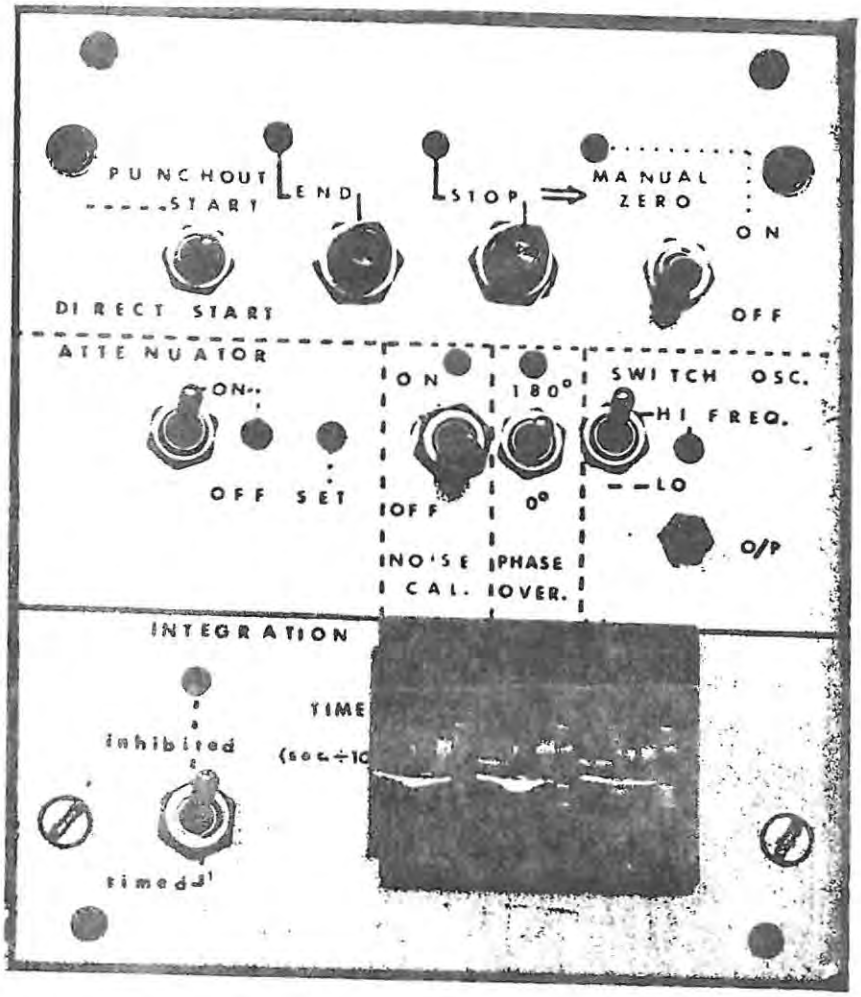

Figure 6.2 Front panel of the "executive" unit

when the "full start" mechanism is actuated, either by a front panel switch or by the paper tape reader logic. The executive then switches the crystal oscillator in the front-end to the second frequency, the value of which is entered into the buffer memory after a delay of 256 seconds. This delay allows the frequency to be counted to an accuracy of 8 decimal digits. The "housekeeping" information, consisting of the run number, the universal time, and the phase-modulation-mode information, are entered into the buffer memory after the second frequency value has been entered. The subsequent operation of the executive is the same for the "full start" as its operation when the "start" switch (figure 6.2) is

depressed. This latter operation starts the first of a series of timed integration runs via the start/stop logic circuitry on circuit board 6. This logic circuitry starts the run by starting the receiver modulation.

The length of the first, and subsequent, integration runs is controlled by the circuit board 4 (figure 6.1). The length of the run is set by the front-panel thumb-wheel switches (figure 6.2), or can be timed manually if the "timed/inhibited" switch is up. The start/stop logic halts a run by stopping the phase synchronous modulation of the receiver. The modulation is halted before the preset time if and when the output voltage of any one of the channels exceeds a certain value, which is selected to prevent saturation of the integrators. When the run is halted by one of the above methods, a pulse from the start/stop control initiates the data readout cycle, during which the channel output voltage values are digitised and stored in the memory of the data processor, in the manner described in section 6.2. At the end of the data readout cycle the executive is restarted by the data processor. During the restart cycle the outputs of the channels are grounded by the reset control on the circuit board 5A; and the housekeeping information for the following run is entered into the memory. (A counter on circuit board 5 counts the number of 'restarts' and serves as a 'run number' counter.) The next timed integration run is then begun, while the contents of the buffer memory are punched onto paper tape.

The executive can be stopped in one of two ways. The 'stop' switch on the front panel serves to stop the executive completely. Alternatively, the 'end' switch may be used. This stores the 'stop' command in a flip flop until the run, the data readout cycle, and the housekeeping readout cycle are completed, and only then stops the executive. During the 'stop' cycle all counters are cleared, and all control flip-flops and gates are disabled. The 'stop' and 'end' commands may also be applied via control lines on a plug at the rear of the executive. When either command has been effected, the executive can be started again by one of the two start methods mentioned above.

The controls affecting the timing of the executive have been discussed. The method of control of the receiver switching is detailed in the next subsection.

6.1b The receiver controls

The three parts of the receiver operation controlled by the executive are the phase synchronous modulation, the grounding of the channel outputs, and the i.f. attenuator switching, as discussed below.

The modulation of the receiver is controlled by circuit boards 6, 5A, and 5B. The circuitry on board 5B selects the type of front-end switching to be employed, whether beam, frequency, or/and Dicke (noise) switching. The front panel oscillator switch selects a high frequency oscillator for beam switching, and a 19 Hz oscillator for frequency switching, and at the same time gates the front-end signal to beam- and frequency-switch controls respectively. The ferrite switch controlling the calibrating argon gas noise source is switched synchronously with the beam- or frequency-modulation, when the front panel 'noise cal.' switch is on. The two modulation oscillators are very stable, and their outputs are passed through a divide-by-two flip-flop to ensure that the front-end spends exactly the same time on the source signal and the reference noise signal.

The relative phases of the front-end and the 100 channel switching (either in- or out-of-phase, see figure 2.1b, page 18) are controlled either manually by the 'phase override' front panel switch, or automatically when this switch is in the mid-position. The automatic phase control on the circuit board 5A reverses the relative phase, of the front-end and the synchronous channel switching, every run. This results in the channel output voltages due to the signal being positive every alternate run, and negative every other alternate run. The integrator drift will always increase the output voltages, and its effect is reduced by combining the run voltage values in pairs and subtracting the negative value in this pair from the positive one.

The channel outputs are grounded either before each run, as was mentioned, or when the 'manual zero' switch on the front panel (figure 6.2) is switched on.

The last part of the executive is the i.f. attenuator (figure ~~1.5b,~~ 2.5a page 28) control on the circuit boards 7 and 6. This logic circuitry switches the calibrating attenuator on for a run at a time, with a predetermined number of runs between such switchings. The paper tape reader logic (figure 2.6) presets the number of runs between switchings; the number is stored in a latch. The front panel attenuator switch can switch the attenuator on (indicated by a display light) at any stage, and can also disable the preset command.

The full logic diagram of the executive appears in the appendix (figure B 6.1, and B 6.2, appendix B). This logic diagram shows the circuit for the working version of the executive, and differs in many places from the original, as logic errors were discovered while the circuit was being built. The method of construction is detailed after the next section, in which the data processor is described.

6.2 The data processor

The data processor consists of two parts. The first part, the "memory signal input" section accepts analogue signals from the channel outputs, digitises them, and provides this information at a common output, with the digital "housekeeping" information. This common output is connected to the second part of the processor, consisting of the 500 word buffer memory, and the paper tape punch control logic. These two sections of the data processor are detailed separately.

6.2a The data processor "memory signal input" logic

The block diagram of the memory input circuitry is shown in figure 6.3.

The timing logic circuitry for the commercial analogue- to- 14 bit digital (a/d) converter is on the circuit board 20. This board also accepts analogue signals from the front panel of the data processor, shown in figure 6.4. The common analogue data bus line,

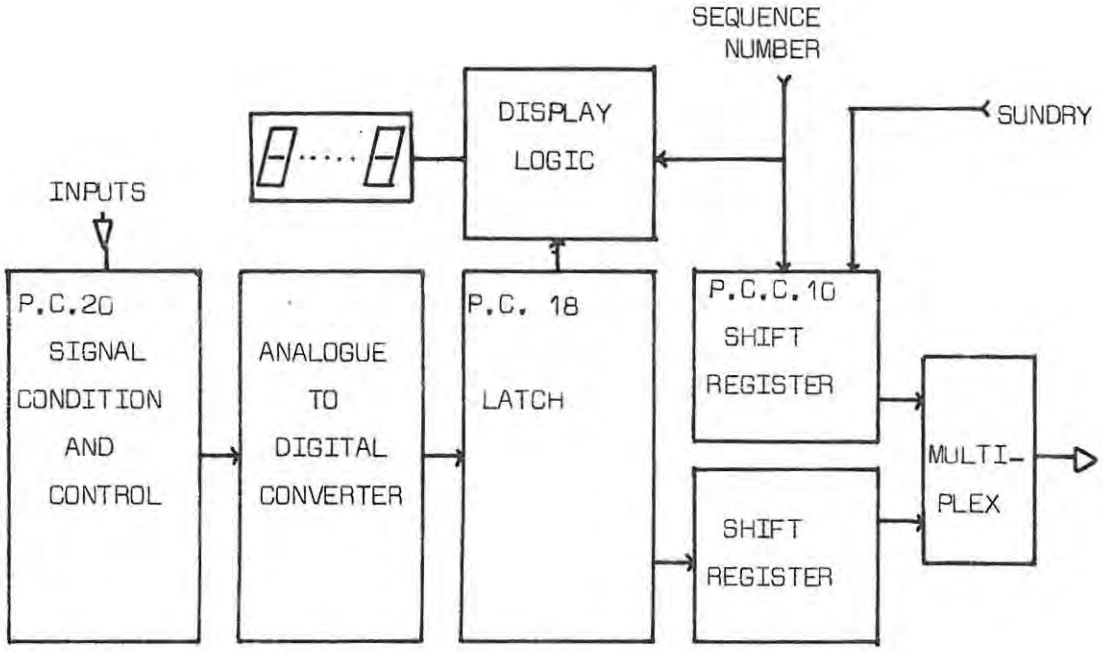

Figure 6.3 Memory signal input

from the outputs of the 100 receiver channels, is attached to the 'output channel' coaxial plug (figure 6.4). The signal from this plug is fed to the a/d converter when the 'source' switch is on 'internal'. The 'input' plug, selected by the 'external' position of the switch, provides a means of using the unit as an ordinary voltmeter, with the voltage being displayed on the 'volts D.C.' display. The a/d converter can convert analogue voltages up to $\pm$ 1,999v, while the channel output voltages are expected to reach $\pm$ 15v. A divide-by-ten attenuator, controlled by the 'volts' switch (figure 6.4), provides a 20v range for the digital voltmeter. During the channel data-readout cycle, a control line from the executive switches the divide-by-ten attenuator on, and the a/d converter input to the analogue busline, regardless of the state of the front panel

switches.

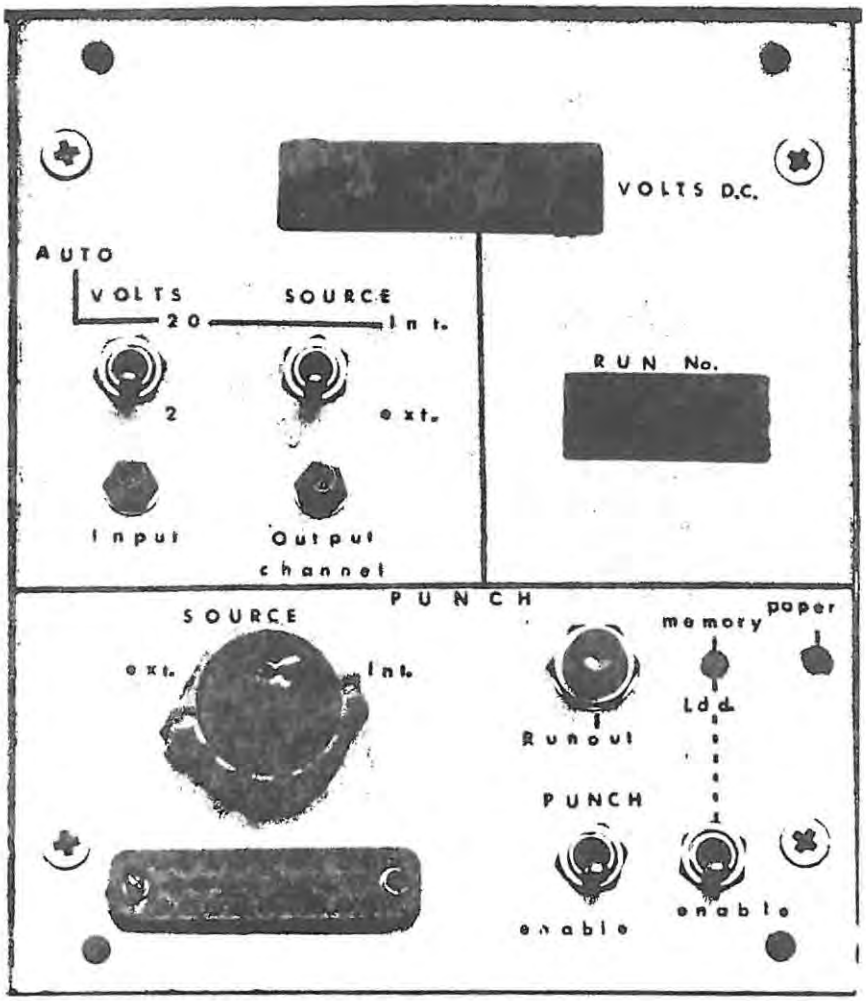

Figure 6.4 Data processor front panel

The input circuit board (20) provides a high input impedance buffer for the analogue signal, before feeding it to the convertor. It also provides a buffered output for a histrogram generator, which will sweep the busline sequentially between the channel outputs (during an integration run), and which will display the outputs in histogram form on an oscilloscope. If at any time one of the channel outputs exceeds a certain value, a voltage

comparator on board 20 will halt the executive to prevent saturation of that output, and the data readout cycle will begin.

A multiplex unit, controlled by the timing circuitry on board 20, switches the channel outputs sequentially to the analogue busline at the end of each conversion. The digital value from the converter is stored in the latch on board 18 (figure 6.3), leaving the converter free for the next conversion. The digital value stored in the latch is displayed continuously, by the display logic circuitry (figure 6.3), on the front panel 'volts' display (figure 6.4). The run number (from the executive) is also displayed on the front panel, by numbers from 0 to 99.

When the data from the channels is being read, the lower (parallel-to-serial) shift register in figure 6.3 stores the digital voltages in the latch, and presents them via the multiplex unit to the 500 word buffer memory. The multiplex unit has a five bit output: four of these bits are used as a data channel, while the fifth bit is used as a "data present" signal to the buffer. The other shift register chain (figure 6.3) is the "housekeeping" information source, and has its parallel inputs attached to the frequency- and universal time clock-counters and the modulation-mode information lines (labelled 'sundry' in figure 6.3), and to the sequence, or run-number, counter. The information in the second chain is entered into the memory, via the multiplex unit before each integration run, on the command of the executive.

6.2b The buffer memory and punch control

The block diagram of the first-in first-out buffer, and the punch circuitry, is shown in figure 6.5.

The 500 word recirculating memory and part of its control circuitry are located on the circuit board 13. The 5 MHz clock on board 10 drives the memory, and provides timing pulses for loading data to it, and offloading data from it. The input-output logic (on three identical P.C. 9 boards) enters information to the memory as soon as it appears at the multiplex output (figure 6.3), and feeds the information from the memory asynchronously to the punch

logic, at the punching rate of 20 words per second. The decoder on board 16, and the parity generator on board 14 code the information into the computer readable ~~ASC II~~ ASCII format. The numerical values in the buffer are converted to the ~~ASC II~~ ASCII numerics, while the numbers 10 to 13 (used for the "+", "-", and housekeeping characters) are coded as "+", "-", "*", and "newline" respectively.

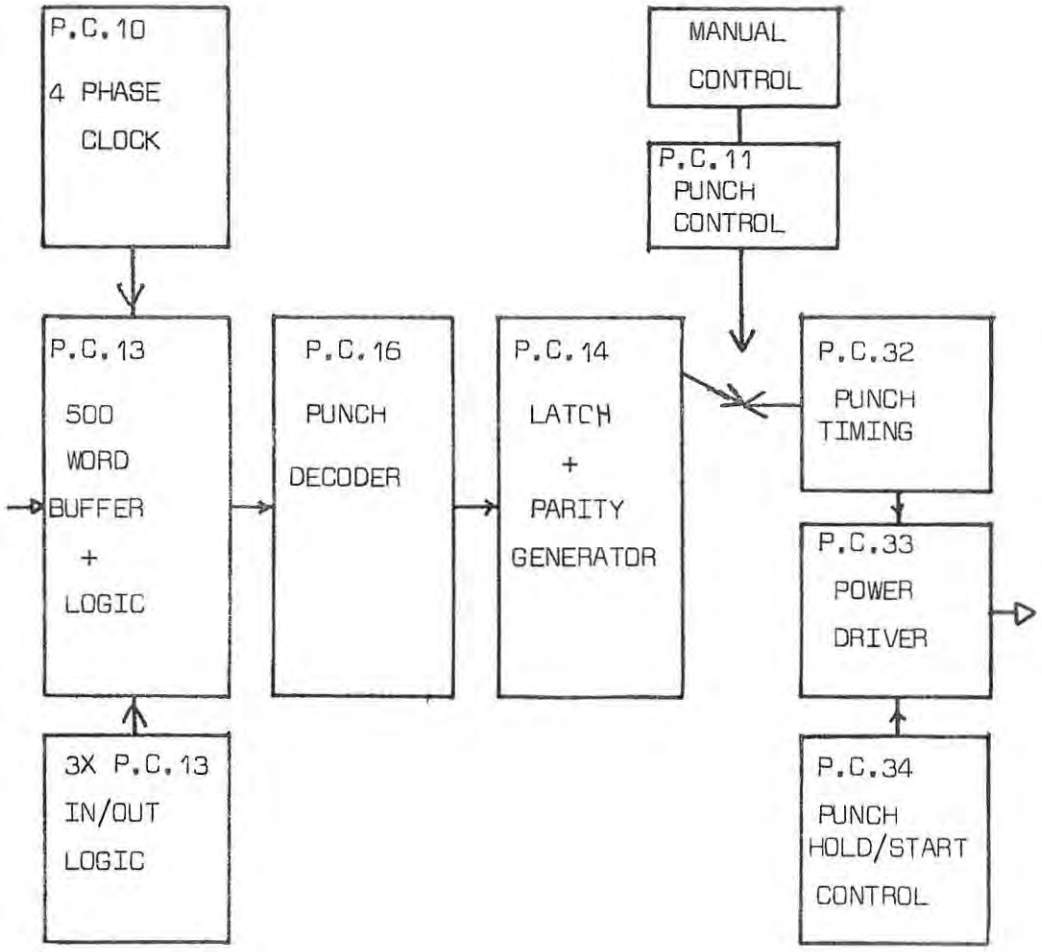

Figure 6.5 Buffer, and Punch Control

The latch on board 14 stores the character to be punched. If the "punch source" switch following this (figures 6.4 and 6.5) is switched to "internal", the punch timing circuitry will punch the character in the latch, via the 8- line power driver circuitry.

When each character has been punched, the punch timing logic loads the latch with the next character and starts the next punch cycle. If the punch source switch is turned to "external", the punch can be controlled manually via the punch control logic and circuit board 11. The manual control is located in a box attached to a long lead, which is plugged into the front-panel multi-socket plug. An operator can punch any ~~ASC II~~ ASCII character singly by selecting the code with thumb-wheel switches, and pressing a "punch" button. This enables the operator to mark, and later to identify, particular events or runs with any codes.

The punch hold/start control board 34 switches the punch motor off when the data in the memory has been punched out, after waiting 20 seconds in case data is loaded into the memory within this period. If information is loaded into the buffer in this period, the motor is left running and punching can begin immediately. If information is loaded while the motor is off, it is switched on and allowed to reach operating speed before the punch is enabled. A light transmitter-receiver combination senses if the paper tape is finished, and stops the motor and punch when this condition is reached.

There are three further controls on the front panel (figure 6.4) which have not been described. The runout button allows a length of blank paper tape to be fed as a leader. The "punch enable" switch can enable the punch to operate, or disable it, while the "memory enable" switch can prevent information transfer to or from the memory, so that information in the memory can be retained indefinitely. The "memory loaded" indicator signals a full memory condition, while the "paper" indicator shows when paper tape has run out.

The full logic diagrams of the data processor appear in appendix B (figure B6.3 to B6.14). The constructional details are given briefly in the next section.

6.3 Construction and testing of the data processor

The layouts for the double-sided printed circuit boards, on which the components for the digital section were mounted, were designed on transparent plastic sheeting. These layouts were reduced photographically

to the correct size, and used to produce the circuit boards using a photosensitive etching technique. Each circuit board plugs into a 50-pin socket, mounted in a tray. Connections between sockets were made underneath the two trays used, and connections external to the trays were made with the sockets mounted at the rear. The two trays used are shown in figure 6.6, mounted in a sliding rack mount. The control panels, shown also in figure 6.2 and 6.4, are shown at the front. The power supply regulators are mounted at the rear of each tray.

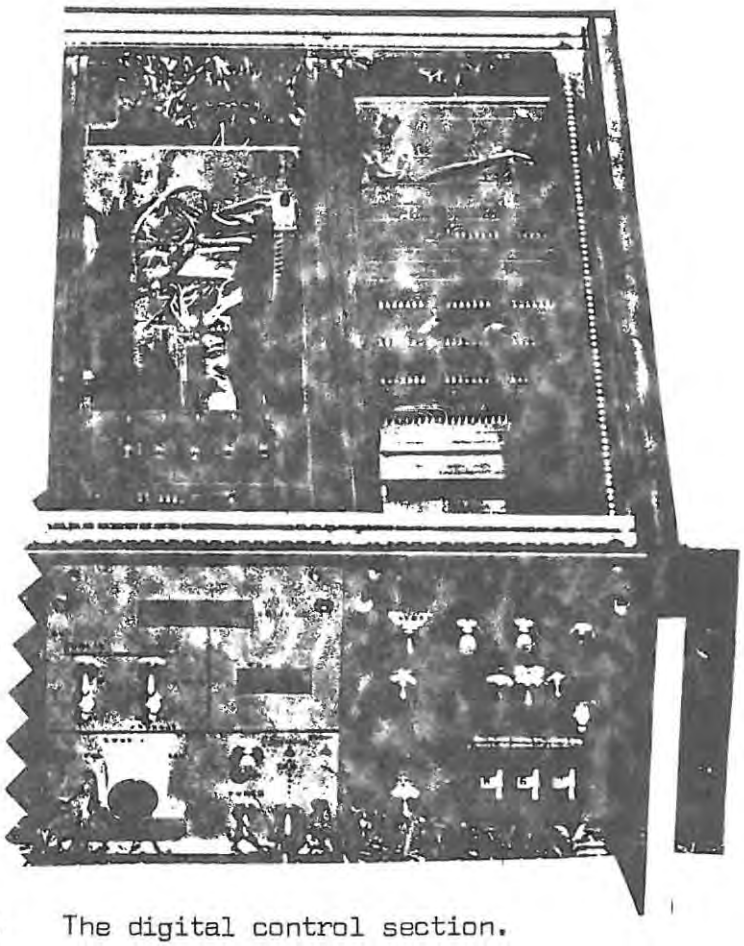

Figure 6.6 The digital control section.

The various circuits detailed in appendix B6 were tested logically, and corrected and redesigned where necessary. The main difficulty encountered during testing was the detection of short pulses, especially when several of these occurred in quick succession.

The executive timing control unit works according to the design specifications, and has already been used to control the switching of ten test channels.

The data processor was not completely working at the time of writing. The "memory signal input" of figure 6.3 worked as expected, but the punch timing (board 32) in figure 6.5 hadn't been completely checked, although the rest of the circuitry in figure 6.5 worked. [The original circuit for the punch timing has been completely redesigned to prevent spurious characters being punched occasionally.]

When the punch timing board has been checked, the data processor can be linked up to the ten test channels for initial spectral line and continuum observations.

CHAPTER SEVEN

CONCLUSIONS

The survey of the properties of interstellar water maser sources in chapter one, and the viability study of the 22 GHz radiometer being built at Rhodes, have shown the extreme usefulness of an instrument of this size for making observations from South Africa.

The front end of the radiometer described in chapter two (section 2.6a), has been assembled, and tested in the continuum and spectral line modes with a second 22 GHz Gunn oscillator simulating a line source. A buffer and ten of the receiver channels were used successfully during the spectral line mode test. The Cassegrain antenna is fully assembled, and awaits precise alignment of the feed system. The executive unit, as previously mentioned, has been successfully used for testing the receiver. The data processor, except for the paper tape punch interface circuit, operates as planned. It is expected that observations of sources will be made in the near future.

Appendix A

A1. General Radio Astronomy Theory

This section, in which the concepts of "brightness", "spin temperature", and "flux density" are defined for radio sources, has been included to make the thesis more comprehensible to the non specialist. More complete descriptions of these parameters appear in Kraus (1968), Kerr (1968), Baars (1970), and Mezger (1972).

Brightness-, Spin-, and Kinetic-temperature

The brightness temperature, $T_{b\nu}$, of a black-body radiator is related to the surface brightness or specific surface intensity, B_ν, of this source. In the centimeter-wavelength region, where the Rayleigh-Jeans approximation to the Planck black-body law holds, the relationship is

$$T_{b\nu} = B_\nu \, c^2/2k \, \nu^2. \qquad \text{A1.1}$$

$T_{b\nu}$ can be seen to depend on the frequency of the radiation, ν, and the values of c, the speed of light, and k, Boltzmann's constant. H_2O and OH maser sources aren't black-body radiators, and so the measured effective brightness temperatures - exceeding 10^{13} K- bear no relation to the kinetic temperatures of these sources.

The spin temperature or excitation temperature, T_s, of a gas is defined by the Boltzmann equation for a transition between two hyperfine sublevels,

$$N = C \exp\left(- h\nu/kT_s\right). \qquad \text{A1.2}$$

N is the 'population ratio' of the two hyperfine energy levels involved in the transition, while C is the ratio of their

statistical weights, and $h\nu$ is the energy difference between them. T_s is thus a measure of the population of the higher level with respect to the lower. For most transitions of galactic disc gases, the collisional deexcitation rate of the upper level far exceeds that of spontaneous deexcitation, and the spin temperature is approximately equal to the kinetic temperature. However, OH and H_2O masing sources will have low spin temperatures due to the radiation-dominated population distributions.

If τ_ν is the optical depth to infinity along a line of sight, and T_s is constant along this line of sight, it can be shown that for an emitting gas characterised by τ_ν and T_s,

$$T_{b\nu} = T_s \left(1 - \exp\left(-\tau_\nu\right)\right). \qquad \text{A1.3}$$

This equation is frequency-dependent. The frequencies that must be considered in the line emission and absorption are determined by the line bandwidth.

The source flux density S_ν is obtained by integrating the brightness B_ν over the solid angle Ω_s subtended by the radio source,

$$S_\nu = \int_{\Omega_s} P_{\eta\nu}(\theta, \Phi)\, B_\nu(\theta, \Phi)\, d\Omega. \qquad \text{A1.4}$$

The polar coordinates θ, and Φ, are referenced to the antenna, and $P_{\eta_\nu}(\theta, \Phi)$ is a normalised, frequency-dependent measure of the antenna response to radiation from the direction (θ, Φ). The flux unit, f.u., is defined by 1 f.u. = 10^{-26} Wm^{-2} Hz^{-1}.

The spectral power received by a radiometer is

$$W_\nu = \frac{Ae}{2} S_\nu \qquad \text{A1.5}$$

where Ae is the effective ~~aperture~~ aperture area of the antenna. The factor of $^1/2$ takes into account the fact that most antennas receive linearly polarised waves.

Appendix A2.

Derivation of Equation 4.10

As is shown in figure 4.4, it was assumed that the weight of the aluminium rods supporting the hyperboloid is neglected. The hyperboloid exerts a torque T at the end of the rod being considered, which is fixed at the other end. These conditions are the boundary conditions, which are expressed mathematically as:

$$y(o) = o \qquad \text{A.2.1}$$

(as the rod is fixed at x = o),

$$y(1) = o \qquad \text{A.2.2}$$

(as the rod is weightless),

$$\left.\frac{dy}{dx}\right|_{x = o} = o \qquad \text{A.2.3}$$

(as the rod is fixed at x = o, and is weightless).

The equations defining the state of the rod are (Pipes 1946):

$$\frac{d^4y}{dx^4} = \frac{W(x)}{EI} = o \qquad \text{A.2.4}$$

where W(x) is the weight per unit length of the rod (= o), E is Young's modulus, and I is the second moment of elasticity of the rod;

Hence by integration,

$$\frac{d^3y}{dx^3} = A \qquad \text{A.2.5}$$

where A is constant. But

$$\frac{d^3y}{dx^3} = \frac{F(x)}{EI} = 0 \qquad \text{A.2.6}$$

where the vertical shear force $F(x)$ is zero for all x;

Again, by integration

$$\frac{d^2y}{dx^2} = C, \qquad \text{A.2.7}$$

and

$$\frac{dy}{dx} = Cx + B \qquad \text{A.2.8}$$

But

$$\frac{d^2y}{dx^2} = \frac{T}{EI} \ , \qquad \text{A.2.9}$$

and using A.2.3, the angle by which the unfixed end of the rod is tilted can be derived from the slope of this end,

$$\left.\frac{dy}{dx}\right|_{x = l} = -\frac{Tl}{EI} \qquad \text{A.2.10}$$

which is equation 4.10. The negative sign arises from T being anticlockwise.

APPENDIX B

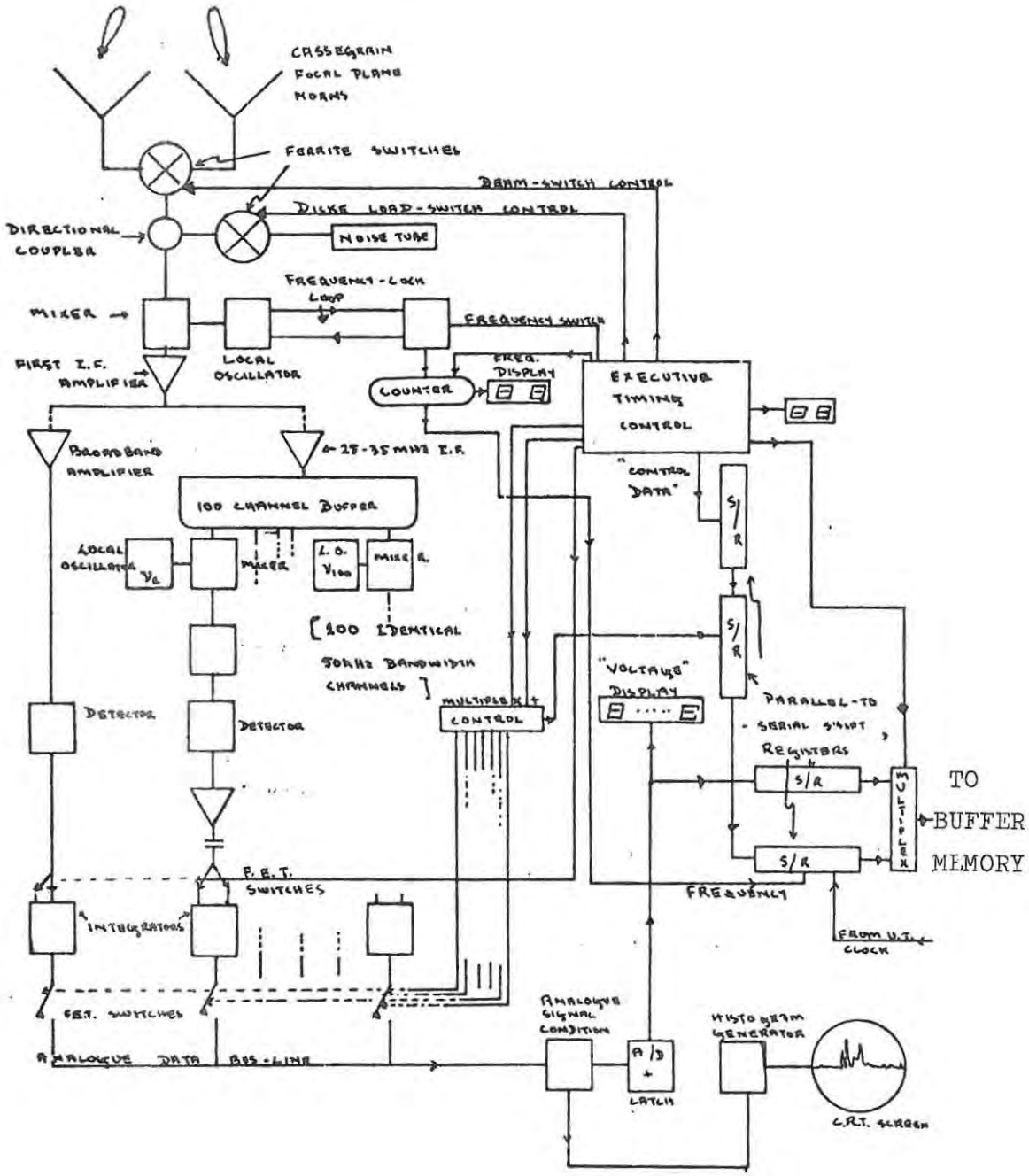

Figure B2.1 22 GHz Receiver and Digital Control

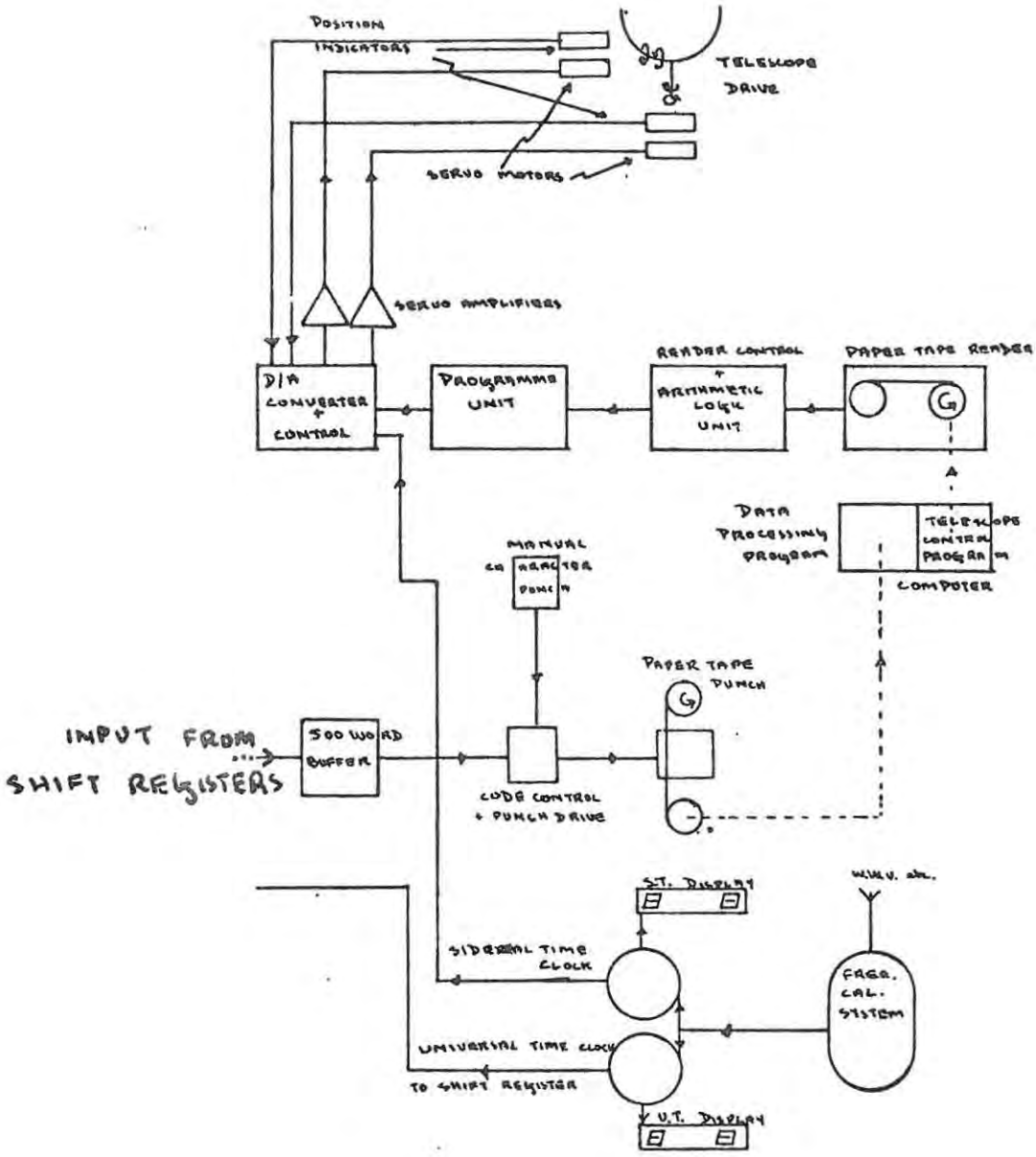

Figure B2.2 22 GHz Receiver Control & Telescope Drive

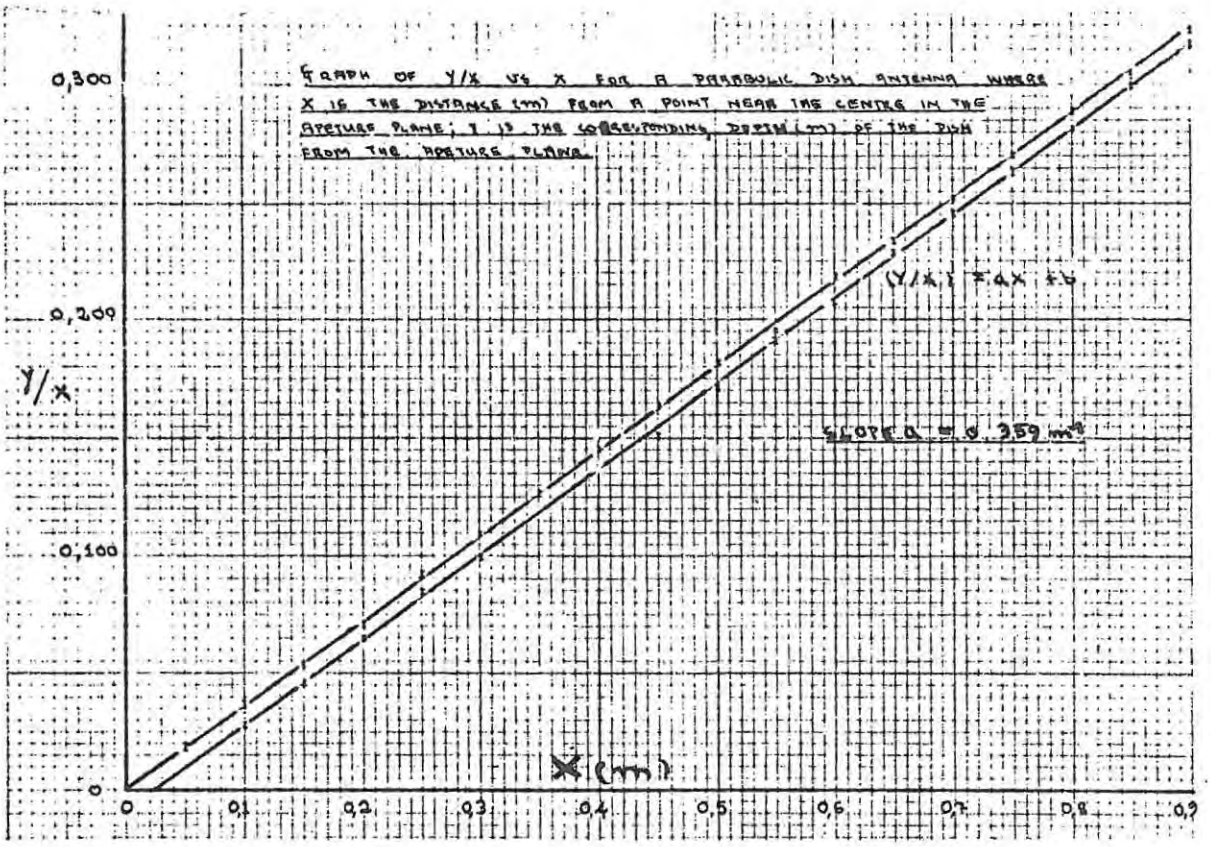

FIGURE B3.1 PLOT TO DETERMINE PARABOLIC FOCUS OF MAIN DISH

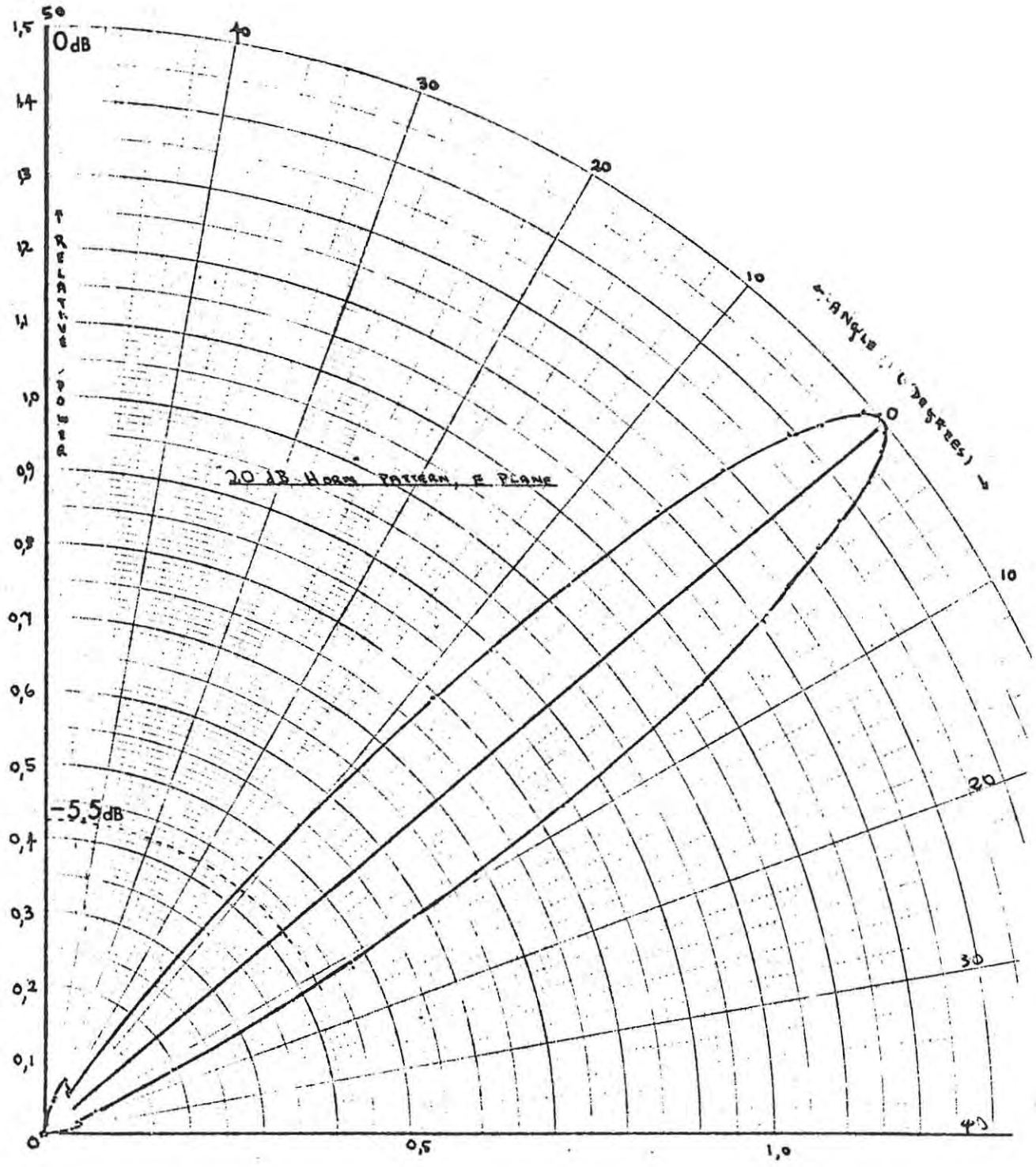

FIGURE 3.2 E - PLANE POWER PATTERN PLOT OF THE 20dB HORN

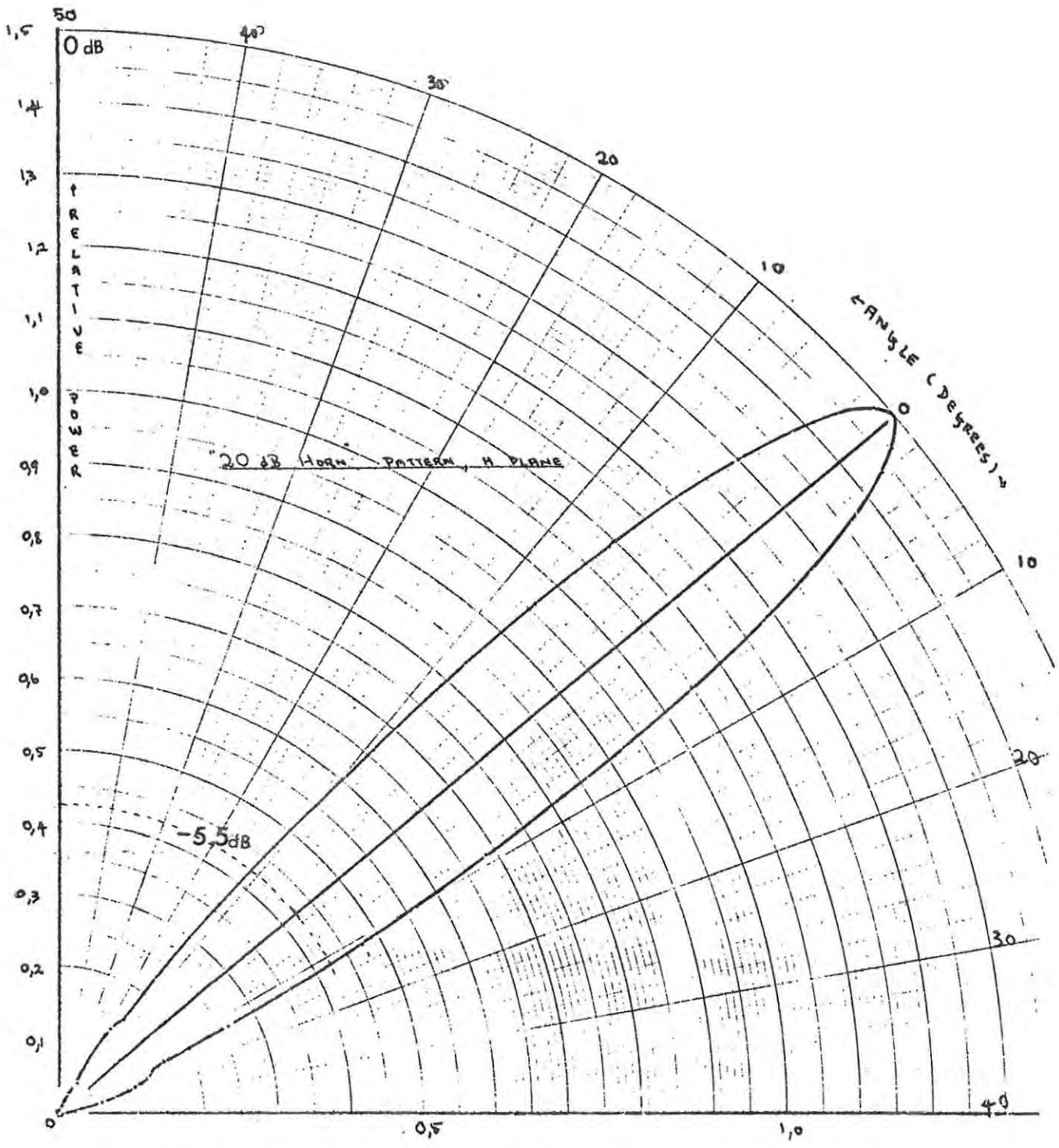

FIGURE B3.3 H- PLANE POWER PATTERN PLOT OF THE 20 dB HORN

```
      MASTER ANTENN
C     THIS PROGRAM CALCULATES THE VARIOUS PARAMETERS
C     REFERRED TO ON PAGE 18 OF 'MICROWAVE ENGINEERS
C     HANDBOOK, VOL 2' COMPILED BY THEODORE S. SAAD. PUBLISHERS ARTECH HOU
C     SE , INC.
C
C     IT ASSUMES THAT THE PARAMETERS DM, FM AND PHIR
C       ARE AVAILABLE. THE PARAMETER FC IS
C       ALSO ENTERED AS A VARIABLE, AND
C     TABLE PRINTED OUT OF THE ASSOCIATED PARAMETERS, WHICH
C     MAY BE USED TO CALCULATE THE DIMENSIONS OF A
C     HYPERBOLIC SUBREFLECTOR WITH THE DESIRED FOCAL LENGTH FC.
C
      REAL LR,LV
      PI=3.1415927
      READ(5,10)DM,FM
10    FORMAT(2F7.3)
C
C     READ IN DIAMETER OF MAIN DISH IN METERS, AND FOCAL LENGTH OF
C     MAIN DISH IN METERS, IN THE FORM:
C     SDD.DDDSDD.DDD ON ONE CARD.
C
      PHIVR=2*ATAN(DM/(4*FM))
      PHIVD=PHIVR*(180.0/PI)
      WRITE(6,20)DM,FM,PHIVD,PHIVR
20    FORMAT(1H ,37X,45HGEOMETRICAL RELATIONS OF CASSEGRAIN ANTENNAS,,//
     1,38X,4HDM =,F7.3,27H METERS (DIAM OF MAIN DISH),/,
     238X,4HFM =,F7.3,35H METERS (FOCAL LENGTH OF MAIN DISH),/,
     336X,6HPHIV =,F7.3,35H DEGREES (ANGLE SUBTENDED AT FOCUS),/,
     436X,5X,1H=,F7.3,8H RADIANS)
C
C     PRINT OUT THE VALUES OF :
C     DM, THE DIAMETER OF THE MAIN PARABOLIC DISH.
C     FM, THE FOCAL LENGTH OF THE MAIN DISH.
C     PHIV, THE ANGLE SUBTENDED AT THE FOCUS.
C
1     READ(5,11)PHIRD
11    FORMAT(F7.3)
C
C     READ IN A VALUE OF PHIR IN DEGREES IN THE FORM
C     SDD.DDD , PUNCHED ONE TO A CARD. TO TERMINATE THE PROGRAM,
C     A VALUE OF PHIR > 90.000 IS ENTERED.
C
      IF(PHIRD-90.0)2,9,9
2     PHIRR=PHIRD*(PI/180.0)
      FE=DM/(4.0*TAN(PHIRR/2.0))
      WRITE(6,21)PHIRD,PHIRR,FE
21    FORMAT(1H ,35X, 6HPHIR =,F7.3,38H DEGREES (ANGLE SUBTENDED BY HYPE
     1RBOLA,/,35X,5X,1H=,F7.3,8H RADIANS,/,35X,4HFE =,F7.3,45H METERS (F
     2OCAL LENGTH OF EQUIVALENT PARABOLA),///)
C
C     PRINT OUT THE VALUES OF:
C     PHIR, THE ANGLE SUBTENDED AT THE FOCUS OF TH HYPERBOLA- THIS IS
C     FE, THE FOCAL LENGTH OF THE EQUIVALENT PARABOLA.
C
      WRITE(6,22)
22    FORMAT(1H ,22X,11HPD METERS, ,11HDS METERS, ,11HLR METERS, ,
     1 11HLV METERS, ,11H C METERS, ,11H A METERS, ,5X,1HE,/)
101   READ(5,100)R
100   FORMAT(F7.3)
      IF(R.GT.999.0)GO TO 9
C     READ IN VALUES OF FD IN FORM DDD.DDD ON
C     SEPARATE CARDS FOLLOWED BY A 999.999CARD.
      FD=R/100.0
      DS=DM*(FD/FM)*((TAN(PHIVR)*TAN(PHIRR))/(2.*TAN(PHIVR/2.)*
     1   (TAN(PHIVR)+TAN(PHIRR))))
      LR=FC/(1+FM/FE)
      LV=FC-LR
      C=FC/2.
      A=(FC-2.*LV)/2.
      E=C/A
3     WRITE(6,23)FC,DS,LR,LV,C,A,E
      GO TO 101
23    FORMAT(1H ,22X,7(2X,F2.3,2X),/)
C
C     PRINT OUT THE VALUES OF :
C     FC, THE DISTANCE BETWEENTHE FOCAL POINTS OF THE MAIN PARABOLA AND
C     THE SUBSIDIARY HYPERBOLA.
C     DS, THE DIAMETER OF THE SUBSIDIARY HYPERBOLA.
C     LR, THE DISTADCE FROM THE FOCUS OF THE HYPERBOLA TO THE SURFACE
C     OF THE HYPERBOLA.
C     LV, THE DISTANCE FROM THE FOCUS OF THE PARBOLA TO THE SURFACE OF
C     THE HYPERBOLA.
C     C AND A ARE CONSTANTS USED IN DETERMINING THE EQUATION OF THE
C     HYPERBOLA.
C     E IS THE ECCENTRICITY OF THE HYPERBOLA.
C
9     STOP
      END

END OF SEGMENT, LENGTH  106, NAME  ANTENN
```

FIGURE B34 FORTRAN PROGRAM TO EVALUATE HYPERBOLOID SUBREFLECTOR PARAMETERS

```
      MASTER HYPZ
C
C     THIS PROGRAM CALCULATES THE FUNCTIONAL VALUES OF A HYPERBOLA WHOSE
C     PARAMETERS HAVE BEEN SUPPLIED.
C     DS = THE DIAMETER OF THE SUB DISH
C     C  = )
C     A  = )  PARAMETERS OF THE HYPERBOLA.
C
      REAL TITLE(10), X(10)
1     READ(5,2)TITLE
2     FORMAT(10A8)
C
C     RAD IN 80 CHARACTER TITLE THAT WILL BE USED TO HEAD EVERY PAGE OF
C     PRINTOUT.
C
      READ(5,3)DS,C,A
3     FORMAT(3F8.4)
C
C     READ IN THE THREE PARAMETERS REQUIRED BY THE PROGRAM.
C     TO TERMINATE THE PROGRAM, INSERT A BLANK CARD FOLLOWED BY 999.9999 0
C     ON THE NEXT CARD.
C
      IF(DS.GE.999.0000)GO TO 8
      AINC=0.0001
C
C     THE STEP LENGTH IS SET AT 1/10 TH OF A MILLIMETER.
C
      DS=DS/2.0
      YMAX=DS+0.02
C
C     THE RANGE OVER WHICH FUNCTIONAL VALUES IS CALCULATED IS GIVEN BY
C     0.5*DS (IN METERS) + 2.0 CENTIMETERS. THIS GIVES A SUFFICIENT OVERLAP
C     AT THE END POINTS TO ENABLE A CONTINUOS SURFACE.
C
      B=C+C-A*A
      Y=0
      DO 7 I=1,80
      WRITE(6,4)TITLE,I
4     FORMAT(1H1,16X,10A8,6H PAGE ,I2,//,
     *11H  LINE NO.  ,5X,1HY,9X,1H0,9X,1H1,9X,1H2,9X,1H3,
     *9X,1H4,9X,1H5,9X,1H6,9X,1H7,9X,1H8,9X,1H9,/,/)
      DO 7 J=1,50
      AY=Y
      DO 5 K=1,10
      X(K)=(A*SQRT((Y*Y/B)+1))-A
      Y=Y+AINC
5     IF(Y.GE.YMAX)GO TO 1
      WRITE(6,6)J,AY,X
6     FORMAT(1H ,6X,I2,4X,11(2X,F8.4))
7     CONTINUE
8     STOP
      END

END OF SEGMENT, LENGTH   118, NAME  HYPZ
```

TEST WITH PARAMETERS OF 20 DB HORN, FC=53CM, DS=20.0CM. PAGE 1

LINE NO.	Y	0	1	2	3	4	5	6	7	8	9
1	0.0000	0.0000	0.0000	0.0000	0.0000	0.0000	0.0000	0.0000	0.0000	0.0000	0.0000
2	0.0010	0.0000	0.0000	0.0000	0.0000	0.0000	0.0000	0.0000	0.0000	0.0000	0.0000
3	0.0020	0.0000	0.0000	0.0000	0.0000	0.0000	0.0000	0.0000	0.0000	0.0000	0.0000
4	0.0030	0.0000	0.0000	0.0000	0.0000	0.0000	0.0000	0.0000	0.0000	0.0000	0.0000
5	0.0040	0.0000	0.0000	0.0001	0.0001	0.0001	0.0001	0.0001	0.0001	0.0001	0.0001
6	0.0050	0.0001	0.0001	0.0001	0.0001	0.0001	0.0001	0.0001	0.0001	0.0001	0.0001
:	:										

FIGURE 3.5 FORTRAN PROGRAM TO FIND SUBREFLECTOR SURFACE COORDINATES

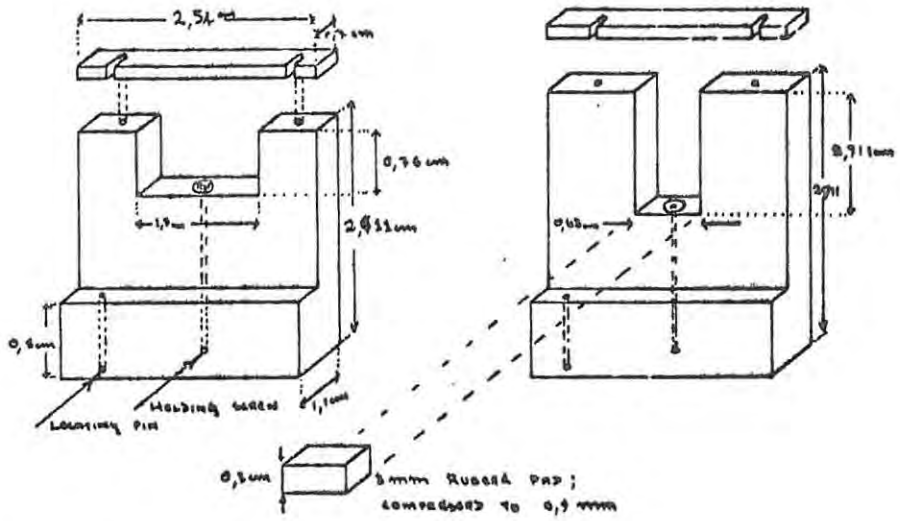

FIGURE B4.1a MICROWAVE TUBING SUPPORT FOR RECEIVER "FRONT-END" MOUNTING.

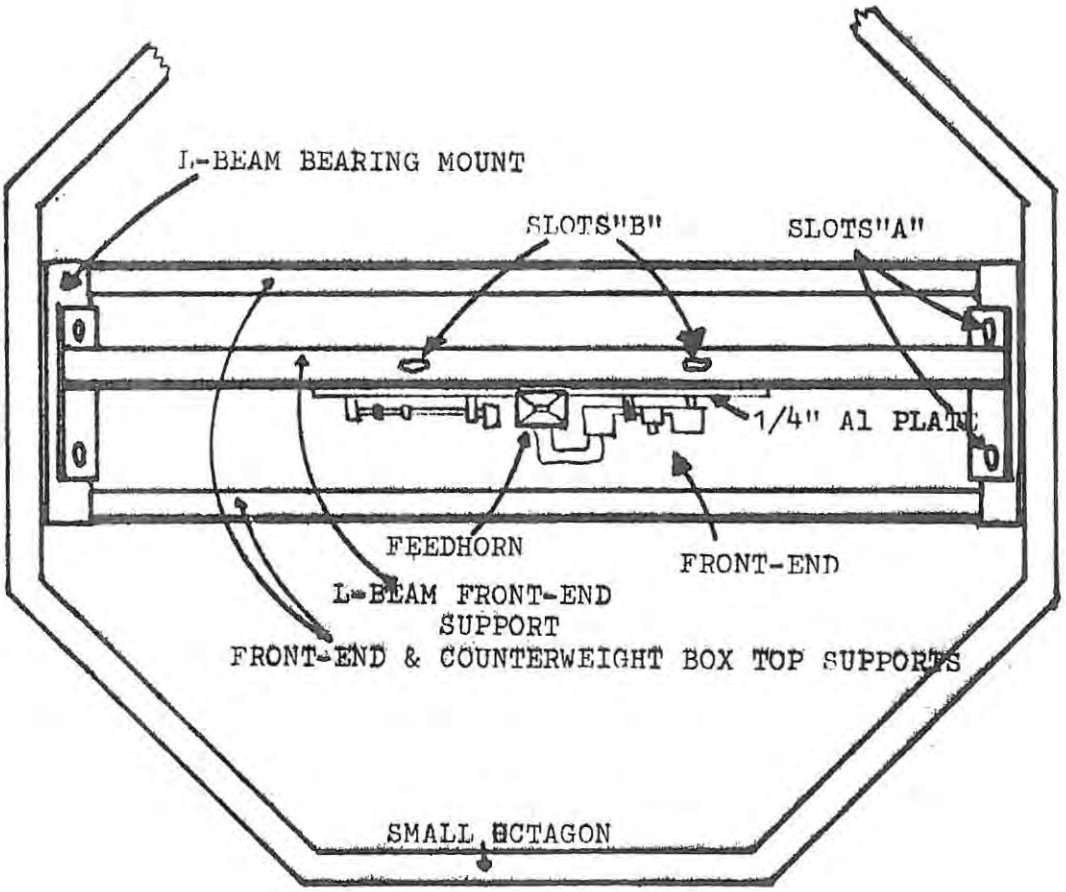

FIGURE B4.1b BEARING MOUNTS & SUPPORTED STRUCTURE.

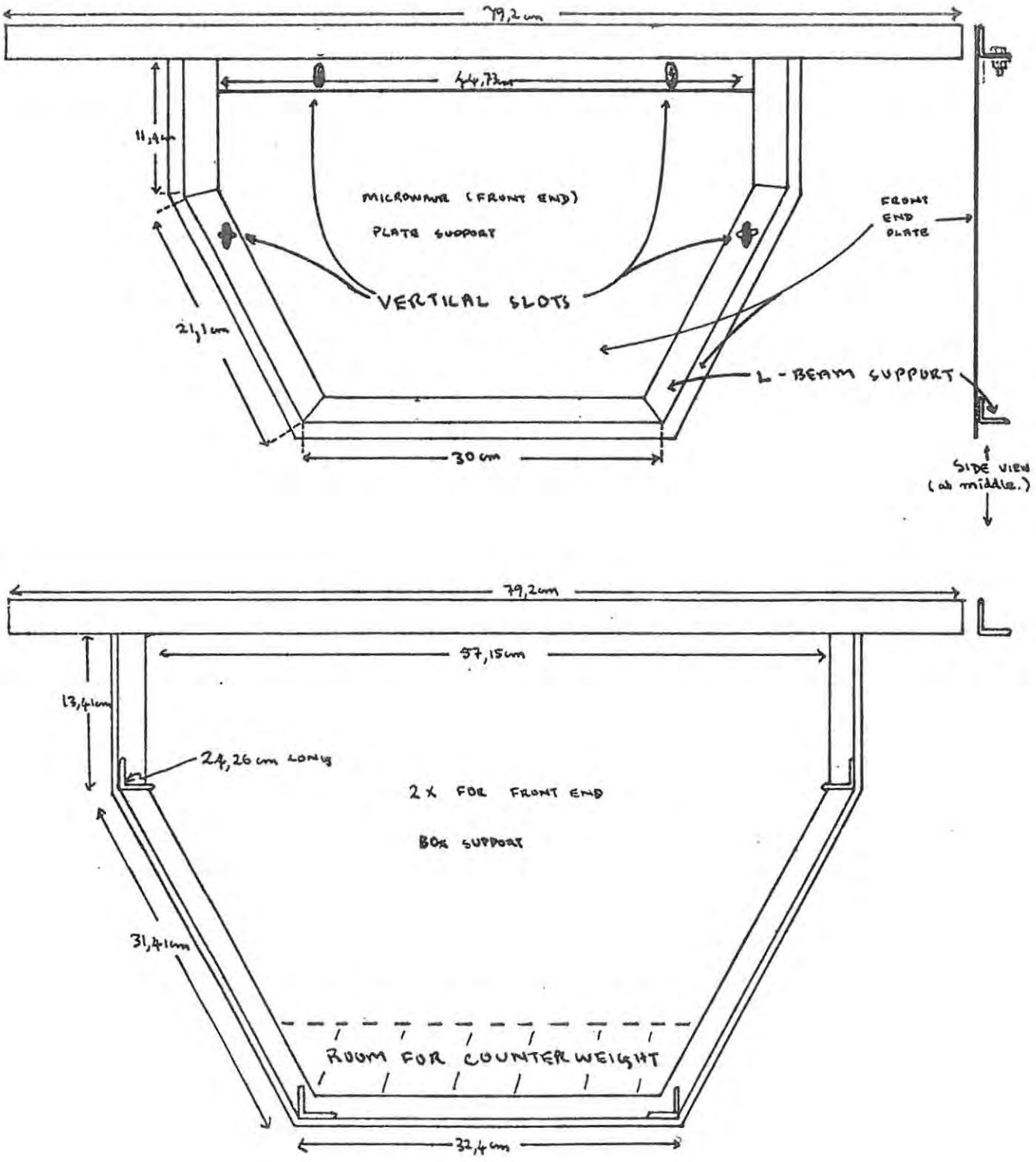

FIGUR B4.2 FRONT-END & COUNTERWEIGHT SUPPORT FRAMEWORKS.

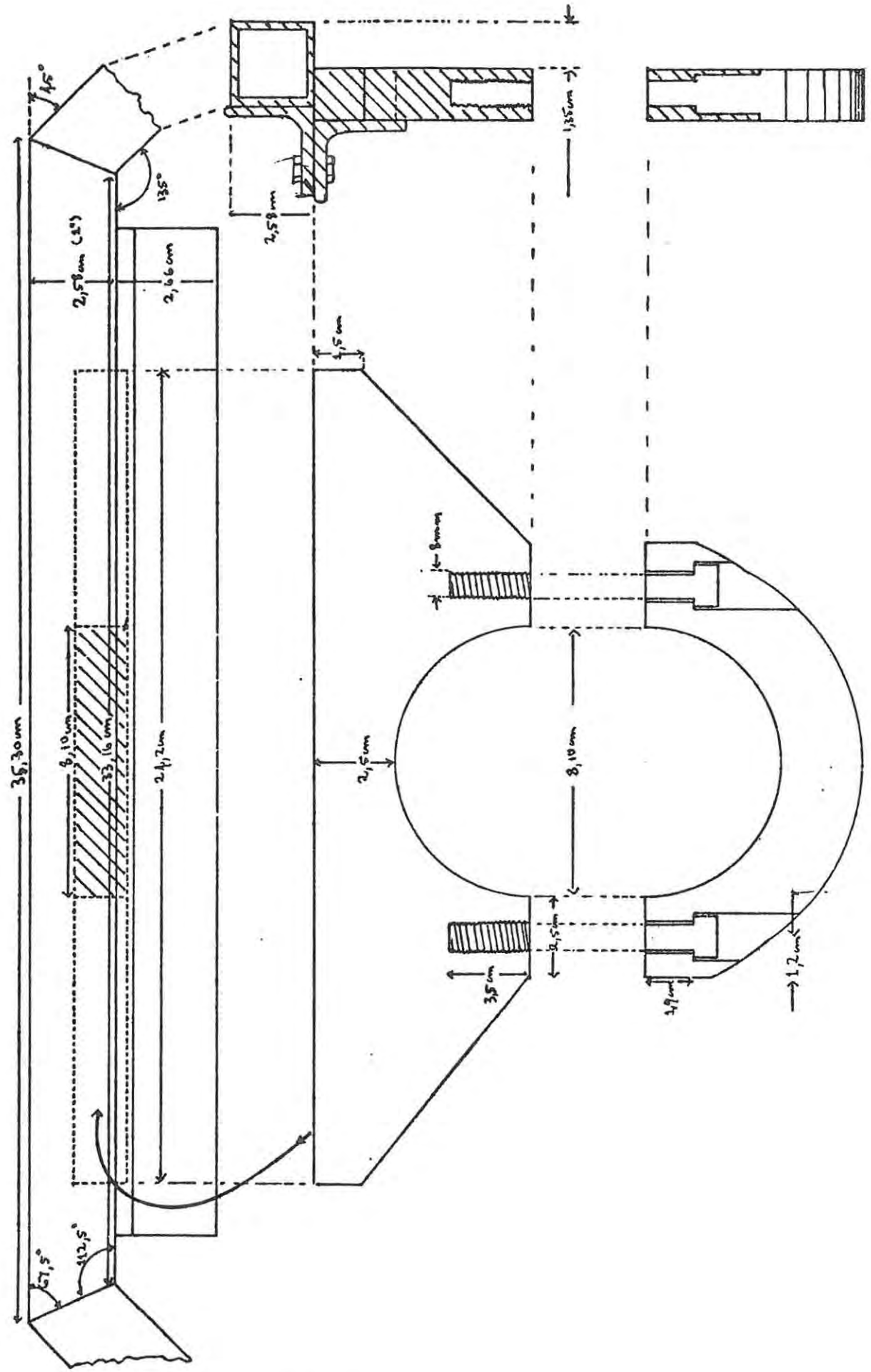

FIGURE B4.3 DETAILS OF BEARING MOUNTS.

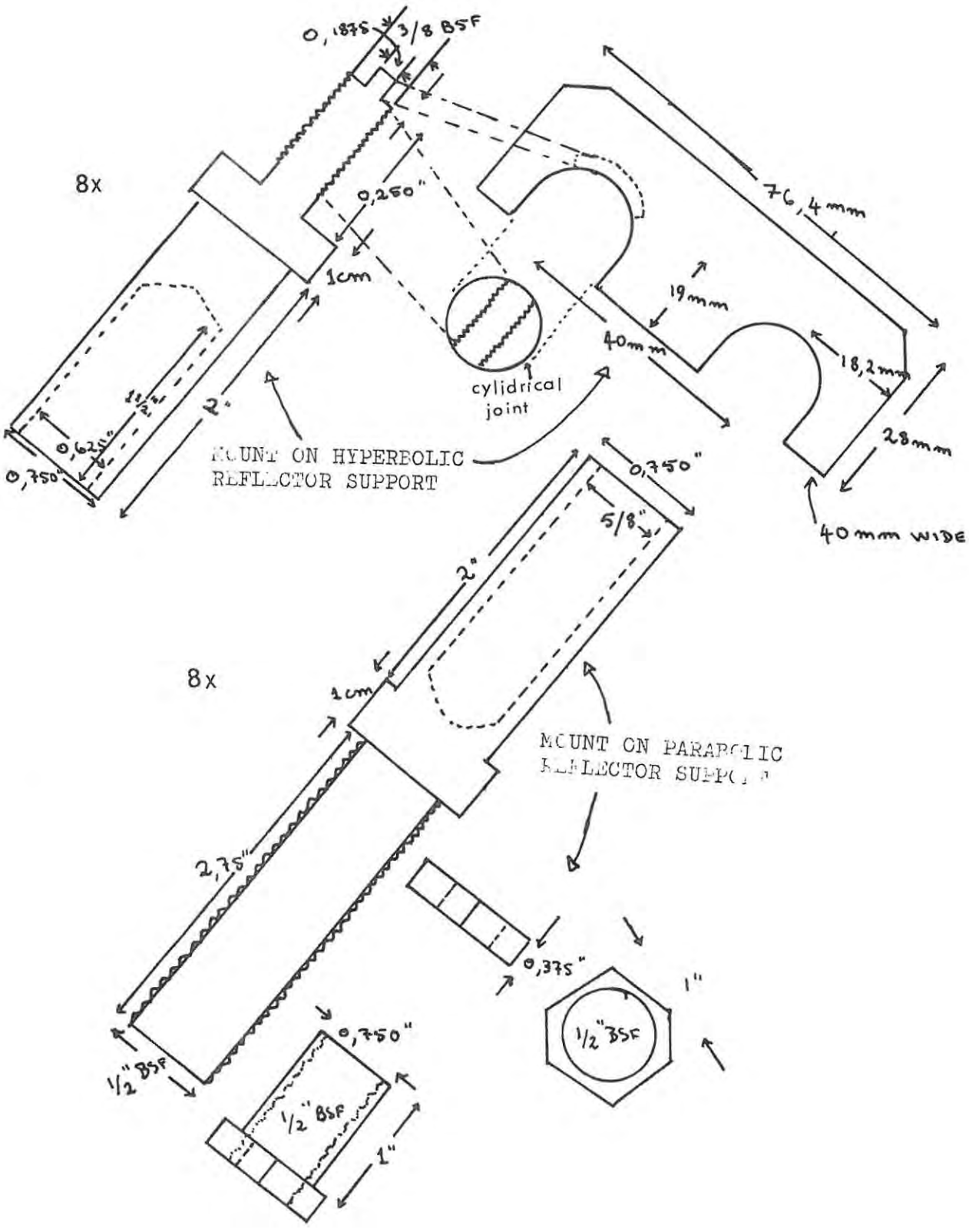

FIGURE B4.4 MOUNTS FOR ALUMINIUM RODS ON HYPERBOLIC SUBREFLECTOR

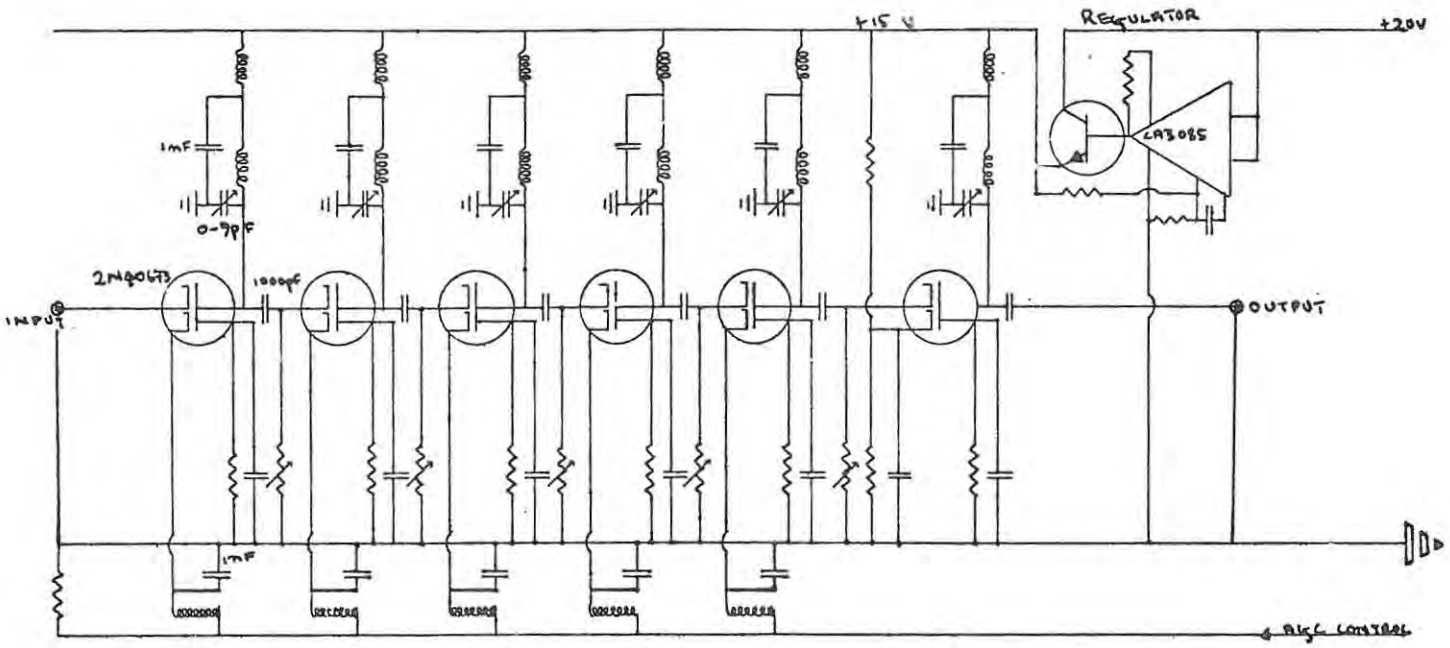

Figure B5.1 The six-stage tuned i.f. amplifier.

Registors (ohms)		Capacitors (~~nano farads~~ nanofarads)		
R_1	3,3k	C_1	1	(ceramic)
R_2	470	C_2	100	(tantalum)
R_3	1k	C_3	1	(ceramic)
R_4	100			
R_5	4,7k	Inductor L : 1 mH.		
R_6	560			
R_7	50	Transistors		
R_8	47k	T_1	5486	
R_9	470	T_2	3906	
R_{10}	10k	Integrated circuit 1 : MC 1590		
R	2,2k			

Figure B5.2 Table of component values of buffer.

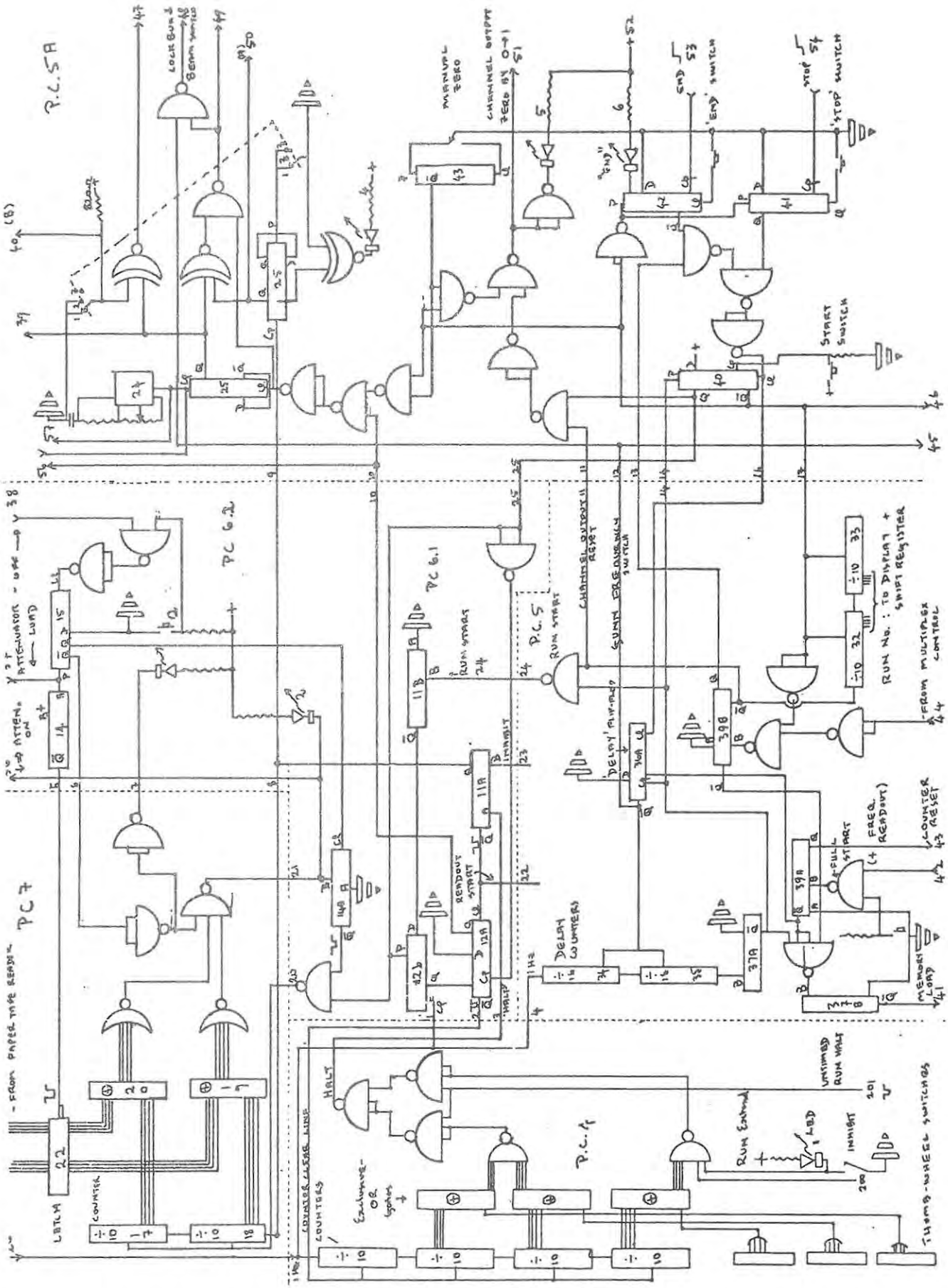

FIGURE B6.1 THE EXECUTIVE TIMING CONTROL

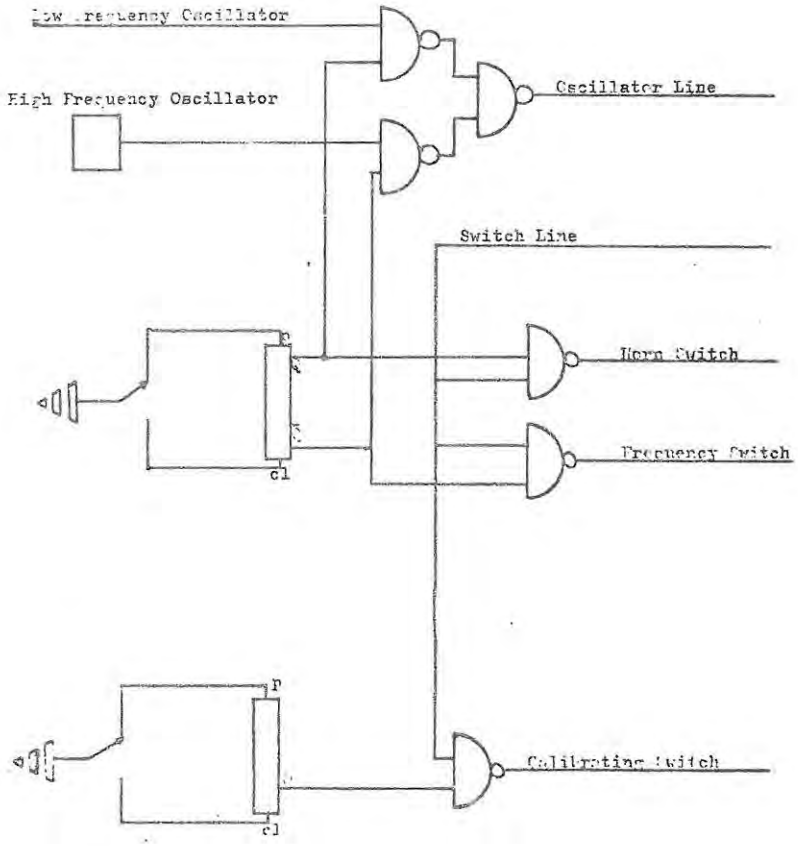

FIGURE B6.2 P.C.5B : FRONT END MODULATOR CONTROL

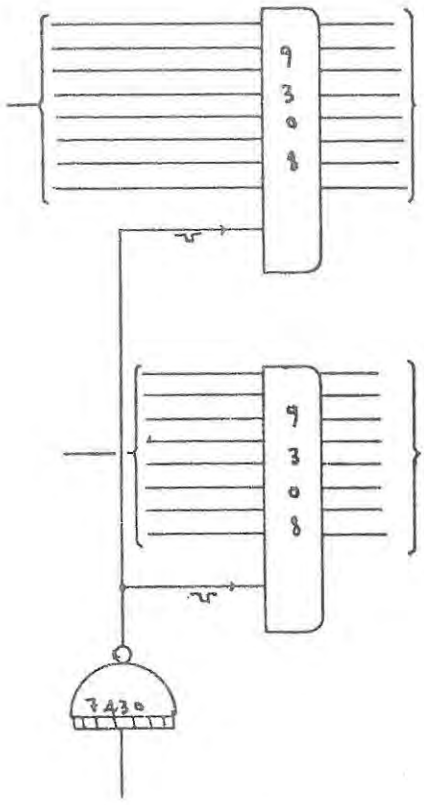

FIGURE B6.3 P.C. 18 DVM OUTPUT LATCH

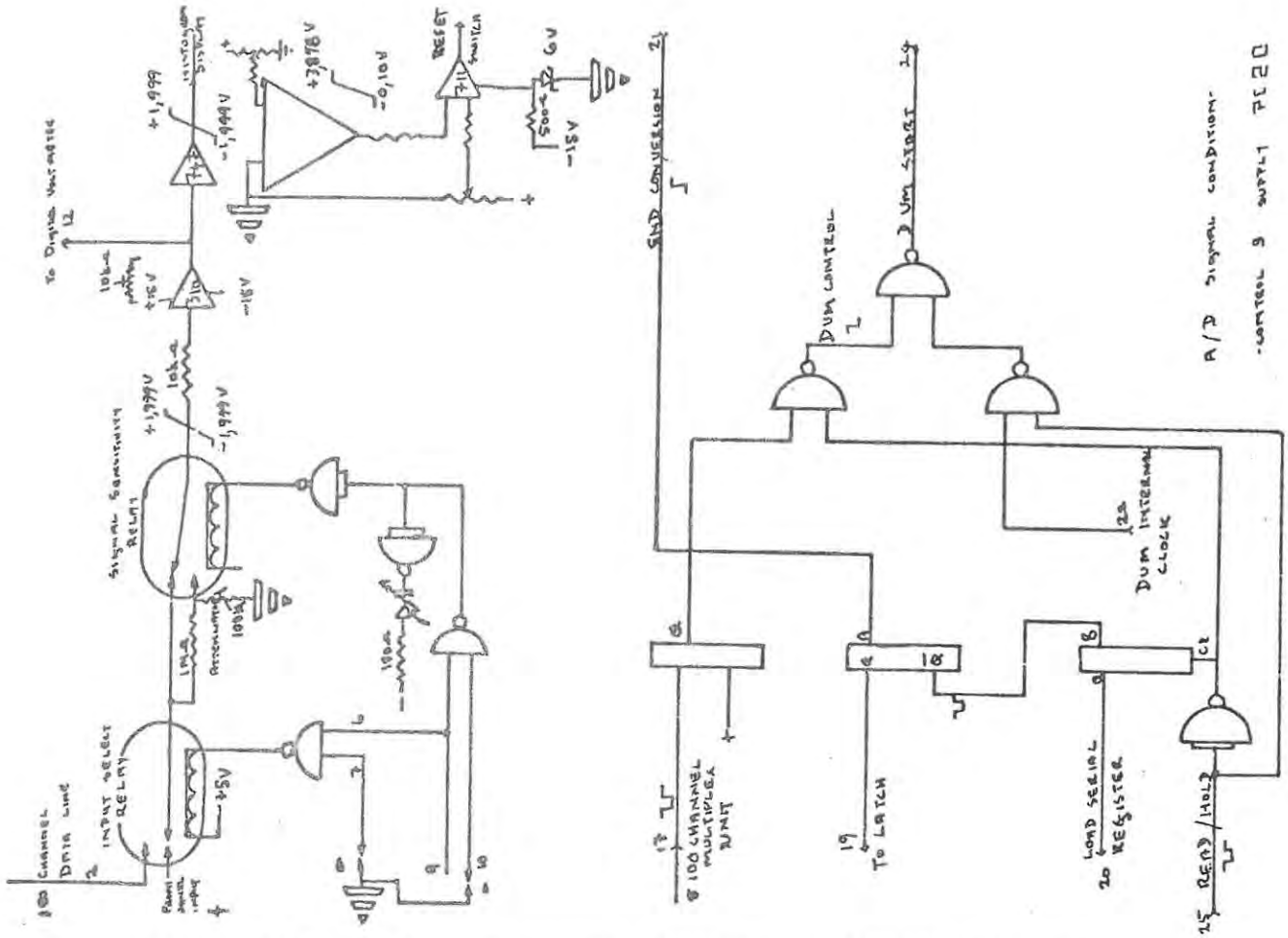

FIGURE B6.4 DIGITAL VOLTMETER ANALOGUE & DIGITAL CONTROL

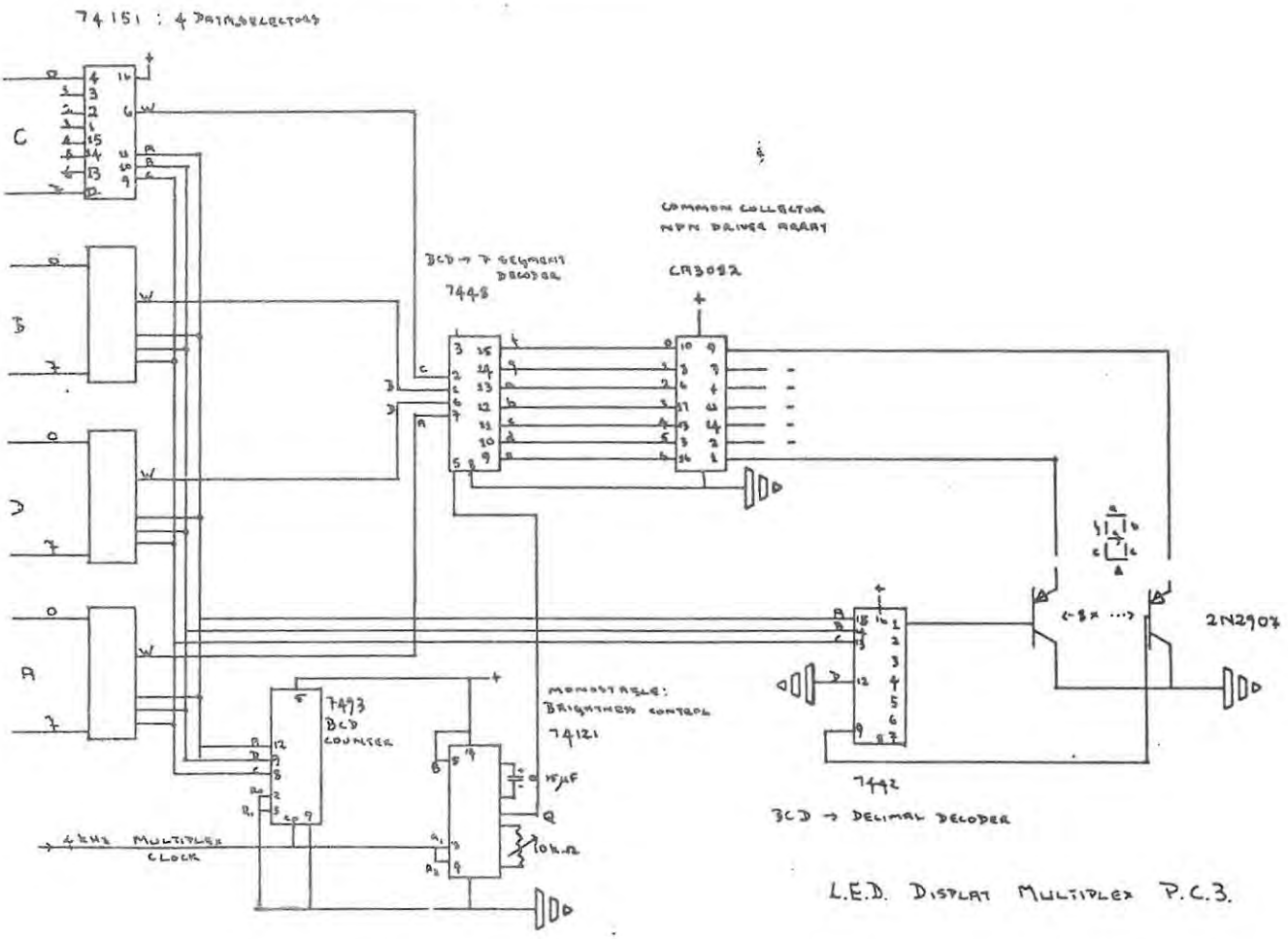

FIGURE B6.5 'L.E.D.' DISPLAY MULTIPLEX & DRIVE

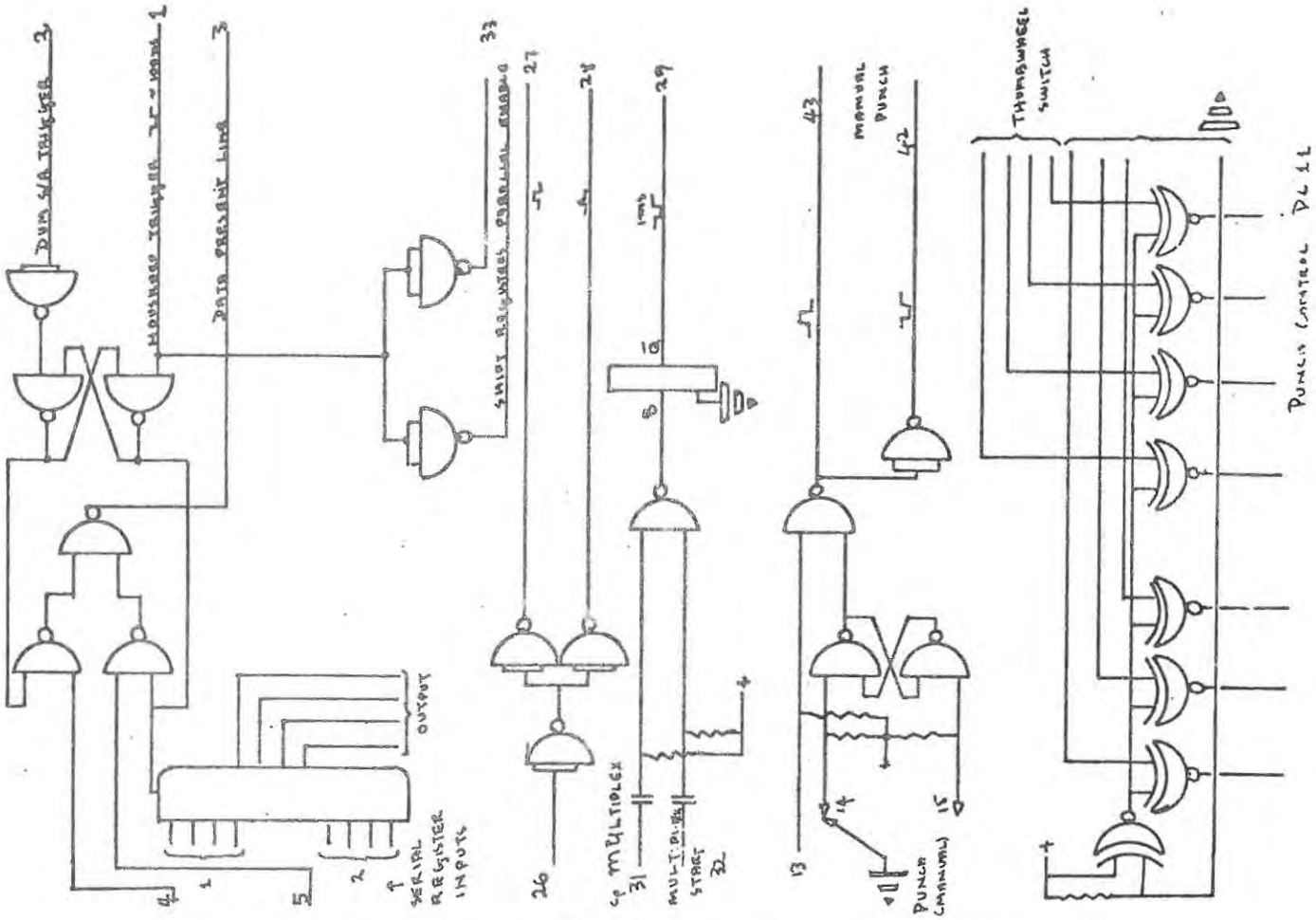

FIGURE B6.6 SHIFT REGISTER MULTIPLEX, & PUNCH CONTROL

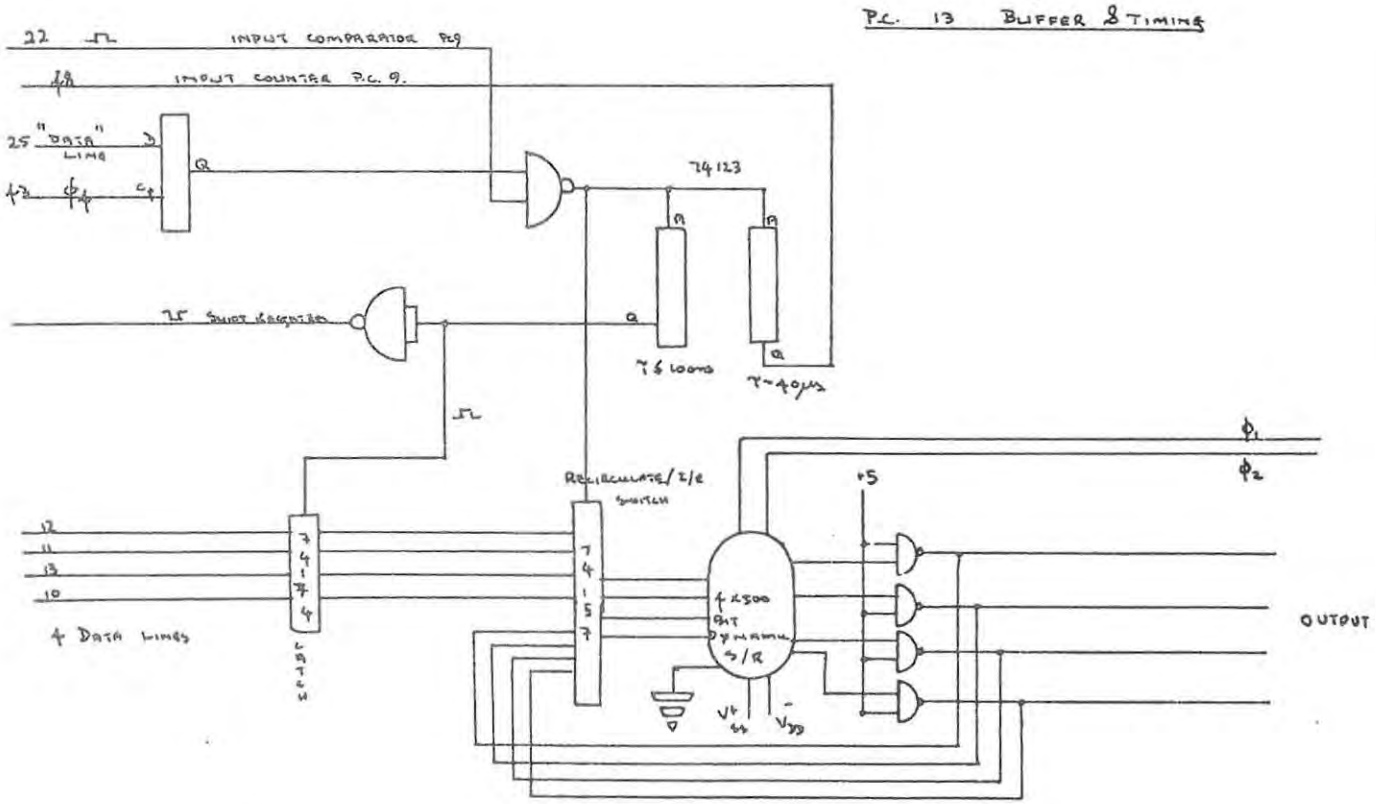

FIGURE B6.7 500 CHARACTER BUFFER MEMORY

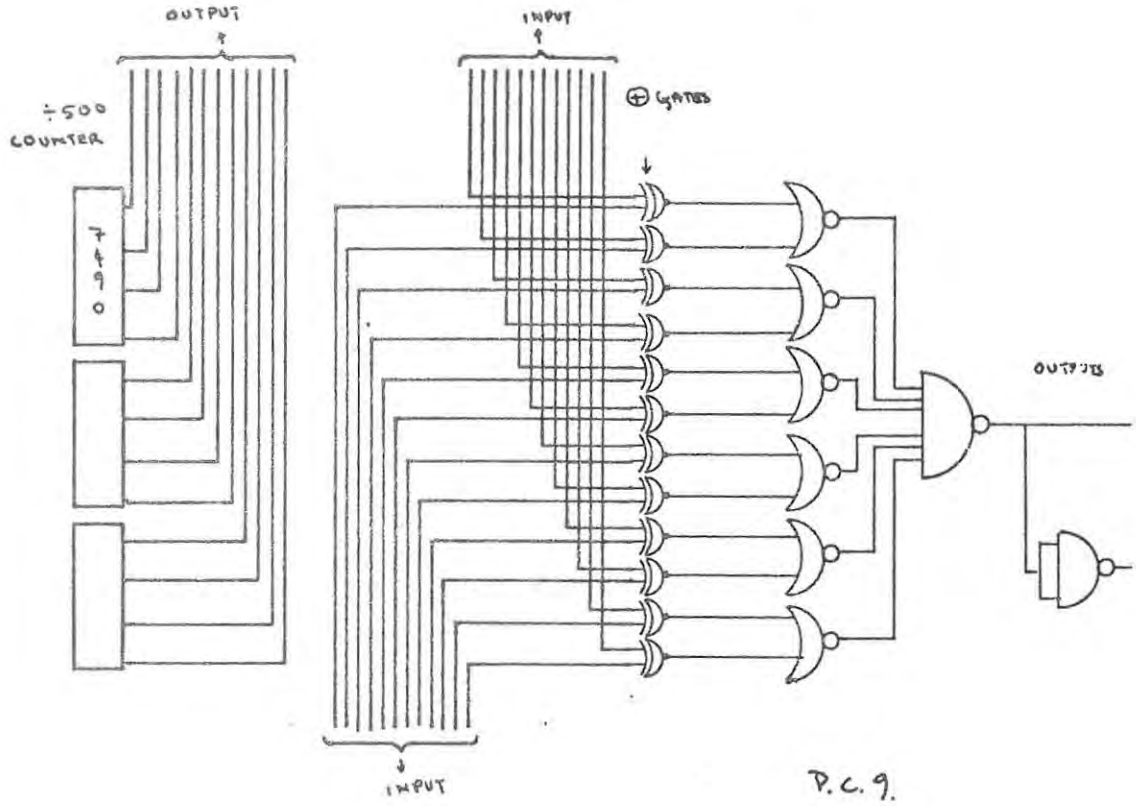

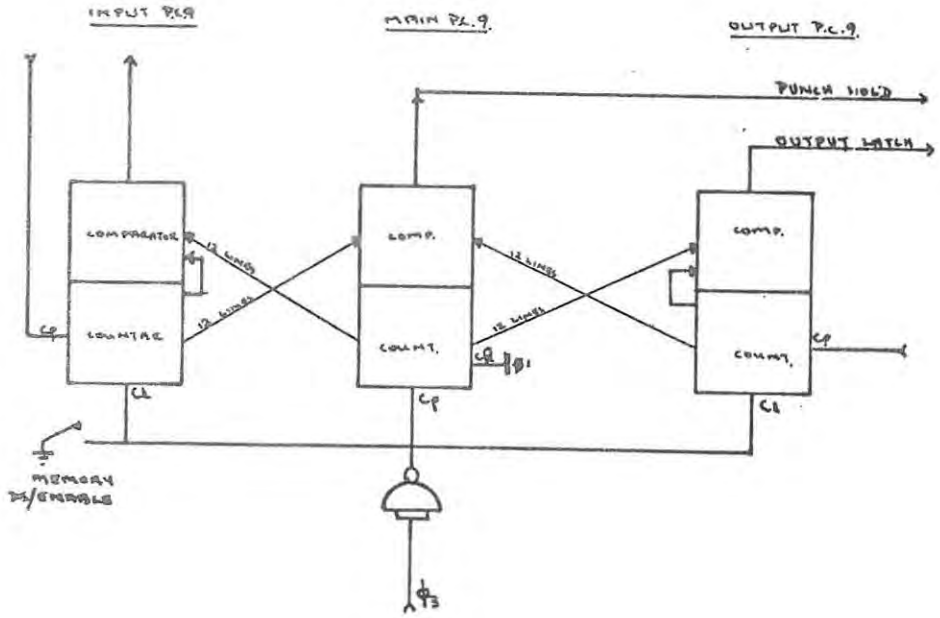

FIGURE B6.8 BUFFER INPUT/OUTPUT CONTROL TIMING CIRCUITRY

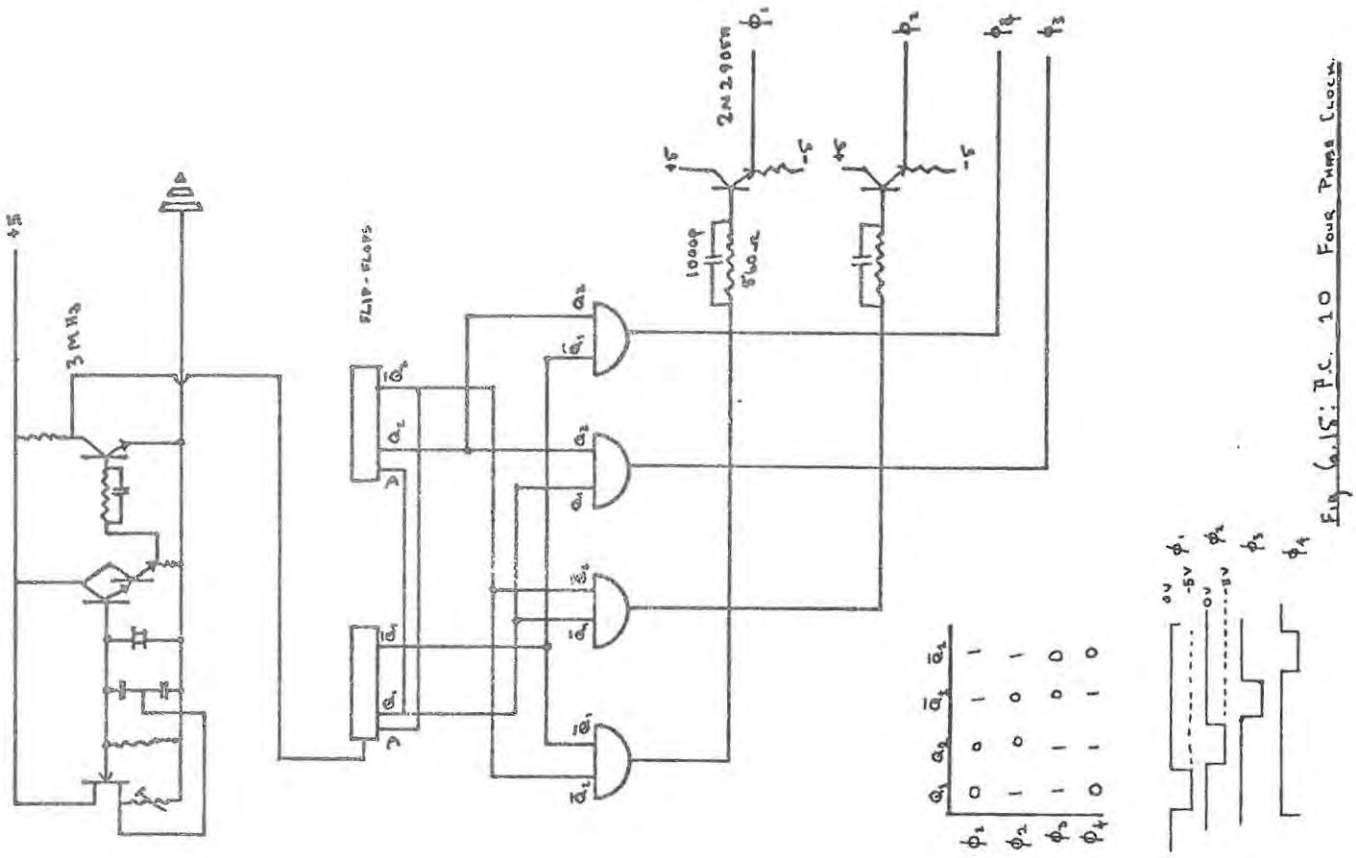

Fig (a.15: P.C. 10 Four Phase Clock.

FIGURE B6.9 FOUR PHASE CLOCK

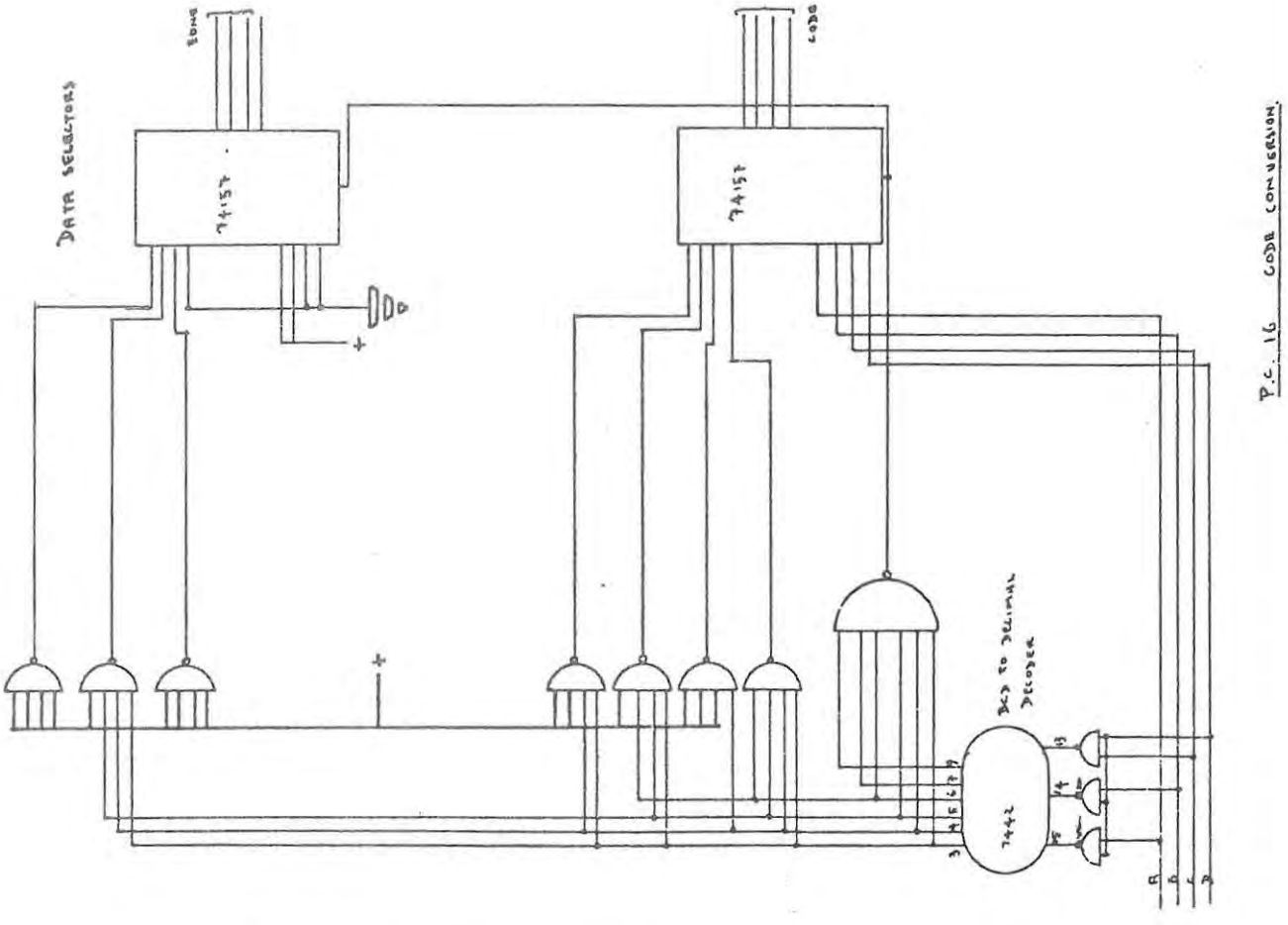

P.C. 16 CODE CONVERSION.

FIGURE B6.10 ASCII CODE CONVERTER

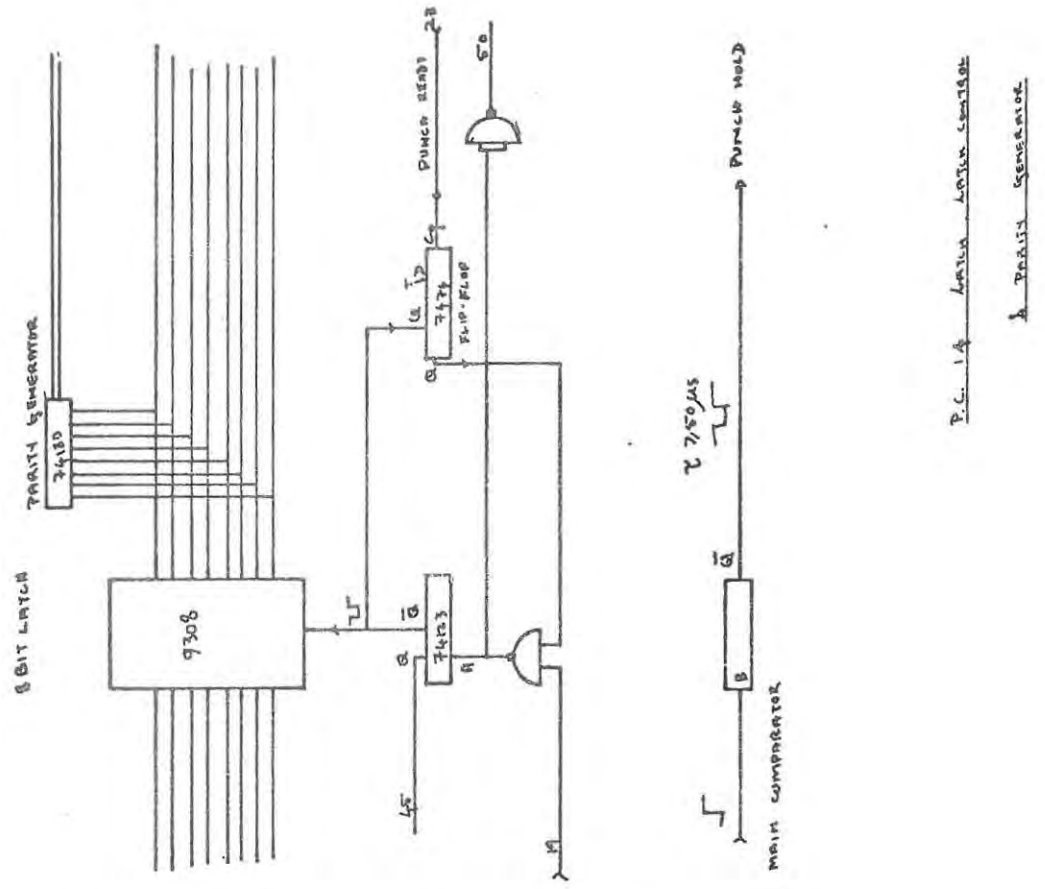

FIGURE 36.11 LATCH & CONTROL. PARITY GENERATOR

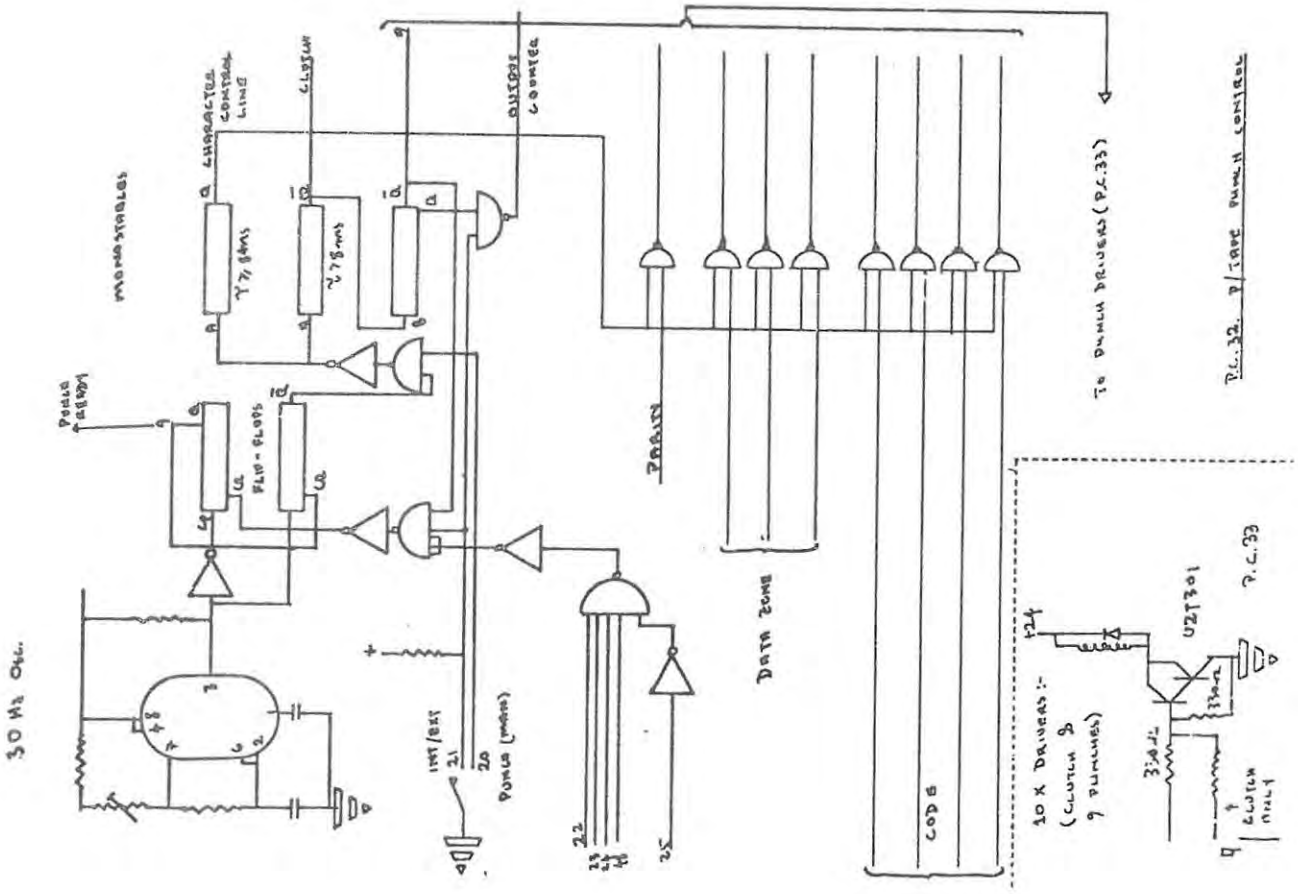

FIGURE 36.12 PAPER TAPE PUNCH CONTROL

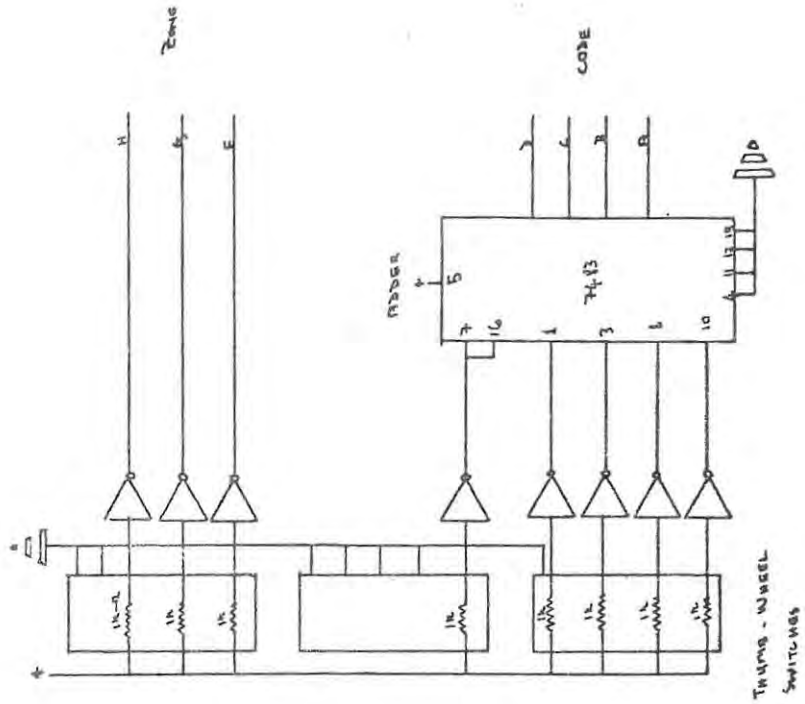

FIGURE B6.13 MANUAL CHARACTER-PUNCH CONTROL

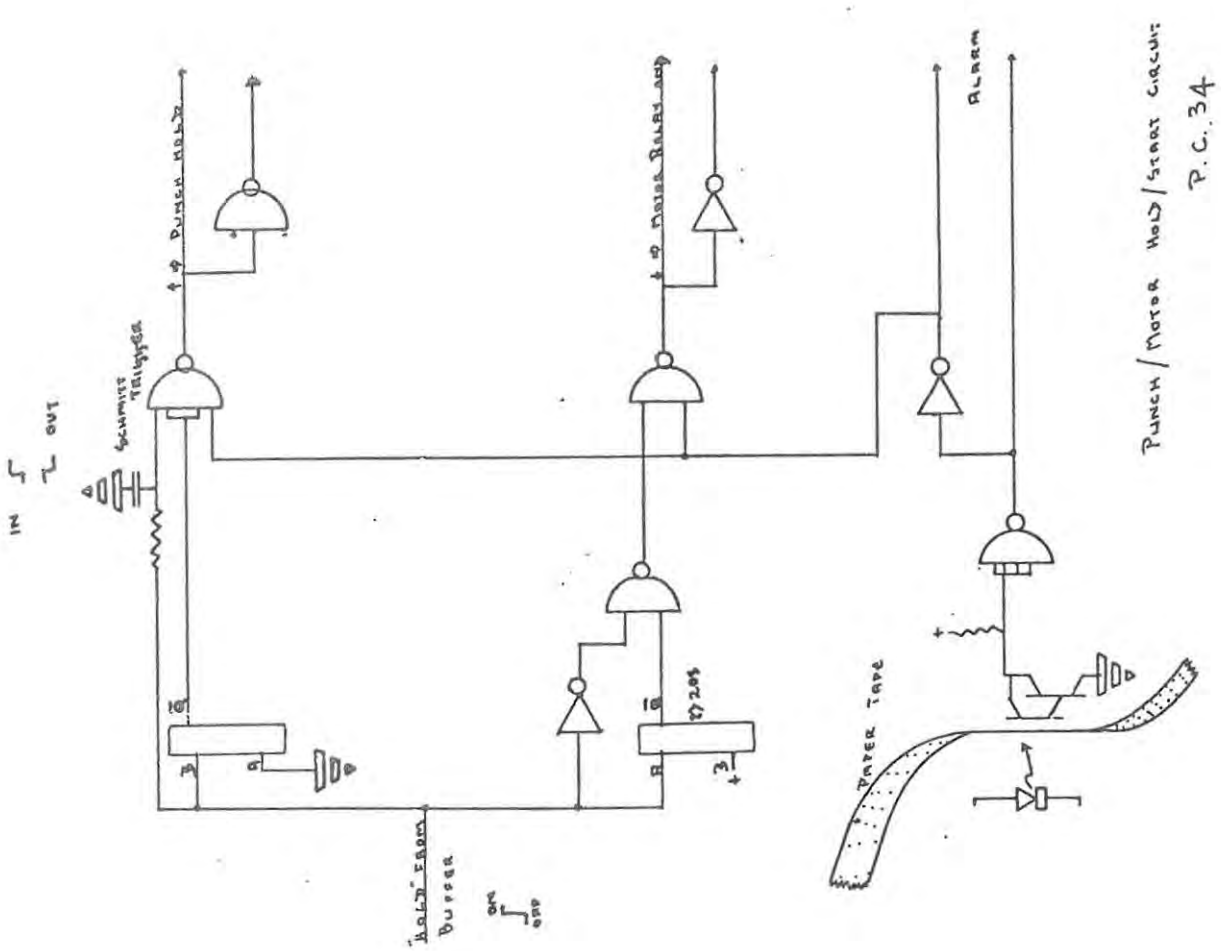

FIGURE B6.14 PUNCH AND MOTOR DISABLE CIRCUIT

BIBLIOGRAPHY

The references below are listed according to the Harvard system, except that the numbers of the pages, on which a reference is quoted, are given in brackets at the end of the reference.

Aannestad, Per A. (1973), "Molecule formation in normal clouds", Ed. Gordon: Molecules in the Galactic Environment, 409-412, Wiley, N.Y. [page 11].

Albaugh, N., and K. H. Wessling (1968), "A novel way of beam-switching, particularly suitable at mm. wavelengths", N.R.A.O. Electronics Div. Int. Report, No.76 [page 20].

Baars, Jacob W. M., P. G. Meyger, and H. Wendker (1965), "The spectra of the strongest non-thermal Radio Sources in the centimeter-wavelength region", Astrophys. J., 142, 1, 122-134. [page 13].

Baars, J. W. M., (1966), "Reduction of Tropospheric Noise Fluctuations at Centimeter Wavelengths", Nature, 212, 494 [page 19].

Baars, Jacob W. M., (1970), Dual-beam parabolic antennae in radio astronomy, Ph.D. thesis, Delft University, Publ. Wolters-Noordhoff Publishing, Gronigen. Chapters 1 & 2 [page 19, Appendix A].

Baars, Jacob W. M., (1973), "The Measurement of Large Antennas with Cosmic Radio Sources", IEEE Transactions on Ant. and Propagat., AP-21:4, 461. [page 46].

Barber, D. (1963), "Planetary Radiation at Centimeter Wavelengths", R. R. E. Journal, 50, 59, Royal Radar Establishment, Ministry of Aviation, Eng. [page 14].

Balister, Michael (1968), "The N.R.A.O. 50-channel spectral line receiver", N.R.A.O. Electronics Div. Int. Report, 70 [page 15].

Barret, Alan H. (1969), "Microwave Spectroscopy of Interstellar Ammonia", Comments on Atomic & Mol. Phys., 1: 2, 60-63 [page 12].

Barret, Alan H. (1970), NASA Acession No. N 65 1970, Rept. No. NASA - CR - 57309 [page 14].

Becklin, E. E., et al. (1973), "Infrared emission from OH/H_2O sources in W49", Astrophys. L., 13, 147 [page 10].

Benson, F. A. (1969), "Attenuation of Rectangular waveguides", Millimeter and Submillimeter waves, Ed. Benson, F. A., Illife books, Hungary, 239. [page 20].

Bhatia, V. B. and J. N. Tandon (1970), "On Solar flare Microwave Spectra", Astrophys. Lett., 6, 113-115 [page 13].

Blake, G. M. (1970), "Observations of Extragalactic Radio Sources having unusual spectra", Astrophys. Lett., 6, 201-5 [page 13].

Bok, B. J. (1972) "The Birth of Stars", Sci. Amer., 227, 48 (August) [page 7].

~~Bolz,~~ Ray E., and George L. Tuve (1973), Handbook of tables for Applied Engineering Science, Chemical Rubber Co. Press, Cleveland, Ohio, Second Ed. [pages 46, 47, 49].

Brown, R. D. (1973), "The New World of Galactochemistry", Chemistry in Britain, 9, No. 10, 450-455 [pages 11, 13].

Buhl, David, et al. (1969), "An investigation of the spectra and time variations of galactic water-vapour sources", Astrophys. J., 158, L 97 [page 10].

Buhl, David, Snyder, Lewis E. and Edrich, Jochem (1972), "An Interstellar Emission line from isocyanic acid at 1,4 cm", Astrophys. J., 177 (3), 625-628 [page 12].

Buhl, David (1973), "Molecular Clouds in the Galaxy", Proc. of the IEEE, 61, 1198 [page 8].

Buhl, David. (1973b), "Molecules and Evolution in the Galaxy", Sky & Telescope, Mar. 1973, 156-158 [page 8].

Burke, B. F. (1969), "Molecular Radio lines including VLB Observations", Proc. of Symp. on "Future Trends in Single Dish Radio Astronomy" held at Bonn, Aug. 27, 1969, Ed. H. J. Wendker, (Max Planck Inst.), 43-48 [page 4].

Caswell, J. L. (1972), "Hydrogen recombination line and continuum observations at 5 000 MHz for 13 Southern H II regions", Aust. J. Phys., 25(4), 443 [page 10].

Cheung, A. C., Rank, D. M., Thornton, D. D., and Townes C. H. (1968), "Detection of NH_3 Molecules in the Interstellar Medium by their Microwave Emission", Phys. Rev. Lett., 21: 25, 1701-1705 [page 12].

Cheung, A. C. et al. (1969), "Detection of water in Interstellar Regions by it's Microwave Radiation", Nature, 221 626-8 [page 3].

Cogdell, John R, and John H. Davis (1973), "On Separating Aberrant Effects from Random Scattering Effects in Radio Telescopes", Proc. IEEE, 61: 9, 1344 [page 45].

Cohen, M. (1973), "I.R. Observations of young stars - IV. Radiative Mechanisms and interpretation", Mon. Not. of the Roy. Astr. Soc., 164, 395 [page 7].

Collin, Robert E. and F. J. Tucker (1969), Antenna theory : Part 2, ~~McGrawhill~~ McGraw-Hill, N.Y., 49 [page 34].

Colvin, R. S. (1961), "A study of radio-astronomy receivers", Scientific Rept. No. 18, Radioscience Lab., Stanford Univ., Calif. [page 18].

Conway, R. G. (1963), "Measurements of Radio sources at centimeter wave-lengths", Nature, 199, 1177 [page 19].

Dalgarno, A., and McCray, R.A. (1973), "The formation of interstellar molecules from negative ions", Astrophys. J.(USA), 181, 1, pt.1, 95-100 [page 11].

Davies, R. D., et al. (1972), "Structure of the OH/infrared object NML cygnus", Nature (Phys. Sci.) (GB), 237, No. 71, 21-4, [page 8].

Dickinson, Dale F., Litvak, Martin M., and Zuckerman, Benjamin M. (1970), "Interstellar Masers", Sky & Telescope, 39: 1, 4-7 [page 11].

Dickinson, Dale F. (1972), "Detection of cyanoacetylene at 18 GHz", Astrophys. Lett., 12 (4), 235-6 [page 12].

Dickinson, D. F., et al. (1973), "New H_2O Sources associated with Infrared Stars", Astrophys. J., 180, 831 [page 7].

Dieter, N. H. et al. (1963), "The Interstellar OH Emission", Sky & Telescope, 31: 3, 132-136 [page 2].

Dieter, N. H., and Goss, W. M. (1966), "Recent work on the interstellar medium", Rev. Mod. Phys. (USA), 38, 256-97 [page 2].

Dolan, James L. (1970), "A Double-Switched Water Vapour Radiometer", N.R.A.O. Electronics Div. Int. Rept., 96 [page 20].

Dolan, James L. (1970b), "General description and operating instructions for the water vapour receiver", N.R.A.O. Electronics Div. Int. Report, 89 [page 20].

Elder, H. E., and V. S. Glinske (1969), "Detector and Mixer Diodes and Circuits", Microwave semiconductor Devices and their Circuit Applications, Ed. Watson, H. A., ~~McGrawhill~~ McGraw-Hill, N. Y. [page 15].

Emerson, S. P. et al. (1973), "Far I.R. observations of H II regions from balloon altitudes", Astrophys. J., 184, 401 [page 9].

Field, G. B., (1970), "Theory of star formation.Introductory report", Mem. Soc. R. Sci. Liege 8° (Belgium), vol 19, No. 1, 29-45 (16th international colloquium on astrophysics, Liege, Belgium, 30 Jun.- 2 Jul. 1969)]page 9].

Finlay, John W. (1964), "Antennas and receivers for Radio Astronomy", Advances in Radio Research, ed. J. A. Saxton, 37-121, Academic Press, London. [page 45].

Findlay, J. W. (1971), "Filled-apeture antennas for radio astronomy", Ann. Rev. Astron. Astrophys., 2, 271, Ed. Goldberg, Leo. [page 20].

Fisher, J. E., and Gatland, H. B. (1966), Electronics from theory into practice, Pergammon Press, London & N.Y., 154 [page 57].

Foley, H. M. (1973), "Introduction to Molecular Spectra", Ed. Carson; Atoms and Molecules in Astrophysics, 156-200, Academic press N.Y., [page 12].

Fürst, E. (1971), "A Statistical Research on Solar Microwave Bursts", Solar Physics, 18, 84-86, (Max Planck Inst.) [page 13].

Gardner, F. F. and Morimoto, M. (1968), "5 GHz Continuum Radiation from Southern Hemisphere Galactic H II regions", Aust. J. Phys., 21, 881-94 [page 11].

Gardner, (1972), "CH_2O Absorption associated with W44", Astron. Astrophys., 21(1), 159-61 (Eng) [page 10].

Goss, W. M., et al. (1973), "Accurate positions of OH emission sources at 1665 and 1667 MHz", Astrophys. J., 183, 843 [page 6].

Grasdalen, G. D., et al. (1973), "A 2-Micron Map of the Ophiuchus dark-cloud region", Astrophys. J., 184, L53 [page 25].

Gulkis, S.,(1973) "Thermal Emission from the Major Planets", Space Science Reviews, 14, 497 [page 14].

Gwinn, W. D., et al. (1973) "Excitation of interstellar OH by the Collisional Dissociation of Water", Astrophys. J., 179, 789-813 [page 11].

Hannan, Peter W. (1961) "Microwave antennas derived from the Cassegrain telescope", IRE trans. on Antennas and Propagation, AP 9, 140-153 [pages 31, 38, 39].

Harvey, A. F., (1963), Microwave Engineering, Academic press, London [pages 13, 14, 20, 22, 27].

Heilies, Carl (1971), "Physical conditions and chemical constitution of dark clouds", Ann. Rev. of Astron. and Ap., Ed. Goldberg, Leo, et al., 9, 293-322 [page 7].

Henderson, C., (1972), "Molecules in Space", Contemp. Phys., 13: 5, 477-499 [pages 7, 15].

Herbig, G. H., (1970), "VY CMa. II Interpretation of Energy Distribution", Astrophys. J., 162, 557 [page 6].

Hey, J. S., (1971), The Radio Universe, Pergamon, Braunschweig, Ger., 68 [pages 13, 27].

Hills, et al.(1972), "Interferometric positions of H_2O vapour emission sources in H II regions", Astrophys. J., 175, (2) pt 2, L59-L64 [page 9].

Hocking, et al. (1972), "Microwave spectrum of HNCO", Astrophys. J., 174: 2, L93-96 [page 12].

Hosking, M. W., (1973), "Realm of microwaves", Wireless World, October 1973, p501-505 [page 35].

Hyland, A. R., et al. (1970), "Observation of the ir object, VY CMa", Astrophys. J., 158, 619 [page 6].

Ingersoll, P. Andrew, Seovy, B. Conway (1971), "The Atmospheres of Mars and Venus", Ann. Rev. of Astron. Astrophys., 9, 147 [page 27].

Irvin, J. C., and N. C. van der Waal, (1969), "Schottky-barrier Devices", Microwave Semiconductor Devices and their Applications, Ed. Watson, H. A., ~~McGrawhill~~ McGraw-Hill N.Y., 1st Ed. [page 15].

Janssen, Michael Allen (1972), "The 20-36 GHz Venus Microwave Emission", Space Sci. Lab. Series, 13 issue 51, (Univ. of California, Berkley) [page 27].

Janssen, M. A., et al. (1973), "Mars & Jupiter : Radio emission at 1,35 cm."Icarus Int. Journ. of Solar System Stud;, 18, 502 [page 27].

Janssen, M., et al. (1973b), "Venus : New microwave measurements show no atmospheric water vapour", Science, 179, 994-997 [page 27].

Jasik, H (1961), Antenna Engineering Handbook, ~~McGrawhill~~ McGraw-Hill N.Y., 2.14 [page 35].

Johnson, H. L., (1966), "Infra-Red Stars", Sky & Telescope, 32: 2 73-77 [page 7].

Johnston, K. J., et al. (1971), "Observations of 1,35 cm H_2O emission in the Southern Hemisphere", Astrophys. J., 167, L93-6 [page 25].

Johnston, K. J., et al. (1971), "An interferometer map of the water vapour sources in W49", Astorphys. J., 166, 621-6 [page 25].

Johnston, K. J. and Robinson, B. J. (1972a), "Water Sources Associated with OH emission in the Southern Milky Way", Astrophys. Lett., 10, 93-98 [pages 9, 25].

Johnston, K. J., et al. (1972b), "Microwave celestial water-vapour sources", Sky & Telescope, 44, No. 2, 88-90 [page 9].

Johnston, et al. (1973), "13 New H_2O sources associated with OH emission in H II regions", Astrophys. J., 182, 67-75 [pages 4, 9, 11].

Jones, et al. (1972), "Spectral Observations of Venus 18,5-24,0 GHz 1964, 1967-8", Astron. Soc. Pac., 84 (499), 435-442 (Eng.) [page 14].

Jones, T. W. (1973), "The Radio Source Sagittarius A West : Thermal or Nonthermal?", Astrophys. Lett., 14, 55 [page 13].

Kerr, F. J. (1968), "Radio-line emission and absorption by the Interstellar Gas", Nebulae and Interstellar Matter, Ed. M. Barbara, (Star and Stellar Systems, Vol. VII, ed. G. P. Kuiper), 575-619 [pages 2, 6. Appendix A].

Knapp, C. R., et al. (1973a), "OH Observation of 16 interstellar Clouds", Astron. J., 78, 453 [page 11].

Knapp, C. R., et al. (1973b), " A search for OH/IR Stars in globular clusters", Astron. J., 78, 458 [pages 10, 11].

Knowles, S. H., et al. (1969a), "Spectra, variability, size and polarisation of H_2O microwave emission sources in the galaxy", Science, 163, 1055-7 [page 7].

Knowles, S. H., et al. (1969b), "Galactic Water vapour emission : further observations of variability", Science, 166, 221-4 [page 7].

Kraus, J. D., (1966), Radio Astronomy, ~~McGrawhill,~~ McGraw-Hill N.Y., [pages 13, 15, 17, 19, 20, 27. Appendix A].

Kurichik, V. M. (1972), "The Nature of Variable Radio Sources", Astrophys. Lett., 10, 115-119 [page 13].

Kuz'min, A. D. et al. (1966) Radiostronomical Methods of Antenna Measurements, Academic Press, N.Y. & London. [page 19].

Larson, Richard B (1973), "Processes in collapsing Interstellar Clouds", Ann. Rev. of Astron. and Ap., Ed. Goldberg et al., 11, 219-238 [page 8].

Law, S. E., and D. H. Stalin, (1968),"Measurement of Venus & Jupiter near 1-cm Wavelength", Astrophys. J., 154, 1077 [page 27]

Lees (1972), "Torsion-vibration-rotation interactions in CH_3OH III", J. Phys. Chem., 57 : 2, 824-826 [page 12].

Leonard, T. W. and P. J. Napier (1973 (Aug.)), "Computation of apeture efficiency and radiation pattern for a Cassegrain antenna", N.R.A.O. Electronics division internal rept., No.131 [page 42].

Litvak, M. M. (1969a), "Hydroxyl and Water Maser in protostars", Science, 165, 855-61 [pages 7, 11].

Litvak, M. M. (1969b), "Infrared Pumping of Interstellar OH", Astrophys. J., 156, 471-492 [page 11].

Litvak, M. M. (1971), "The Meaning of $OH-H_2O$ Maser Maps", Astrophys. J., 170, 71-80 [page 8].

Litvak, M. M. (1972b), "Non-equilibrium processes in interstellar molecules", Atoms and molecules in astrophysics, Ed. T. R. Carson, Academic Press, Lon. & N.Y., 201 [pages 3, 11].

Litvak, M. M. (1973a), "Radiative Transport in Interstellar Masers", Astrophys. J., 182, 669 [pages 8, 10, 11].

Litvak, M. M. (1973b), "Maser and Optical Pumping", Ed. Gordon : Molecules in the Galactic Environment, 267-288, Wiley, N.Y. [pages 11, 12].

McNally, D. (1968), "Interstellar molecules", Advances in Astronomy & Astrophysics, Ed. Z. Kopal, 6, 173-198 [page 2].

Matveenko, L. I., and M. Z. Meeks (1972), "Radio brightness and distribution over the Crab Nebula at 3,55 cm and 1,28 cm", Astron. Zh., 49, 965 [Sov. Astron. - A.J. 16 : 5, 790-4, (1973)] [page 13].

Mayer, C. H., et al. (1973), "Ammonia in DR 21 (OH) and NGC 2264", Astrophys. J., 182, L65 [page 12].

Meeks, M. L. et al. (1969), "Water vapour : observations of galactic sources", Science, 165, 180-4 [page 13].

Mezger, P. G. (1971), "Molecules in Dense Clouds and Protostars", Highlights of Astronomy, De Jager (ed.), 336-377 [page 9].

Mezger, P. G. (1972), "Interstellar Matter : An observer's point of view" Interstellar Matter, ed. N. C. Wickramasinghe, et al., publ. Geneva Observatory, CH-1290 Sauverny, Switzerland, 1-191 [page 12, Appendix A].

Moran, J. M. et al. (1973), "Very long baseline interferometric observations of the H_2O sources in W49N, W3(OH), Orion A, and VY Canis Majoris", Astrophys. J., 185, 535 [pages 4, 8, 9].

Morrison, David (1969), "Venus : Absence of a Phase effect at a 2-cm Wavelength", Science, 163, 815-817 [page 14].

Morrison, David and Michael J. Klein, (1970), "The Microwave Spectrum of Mercury", Astrophys. J., 160, 325 [page 27].

Neugebauer, Gerry, et al. (1971), "Infrared sources of radiation", Annual Review of Astronomy and Astrophysics, Ed. Goldberg, Leo et al. 9, 67-102 [page 6].

Newburn, R. L., and S. Gulkis Sr. (1973), "A survey of the outer planets Jupiter, Saturn, Uranus, Neptune, Pluto and their satellites", Space Sci. Rev., 14, 1794 [pages 14, 27].

Parker, E. N., (1966), "The dynamical state of the interstellar gas and field", Astrophys. J., (USA), 145: 3, 811-33 [page 9].

Pauliny-Toth, I. I. K. and K. I. Kellermann, (1970), "MM - Wavelength measurements of Uranus and Neptune", Astrophys. Lett., 6, 185-7 [page 27].

Pipes, Louis A. (1946), Applied Mathematics for Engineers and Physicists, ~~McGrawhill~~ McGraw-Hill, N.Y., First ed., 209 [page 50].

Potter, P. D. (1963), "Apeture illumination and gain of a Cassegrain system", IEEE Trans., AP-11 373-375 [page 42].

Potter, Philip D. (1967), "Application of spherical wave-theory to Cassegrain-fed Paraboloids" IEEE Trans. Antennas and Propagation, AP-15, 727-36 [page 42].

Raimond, et al. (1969), "Positions and Stokes Parameters of Seven OH-emission sources", Astrophys. J., 155, 817 [page 6].

Robinson, B (1973), "Interstellar Molecules" I.A.U. 1973; Rhodes Physics I.A.U. Report by Baart, E. E.

Rudnitskii, G. M. et al. (1973), "Constraints on cosmic maser intensity, and the possibility of detecting new OH and H_2O sources by a rapid sky survey", Soviet Astronomy-A.J., 16: 6, 1049-1050 [page 25].

Rusch, W. V. T. and P. D. Potter (1970), Analysis of Reflector Antennas, Academic Press, London [Page 31].

Saad, Theodore S. (1971), Microwave Engineers Handbook, 2, Artech House, Massachusetts, 18 [page 32, section 4.2].

Sarma, N. V. G. (1972), "A 50- channel multifilter Receiver", N.R.A.O. Electronics Div. Int. Report, 117 [page 15].

Schwartz, P. R. and Barret, A. H. (1970), "Observations of water-vapour emission associated with infrared stars", Astrophys. J., 159, L123 [page 11].

Shu, Frank H. (1970a & b), "On the Denisty-Wave theory of Galactic Spirals. I. Spiral structure as a normal mode of oscillation II. The propagation of the density wave action", Astrophys. J., 160, a) 89 b) 99 [page 9].

Shu, Frank H., et al. (1972), "Galactic shocks in an interstellar medium with two stable phases", Astrophys. J., (USA), 173: 3, pt 1, 557-92 [page 9].

Silver, Samuel (1965), Microwave antenna theory and design, Dover Publications, N.Y., 432 [pages 35, 41, 45].

Snyder, Lewis, E. and Buhl, David (1970a & b), "Molecules in the interstellar Medium", Sky & Telescope, a) 40: 5 267-270; b) 40: 6 345-348 [page 3].

Snyder, et al. (1972), "Detection of several new interstellar molecules", Ann. N.Y. Acad. Sci., 194, 17-20 (Eng.) [page 12].

Solomon, Philip M. (1973), "Interstellar Molecules", Phys. Today, Mar. 1973, 32-40 [page 7].

Sommerfeld, Arnold (1964), Mechanics of deformable bodies, Translated by G. Kuerti, Academic Press, N.Y. 295 [page 49 and Appendix A.2].

Spinrad, Hyron and Newburn, Ray L. (1965), "A Low-Dispersion Sepctroscopic Search for water vapour in cool stars", Astrophys. J., 141 (3), 965-975 [page 12].

Steinberg, Jean Louis, and J. Lequeux (1963), Radio Astronomy, translated by R. N. Bracewell, ~~McGrawhill~~ McGraw-Hill, N.Y., p.p.127, 166, 35 [pages 13, 14, 37 respectively].

Strull, M. A. and R. D. Carpenter (1973), "Some Radio Sources with enhanced spectra at centimeter Wavelengths", Astrophys. Lett., 13, 73 [page 13].

Sullivan, W. T. (1973), "Microwave water vapour emission from galactic sources", (Astrophys. J. suppl. 222) Abstract: Astrophys. J., 181, 1065 [page 8].

Townes, C. H. (1957), "Microwave and Radio-frequency resonance lines of interest to Radio Astronomy", Radio Astronomy (I.A.U. Symp. No.4) ed. H. C. van de Hulst, Cambridge : Cambridge university press. 92-103 [pages 2, 3, 13].

Turner, B. E. (1970), "Fifty New OH sources associated with H II regions", Astrophys. Lett., 6, 99-408 [page 11].

Turner, B. E. (1973), "The distribution of interstellar molecules", Molecules in the Galactic Environment, 144-154, ed. Gordon, M. A. et al. John Wiley & Sons Inc. [page 8].

Wallerstein, George (1971), "On the I.R. Excess of W. Cephei and Similar Stars", Astrophys. J., 166, 725-729 [pages 7, 8].

Watson, W. D. and Saltpeter, E. E. (1973), "Molecule formation on Interstellar Grains", Ed. Gordon, Molecules in the Galactic Environment, Wiley N.Y., 375-380 [page 11].

Weinreb, S. and Jansson, S. (1970), "Antenna feed efficiency and spillover calculation program", N.R.A.O. (Greenbank, West Virginia) Electronics Division internal rept., No.93, June 1970 [page 42].

White, Raymond E. (1970), "A bibliography of Colour-Magnitude diagrams for Globular Clusters", Abstract : Astrophys. J., 160, 379 [Astrophys. J. suppl. 177] [page 10].

Wickramasinghe, N. C., et al. (1972), Interstellar Matter, Publ. Geneva Observatory, CH-1290 Sauverny, Switzerland pages 118, 209 [pages 5, 8].

Williams, David A. (1971), "Association Reactions", Astrophys. Lett., 10: 1, 17-19, [page 11].

Wilson, W. J., et al.(1970), "OH Emission Associated with I.R. stars", Astrophys. J., 160, 545 [page 6].

Wilson, W. J., et al. (1972), "I.R. Stars with strong 1665/1667 MHz OH", Astrophys. J., 177 (2) (pt 1), 523-540 [page 6].

Wilson, W. J. (1973), "OH and H_2O Microwave Emission from Infrared Stars", Molecules in the Galactic Environment, Ed. Gordon, M. A. et al., John Wiley & Sons, N.Y. [page 6]

Winnberg, A. et al. (1973), "New OH sources discovered at 1612 MHz", Astrophys. Lett., 13, 125 [page 6].

Wrixon, et al. (1971), "The Spectrum of Jupiter at millimeter Wavelengths", Astrophys. J., 169, 171 [page 27].

Wynn-Williams, C. G. (1970), "Observations of NGc 7027 at 5 GHz", Astrophys. Lett., 6, 189-92 [page 13].

SUPPLEMENTARY BIBLIOGRAPHY

The following references were found useful during the course of the investigations for the thesis, but are not referred to in the text.

Avery, Roger (1961), "Mechanical considerations in Antenna design", Antenna Engineering Handbook, Ed. Jasik, Henry, McGraw-Hill, N.Y.

Balister, Michael (1971), "A 50-channel multifilter receiver", N.R.A.O. Electronics Div. Int. Report, 112.

Barret, A. H. (1969), "Discovery of interstellar water vapour", Comm. At. Mol. Phys., 1 93-6.

de Jong, Teije (1973), "Water masers in a Protostellar Gas Cloud", Astron. and Astrophys., 26, 297-313.

Dickinson, D. F. and Chaisson, E. J. (1971), "Search for Extragalactic H_2O", Astrophys. J., 169, 207-8.

Dickinson, Dale F. (1973b), "Long Period variables : Correlation of Stellar period with OH Radial-velocity pattern", Astrophys. J., 181, L135.

Frogel, J. A. (1970), "Water absorption in the infrared spectrum of long-period variable stars and associated microwave emission", Astrophys. J., 162, 15-19.

Jonson, Harold L. (1970), "Infrared Stars", Sky & Telescope, 32: 2, 73-77.

Knowles, S. H. et al. (1969), "Galactic water vapour emission : further observations of variability", Science, 166, 221-4.

McCraken, Daniel D. (1965), A guide to FONTRAN IV programming, John Wiley & Sons, Inc., N.Y. & London.

Oka, Takeshi (1973), "Selective Predissociation as a Possible Mechanism for the Population inversion of interstellar H_2O", Ed. Gordon : Molecules in the Galactic Environment, John Wiley & Sons, N.Y., 257-266.

Penzias, A. A., Burrus, C. A. (1973), "Millimeter-Wavelength Radio Astronomy Techniques", Ann. Rev. Astr. Ap., Ed. Goldberg, Leo et al.

Reisz, A. C. et al. (1973), "W_3(OH) : Accurate relative positions of water-vapour emission features", Astrophys. J., 186, 537.

Snyder, Lewis E., Buhl, David (1969), "Water-vapour clouds and the interstellar Medium", Astrophys. J., 155, L65-L70.

Snyder, Lewis E., Buhl, David, Zuckerman, B., Palmer, Patrick (1969), "Microwave Detection of Interstellar Formaldehyde", Phys. Rev. Lett., 22: 13, 679-681.

Snyder, et al. (1973), "Radio Astronomy - Interstellar methyl acetylene and isocyanic acid", Nature Phys. Sci., 243 (125) 45.

Sullivan, W. T. (1971), "Variations in the frequency and intensity of 1,35 cm water emission profiles in galactic H II regions", Astrophys. J., 160, 321.

Turner, B. E. and Rubin, R. H. (1971), "New galactic H_2O sources associated with H II regions", Astrophys. J., 170, L113-L118.

Weinreb, Sander (1963), A digital Spectral analysis technique and it's application to radio astronomy, Ph.D. thesis, M.I.T. technical report 412.

Wilson, W. J., Barret, Alan H (1968), "Discovery of Hydroxyl Radio Emission from Infrared Stars", Science, 161, 778-779.